Journal Title
XX(X):1–27

DOI: 10.1177/ToBeAssigned
www.sagepub.com/
SAGE

Set-Valued Rigid Body Dynamics for Simultaneous Frictional Impact

Mathew Halm[1] and Michael Posa[1]

Abstract

Robotic manipulation and locomotion often entail nearly-simultaneous collisions—such as heel and toe strikes during a foot step—with outcomes that are extremely sensitive to the order in which impacts occur. Robotic simulators commonly lack the accuracy to predict this ordering, and instead pick one with a heuristic. This discrepancy degrades performance when model-based controllers and policies learned in simulation are placed on a real robot. We reconcile this issue with a *set-valued* rigid-body model which generates a broad set of physically reasonable outcomes of simultaneous frictional impacts. We first extend Routh's impact model to multiple impacts by reformulating it as a differential inclusion (DI), and show that any solution will resolve all impacts in finite time. By considering time as a state, we embed this model into another DI which captures the continuous-time evolution of rigid body dynamics, and guarantee existence of solutions. We finally cast simulation of simultaneous impacts as a linear complementarity problem (LCP), and develop a probabilistically-complete algorithm for approximating the post-impact velocity set. We demonstrate our approach on several examples drawn from manipulation and legged locomotion.

Keywords

Rigid-body Dynamics; Simulation; Contact Modeling; Legged Locomotion; Manipulation; Linear Complementarity Problems

1 Introduction

Modern robots are fast and strong, and their capabilities often eclipse those of humans. However, when these robots interact with their environment, whether by manipulating objects or traversing over uneven surfaces, they do so with far less skill than their human counterparts. Critical challenges facing the field lie in modeling, planning, and control of robots in these complex, multi-contact settings, particularly for locomotion (Wieber et al. 2016) and manipulation (Kemp et al. 2007).

Chief among the difficulties induced by frictional contact are collisions between robots and the objects in their environments. Even a single collision is a complex interaction, in which object interpenetration is prevented by material deformation. Often, this process occurs on a spatial and temporal scale far below the resolution of practical robotics sensors. Truly accurate capture of these effects requires an impractically precise set of knowledge of the constituent materials, geometries, and initial conditions, let alone the burdensome computation to produce predictions from such information (Chatterjee 1997). In the face of these challenges, many robotics approaches make a *rigid-body* assumption, a tractable but coarse approximation of contact mechanics in which objects do not deform (see Stewart (2000) or Brogliato (1999) for a detailed overview).

Deeply ingrained into robotics simulation, planning, and control methodology is the philosophy of 1) picking a rigid-body model for its mathematical convenience and 2) assuming that an arbitrary prediction from the model is unique and closely matches real-world behavior (Posa et al. 2014; Mordatch et al. 2015; Coumans and Erwin 2015; Hogan and Rodriguez 2016; Chavan-Dafle and Rodriguez 2017; Salehian and Billard 2018). This approach is sometimes reinforced by underlying models which intentionally select unique outcomes based on a heuristic such as maximum dissipation (Drumwright and Shell 2010), minimum potential energy (Uchida et al. 2015), or symmetry constraints (Kaufman et al. 2008). Popular linear complementarity problem (LCP) formulations may have a finite number of non-unique solutions (as opposed to infinite realistic outcomes), but practically rely on a numerical solver which may be biased toward a particular solution (Anitescu and Potra 1997; Stewart and Trinkle 1996; Halm and Posa 2018; Horak and Trinkle 2019; Remy 2017).

However, seemingly minor mathematical differences between models can result in wildly different predictions from identical initial conditions; in many cases, *no* available model reasonably captures real-world behaviors (Fazeli et al. 2017; Chatterjee 1999; Stoianovici and Hurmuzlu 1996; Remy 2017). These discrepancies are particularly pronounced when multiple impacts occur so quickly that their order cannot be practically distinguished—for instance, heel and toe strikes in flat-footed running. The extreme sensitivity of simultaneous impacts to their ordering has been widely studied (Wang et al. (1992); Hurmuzlu and Marghitu (1994); Ivanov (1995); Smith et al. (2012); Uchida et al. (2015) and others). A ubiquitous manifestation of

[1]GRASP Laboratory, University of Pennsylvania

Corresponding author:
Mathew Halm
GRASP Laboratory
University of Pennsylvania
Philadelphia, PA, 19104
Email: mhalm@seas.upenn.edu

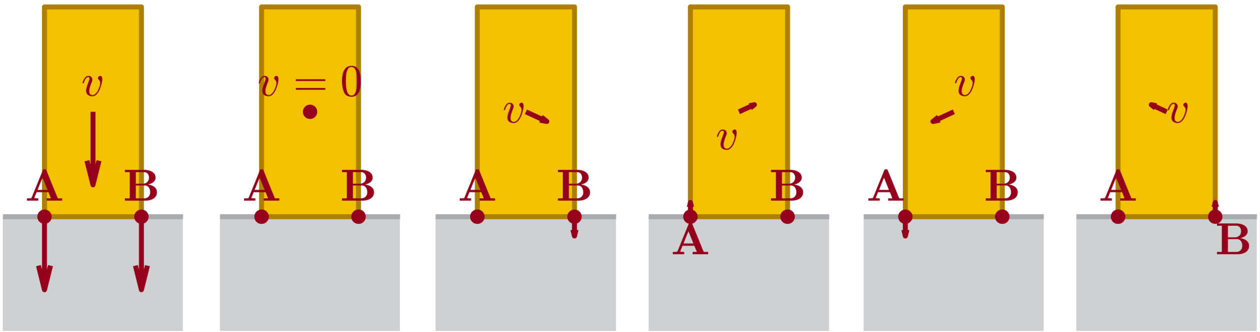

(a) Initial condition **(b)** Symmetric impact **(c)** A-then-B sequential impacts **(d)** B-then-A sequential impacts

Figure 1. (a) A cell phone (yellow) with velocity v is dropped onto flat ground (gray), colliding at two corners; multiple physically-realistic results may emerge from these simultaneous impacts. (b) As the system is symmetric about the vertical axis, one possibility is that the phone comes to rest; the model in Anitescu and Potra (1997) produces this outcome. (c) With sufficient friction, any impact at a single corner can stick. Therefore, if point A impacts first, the resulting torque would cause the phone to rotate counter-clockwise. This causes a second impact at point B, causing the phone to pivot about B with A lifting off the ground. (d) If the impacts are instead ordered B-then-A, the end result by symmetry is A pivoting and B lifting off.

this phenomenon is the difficulty of predicting a billiards break, though sensitivity to impact also occurs in far simpler systems. Figure 1 for instance shows how qualitatively and quantitatively distinct outcomes can results from a single, slender object impacting flat ground.

As the motivating examples in Section 3.1 will demonstrate, simultaneous impacts are not limited to unlikely, pathological events; they are, in fact, regular occurrences in robotics. Such behaviors require careful analysis that unique-outcome models do not readily provide. From the perspective of planning, learning, and control, it is critical to understand the role of this non-uniqueness (alternatively, extreme sensitivity), as some of the broad challenges in executing dynamic, multi-contact motion likely arise from these issues. For example, methods which use a simulator to learn or plan a motion may, unwittingly, be planning for an ambiguous and therefore unstable outcome due to multi-contact. Furthermore, as the set of these ambiguous outcomes is often non-convex, it is insufficient to try to capture this sensitivity via simple models of uncertainty. To address these issues, we propose the development of *set-valued* rigid-body models that attempt to generate all physically-reasonable outcomes. While some predictions from such a model may not ultimately occur, controllers guaranteed to stabilize the model—as well as learned policies trained on the the model's predictions—are well-positioned to perform reliably in the real world. In this work, we present a rigorously-derived, set-valued rigid body model which captures arbitrary impact sequencing in multi-contact scenarios. This work extends our previous conference publication Halm and Posa (2019), in which we first extended of Routh's impact method to simultaneous frictional impacts. This paper supplements the scope of this work with the following:

- In Section 3, we provided a significantly simplified theoretical analysis of the impact model in Halm and Posa (2019), including guarantees on existence of solutions (Lemma 14) and impact termination (Theorem 23). We additionally include new motivating examples which highlight the inconsistencies which arise between existing models of simultaneous impact.
- In Section 4, we embed this approach into a unified rigid body dynamics model, capturing both impacts and continuous-time evolution with a differential inclusion. We prove that our differential model exhibits desirable physical and mathematical properties. Notably, we prove existence of solutions (Theorem 28) and amortized time advancement (Theorem 31) in spite of pathological multi-contact behaviors including Zeno's paradox.
- In Section 5, we formulate a time-stepping simulation of the impact model as a linear complementarity problem (LCP). We provide probabilistic bounds on computation time for both sampling from (Theorem 37) and global approximation of (Theorem 43) the feasible post-impact velocity set.
- In Section 6, we apply our model to several examples from robotic locomotion and manipulation.

2 Background

We now introduce notation for and review frictional impact dynamics of rigid multibody systems. In the breadth of developing both a continuous-time model and a discrete simulator, there are several prerequisite topics to review. We offer a thorough introduction to each, and summarize related notation in Appendix A. For readers already well-versed in most of these topics, it may be advisable to skip to Section 3 and use this section and the appendix as required.

We will begin with the mathematical foundations of our models: functional analysis (2.1), sampling-based set approximation (2.2), differential inclusions (2.3), and linear complementarity problems (2.4). We will make use of several set-, matrix-, and vector-valued operations and constants; the most common of these are listed in Appendix A, Table 2. We conclude the section with an overview of continuous-time evolution (2.5), discrete-time simulation

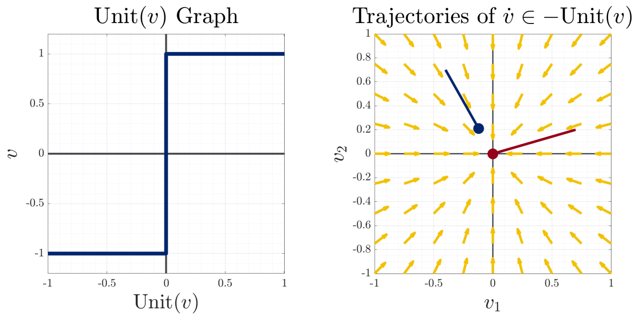

(a) **(b)**

Figure 2. (a) Graph of $\mathrm{Unit}(\boldsymbol{v})$ for $n = 1$. Note that $\mathrm{Unit}(\boldsymbol{v})$ is continuous on $\boldsymbol{v} \neq 0$. At $\mathbf{0}$, Unit takes the value $[-1, 1]$, which contains a continuous extension of $\widehat{\boldsymbol{v}}$ from both the left (-1) and the right $(+1)$, so that Unit is u.s.c.. (b) Flow field (yellow) of the solutions (blue, red) to $\dot{\boldsymbol{v}} \in -\mathrm{Unit}(\boldsymbol{v})$ for $\boldsymbol{v} \in \mathbb{R}^2$.

(2.6), and impact resolution (2.7) of rigid bodies undergoing frictional contact; a listing of the associated system terms is in Section 2.5, Table 1. For notational brevity, we will frequently write a singleton set $\{a\}$ without braces (e.g. $a + B$ is the Minkowski sum of $\{a\}$ and B) and suppress the dependence of system terms on their inputs whenever clear (e.g. $\boldsymbol{G}$ instead of $\boldsymbol{G}(\boldsymbol{q})$).

2.1 Functional Analysis

The results in this work are derived using tools from measure theory and functional analysis; for a thorough background, see Rudin (1986, 1991). For a domain $\Omega \subseteq \mathbb{R}^n$, we equip Ω with the Euclidean metric and norm, and integrate over Ω with respect to the Lebesgue measure by default. The total time derivative $\dot{\boldsymbol{f}}(t)$ of an absolutely continuous function $\boldsymbol{f}(t)$ is taken in the Lebesgue sense (i.e. $\boldsymbol{f}(t)$ is the anti-derivative of $\dot{\boldsymbol{f}}(t)$, which is defined almost everywhere (a.e.)). Convergence of a sequence of functions f_n to f almost everywhere and uniformly are denoted $f_n \xrightarrow{a.e.} f$ and $f_n \xrightarrow{u} f$, respectively. A key result for the derivations in this work is the Arzelà-Ascoli Theorem (Rudin 1991):

Theorem 1. Arzelà-Ascoli. *Every uniformly bounded sequence $(\boldsymbol{f}_n)_{n \in \mathbb{N}}$ of equicontinuous $\mathbb{R}^n$-valued functions on a compact interval $[a, b]$ has a subsequence $(\boldsymbol{f}_{n_k})_{k \in \mathbb{N}}$ that converges uniformly.*

In particular, we will apply this theorem to sequences of functions that are equicontinuous because they are all Lipschitz with the same constant. We say a function $f : A \to B$ is Lipschitz with constant L if for each a_1, a_2 in A, $\|f(a_1) - f(a_2)\|_2 \leq L \|a_1 - a_2\|_2$. For instance, an absolutely continuous function $\boldsymbol{f}(t)$ has this property if $\left\|\dot{\boldsymbol{f}}(t)\right\|_2 \leq L$ almost everywhere. When Lipschitz functions are composed, the resulting function is Lipschitz as well:

Proposition 2. *let $f, g : A \times B \to A$ be two Lipschitz functions with constants L_f and L_g. Then $h(a, b_1, b_2) = f(g(a, b_1), b_2)$ is Lipschitz with constant $L_f L_g$.*

Our analysis will also make use of positive definite functions; a function $\alpha(s) : \Omega \to \mathrm{cl}\mathbb{R}^+$ is positive definite if it is positive on $\Omega \setminus \{0\}$ and $\alpha(0) = 0$.

2.2 Set Approximation via Sampling

Intractable problems in robotics can often be approximately solved with arbitrary precision via stochastic, sampling-based methods (e.g. "probabilistic completeness" and "asymptotic optimality" of RRT* (Karaman and Frazzoli 2011)). In Section 5, we will use random sampling to approximate the set of possible post-impact velocities corresponding to a pre-impact state. We will show that finite set of samples can approximate the whole set as an ε-*net*:

Definition 3. *For $\varepsilon \geq 0$, an ε-net of a set $\mathcal{X}$ is a set $\mathcal{X}' \subseteq \mathcal{X}$ such that for each $x \in \mathcal{X}$, there exists an $x' \in \mathcal{X}'$ with $\|x - x'\|_2 \leq \varepsilon$.*

In the spirit of probabilistic completeness, we will show that, with sufficient samples, our simulation scheme can approximate this set to arbitrary precision with arbitrary confidence. We will prove this by leveraging a similar behavior for the image of a box under a Lipschitz continuous function:

Proposition 4. *Let $g(x) : \mathbb{R}^n \to \mathbb{R}^m$ be Lipschitz continuous with constant L. Consider a set of N uniform i.i.d. samples $\mathcal{X} = \{x_1, \ldots, x_N\}$ from $[0, h]^n$. Then $g(\mathcal{X})$ is an ε-net of $g([0, h]^n)$ with probability at least $1 - \frac{(1-\Omega)^N}{\Omega}$, where*

$$\Omega = \left\lceil \frac{hL\sqrt{n}}{\varepsilon} \right\rceil^{-n} . \tag{1}$$

Proof. See Appendix C.1.

2.3 Differential Inclusions

The dynamics of many robots can be captured with a system of ordinary differential equations (ODEs) $\dot{\boldsymbol{x}} = \boldsymbol{f}(\boldsymbol{x}, \boldsymbol{u})$, which relates $\boldsymbol{x}$, the state of the robot (typically some notion of position and velocity), to $\boldsymbol{u}$, a set of inputs (such as motor torques) that can be manipulated. However, the dynamics of rigid bodies under frictional contact present complexities that this formulation cannot capture. Impacts between bodies induce instantaneous jumps in velocity that in general cannot described by an ODE (*non-smooth* behaviors) (Brogliato 1999). Additionally, when contact occurs at many points, multiple frictional forces that obey Coulomb's law of friction may exist (*non-unique* behaviors) Stewart (2000). It is then useful to define an object that, unlike ODEs, allows for the derivative at each state to lie in a set of possible values

$$\dot{\boldsymbol{v}} \in D(\boldsymbol{v}) . \tag{2}$$

As the set-valued map $D(\boldsymbol{v})$ associated with friction may not be continuous, conditions for a function $\boldsymbol{v}(t)$ to be a solution to this *differential inclusion* (DI) are weakened from those of an ODE:

Definition 5. *For a compact interval $[a, b]$, $\boldsymbol{v} : [a, b] \to \mathbb{R}^n$ is a solution to the differential inclusion $\dot{\boldsymbol{v}} \in D(\boldsymbol{v})$ if $\boldsymbol{v}$ is absolutely continuous and $\dot{\boldsymbol{v}}(t) \in D(\boldsymbol{v}(t))$ a.e. on $[a, b]$. Denote the set of such solutions as* $\mathrm{SOL}\left(D, [a, b]\right)$.

Solutions to initial value problems for (2) are defined similarly:

Definition 6. *The set of solutions to* $\dot{\boldsymbol{v}}(t) \in D(t)$ *with initial condition* $\boldsymbol{v}(a) = \boldsymbol{v}_0$ *over the interval* $t \in [a, b]$ *are denoted as* $\mathrm{IVP}\left(D, \boldsymbol{v}_0, [a, b]\right)$.

In Figure 2, we consider an example DI

$$\dot{\boldsymbol{v}} \in -\mathrm{Unit}\left(\boldsymbol{v}\right), \tag{3}$$

where $\mathrm{Unit}\left(\boldsymbol{v}\right)$ is the set-valued unit direction function

$$\mathrm{Unit}\left(\boldsymbol{v}\right) = \begin{cases} \{\widehat{\boldsymbol{v}}\} & \boldsymbol{v} \neq \boldsymbol{0}, \\ \{\boldsymbol{v} : \|\boldsymbol{v}\|_2 \leq 1\} = \mathrm{cl}(\mathrm{Ball}(1)) & \boldsymbol{v} = \boldsymbol{0}. \end{cases} \tag{4}$$

The only solution to the initial value problem starting from $\boldsymbol{v}(0) = \boldsymbol{v}_0$ has the form

$$\boldsymbol{v}(t) = \max\left(\|\boldsymbol{v}_0\|_2 - t, 0\right) \hat{\boldsymbol{v}}_0 . \tag{5}$$

This solution is non-differentiable at $t = \|\boldsymbol{v}_0\|_2$ and thus is not a solution of any ODE. In general, non-emptiness and regularity of the initial value problem depends on the structure of $D(\boldsymbol{v})$; fortunately, we will later show that solution sets for frictional dynamics are well-behaved due to their *upper semi-continuous (u.s.c.)* structure:

Definition 7. *A function* $D : A \to \mathbb{P}\left(B\right)$ *is upper semi-continuous if for any input* a *and neighborhood* B' *of* $D(a)$*, there exists a neighborhood* A' *of* a *with* $B' \subseteq D(A')$*. Equivalently, if* B *is compact, for all convergent sequences* $(a_n)_{n\in\mathbb{N}}$ *and* $(b_n)_{n\in\mathbb{N}}$*,*

$$b_n \in D(a_n), \forall n \implies \lim b_n \in D(\lim a_n).$$

Proposition 8. (Aubin and Cellina 1984). *Let* $\boldsymbol{v}_0 \in \mathbb{R}^n$ *and* $[a, b]$ *be a compact interval. Suppose* $D(\boldsymbol{v})$ *is uniformly bounded (i.e.* $D(\boldsymbol{v}) \subseteq \mathrm{Ball}(c)$ *for some* $c > 0$*). If* $D(\boldsymbol{v})$ *is u.s.c., and closed, convex, and non-empty at all* $\boldsymbol{v}$*, then* $\mathrm{IVP}\left(D, \boldsymbol{v}_0, [a, b]\right)$ *is non-empty and u.s.c. in* $\boldsymbol{v}_0$.

Intuitively, a map is u.s.c. if its value at each $\boldsymbol{v}$ is not significantly smaller than its value at any $\boldsymbol{v}'$ near $\boldsymbol{v}$. U.s.c. functions have the useful property that they map compact sets to closed sets, and Proposition 8 immediately and crucially implies that $\mathrm{SOL}\left(D, [a, b]\right)$ and $\mathrm{IVP}\left(D, \boldsymbol{v}_0, [a, b]\right)$ are non-empty and closed under uniform convergence. The DI in Figure 2 for example exhibits this structure.

Similar to continuous functions, there are several useful compositional rules which preserve upper semicontinuity; finite combination of u.s.c. functions by cartesian product, convex hull, composition, union, and addition are all u.s.c..

2.4 Linear Complementarity Problems

We will formulate multi-impact simulation as a sequence of linear complementarity problems (LCP's), which have been widely used for frictional contact simulation (e.g. Stewart and Trinkle (1996); Anitescu and Potra (1997)). We refer the reader to Cottle et al. (2009) for a complete description and briefly describe some essential properties.

Definition 9. *The linear complementarity problem with parameters* $\boldsymbol{W} \in \mathbb{R}^{n\times n}$ *and* $\boldsymbol{w} \in \mathbb{R}^n$ *is the constraint satisfaction problem*

$$\begin{aligned} &\textit{find} && \boldsymbol{z} \in \mathbb{R}^n, && (6)\\ &\textit{subject to} && \boldsymbol{z}^T\left(\boldsymbol{W}\boldsymbol{z} + \boldsymbol{w}\right) = \boldsymbol{0}, && (7)\\ & && \boldsymbol{z} \geq \boldsymbol{0}, && (8)\\ & && \boldsymbol{W}\boldsymbol{z} + \boldsymbol{w} \geq \boldsymbol{0}, && (9) \end{aligned}$$

for which the set of solutions is denoted $\mathrm{LCP}(\boldsymbol{W}, \boldsymbol{w})$*. The* ***complementarity constraints*** *(7)–(9) are often abbreviated as* $\boldsymbol{0} \leq \boldsymbol{z} \perp \boldsymbol{W}\boldsymbol{z} + \boldsymbol{w} \geq \boldsymbol{0}$.

For LCPs related to frictional behavior, $\boldsymbol{W}$ is often copositive (i.e. $\boldsymbol{x}^T\boldsymbol{W}\boldsymbol{x} \geq 0$ for all $\boldsymbol{x} \geq \boldsymbol{0}$). This property is theoretically useful, as it provides a sufficient condition for LCP feasibility and computability:

Proposition 10. (Cottle et al. 2009). *Let* $\boldsymbol{w} \in \mathbb{R}^n$*, and let* $\boldsymbol{W} \in \mathbb{R}^{n\times n}$ *be copositive. If* $\boldsymbol{w}^T\mathrm{LCP}(\boldsymbol{W}, \boldsymbol{0}) \geq 0$*, then* $\mathrm{LCP}(\boldsymbol{W}, \boldsymbol{w})$ *contains a solution which Lemke's Algorithm can find in finite time.*

While uniqueness of the solution is not guaranteed, if mapping the solution through a matrix $\boldsymbol{A}$ produces uniqueness, it also produces Lipschitz continuity:

Proposition 11. (Facchinei and Pang 2003). *For all matrices* $\boldsymbol{W} \in \mathbb{R}^{n\times n}$*,* $\boldsymbol{A} \in \mathbb{R}^{m\times n}$*, if the function* $\boldsymbol{f}(\boldsymbol{w}) = \boldsymbol{A}\mathrm{LCP}(\boldsymbol{W}, \boldsymbol{w})$ *is unique over a convex domain* $\Omega \subseteq \mathbb{R}^n$*, it is also Lipschitz on* Ω.

2.5 Continuous-time Dynamics of Rigid Bodies and Friction

We new describe the motion of rigid bodies undergoing frictional contact; related mathematical terms are listed in Table 1.

Many robots' dynamics can be modeled as a system of rigid bodies experiencing contact at up to m pairs of points (for a thorough introduction, see Stewart (2000) and Brogliato (1999)); each pair is referred to as *a contact*. The state

$$\boldsymbol{x}(t) = \begin{bmatrix} \boldsymbol{q}(t) \\ \boldsymbol{v}(t) \end{bmatrix}, \tag{10}$$

of such a system can be represented by a configuration $\boldsymbol{q}(t) \in \mathbb{R}^{n_q}$ and velocity $\boldsymbol{v}(t) \in \mathbb{R}^{n_v}$. Though $\boldsymbol{v} = \frac{\mathrm{d}\boldsymbol{q}}{\mathrm{d}t}$ for some systems, others (e.g. those representing rotations with angular velocities and quaternions) obey the more general

$$\mathrm{d}\boldsymbol{q} = \boldsymbol{\Gamma}(\boldsymbol{q})\boldsymbol{v}\mathrm{d}t, \tag{11}$$

for some smooth, bounded, full-rank $\boldsymbol{\Gamma}(\boldsymbol{q})$.

The geometry of the contacts is represented by a Lipschitz continuous and continuously differentiable *signed-distance* function $\boldsymbol{\phi}(\boldsymbol{q}) \in \mathbb{R}^m$ for which the ith component is positive when the ith contact is inactive; zero if it is active; and negative if there is interpenetration. Impactless evolution of the system is governed by the *manipulator equations*

$$\boldsymbol{M}(\boldsymbol{q})\mathrm{d}\boldsymbol{v} = \left(\begin{bmatrix} \boldsymbol{J}_n(\boldsymbol{q}) \\ \boldsymbol{J}_t(\boldsymbol{q}) \end{bmatrix}^T \begin{bmatrix} \boldsymbol{\lambda}_n \\ \boldsymbol{\lambda}_t \end{bmatrix} + \boldsymbol{u} - \boldsymbol{C}(\boldsymbol{x}) - \boldsymbol{G}(\boldsymbol{q})\right)\mathrm{d}t. \tag{12}$$

Here, the continuous function $\boldsymbol{M}(\boldsymbol{q}) \succ 0$ is the generalized inertial matrix, and the kinetic energy $K(\boldsymbol{q}, \boldsymbol{v})$ of the system can be calculated as

$$K(\boldsymbol{q}, \boldsymbol{v}) = \frac{1}{2}\|\boldsymbol{v}\|^2_{\boldsymbol{M}(\boldsymbol{q})} = \frac{1}{2}\boldsymbol{v}^T\boldsymbol{M}(\boldsymbol{q})\boldsymbol{v}. \tag{13}$$

By assumption there exist $c_1, c_2 > 0$ such that $c_1\boldsymbol{I} \succeq \boldsymbol{M} \succeq c_2\boldsymbol{I}$ (thus $\boldsymbol{M}$ and $\boldsymbol{M}^{-1}$ are bounded over configuration

Table 1. Dynamics terms for rigid bodies undergoing frictional contact. When clear, some terms may be written with the dependence on their inputs suppressed.

Term	Meaning
n_q	number of configuration variables
n_v	number of generalized velocities
m	number of contacts
t	time
$\boldsymbol{q}$	robot/environment configuration
$\boldsymbol{v}$	robot/environment velocity
$\boldsymbol{x}$	robot/environment state (10)
$\bar{\boldsymbol{x}}$	robot/environment time-augmented state (63)
$\boldsymbol{u}$	robot/environment input forces
$\boldsymbol{\Gamma}(\boldsymbol{q})$	generalized velocity jacobian (11)
$\boldsymbol{M}(\boldsymbol{q})$	generalized mass-inertia matrix
$\boldsymbol{C}(\boldsymbol{x})$	Coriolis and centrifugal effects
$\boldsymbol{G}(\boldsymbol{q})$	conservative (potential) forces
$K(\boldsymbol{q},\boldsymbol{v})$	total kinetic energy (13)
$U(\boldsymbol{q})$	total potential energy (14)
$\boldsymbol{J}_n(\boldsymbol{q})$	normal velocity Jacobian
$\boldsymbol{J}_t(\boldsymbol{q})$	tangential velocity Jacobian
$\boldsymbol{J}(\boldsymbol{q})$	full contact velocity Jacobian (26)
$\boldsymbol{\lambda}_n$	normal forces vector
$\boldsymbol{\lambda}_t$	frictional contact forces vector
$\boldsymbol{\lambda}$	full contact forces vector (27)
$\boldsymbol{\mu}_i$	ith contact Coulomb friction coefficient
$\mathrm{FC}\left(\boldsymbol{q},\boldsymbol{v}\right)$	Coulomb friction cone at state $[\boldsymbol{q};\ \boldsymbol{v}]$ (22)
$\boldsymbol{J}_D$	linearized tangential velocity Jacobian (40)
$\boldsymbol{\lambda}_D$	linearized friction forces vector (39)
$\bar{\boldsymbol{J}}$	linearized velocity Jacobian (40)
$\bar{\boldsymbol{\lambda}}$	linearized contact forces vector (39)
$\mathrm{LFC}\left(\boldsymbol{q},\boldsymbol{v}\right)$	linear friction cone at state $[\boldsymbol{q};\ \boldsymbol{v}]$ (41)
$\mathcal{C}$	set of all contacts
$C_A(\boldsymbol{q})$	set of active (touching) contacts at $\boldsymbol{q}$ (24)
$C_P(\boldsymbol{q})$	set of interpenetrating contacts at $\boldsymbol{q}$ (25)
$\mathcal{Q}_A$	set of active-contact configurations
$\mathcal{Q}_P$	set of penetrating-contact configurations
$\mathcal{X}_A$	set of active-contact states
$\mathcal{X}_P$	set of penetrating-contact states
$\mathcal{I}(\boldsymbol{q})$	set of impact-causing velocities at $\boldsymbol{q}$ (28)
$\mathcal{S}(\boldsymbol{q})$	set of separating velocities at $\boldsymbol{q}$ (29)

space). The continuous function $\boldsymbol{C}(\boldsymbol{x})$ encompasses Coriolis and centrifugal effects and grows at most quadratically in $\boldsymbol{x}$. $\boldsymbol{G}(\boldsymbol{q})$ are conservative forces, related to the system's potential energy $U(\boldsymbol{q})$ as

$$\boldsymbol{G}(\boldsymbol{q}) = \boldsymbol{\Gamma}(\boldsymbol{q})^T \frac{\partial U}{\partial \boldsymbol{q}}^T . \tag{14}$$

$\boldsymbol{u}$ are external inputs, modeled as generalized forces (i.e. motor torques). $\boldsymbol{J}_n = \frac{\partial \boldsymbol{\phi}}{\partial \boldsymbol{q}}\boldsymbol{\Gamma} \in \mathbb{R}^{m \times n_v}$ projects $\boldsymbol{v}$ onto the contact normals, and thus $\boldsymbol{J}_n^T$ maps contact-frame normal forces $\boldsymbol{\lambda}_n(t) \in \mathbb{R}^m$ to corresponding generalized forces. To prevent degenerate behaviors, we assume that for all active contacts, there exists a generalized velocity for which the contact is separating:

Assumption 12. $\forall i,\ \boldsymbol{\phi}_i(\boldsymbol{q}) = 0 \implies \boldsymbol{J}_{n,i}(\boldsymbol{q}) \neq \boldsymbol{0}$.

$\boldsymbol{J}_t \in \mathbb{R}^{2m \times n_v}$ similarly maps between generalized velocities/forces and contact tangential velocities/friction forces $\boldsymbol{\lambda}_t(t) \in \mathbb{R}^{2m}$. For $i \in 1,\dots,m$, we associate the submatrices corresponding to the ith contact as $\boldsymbol{J}_{n,i}$ and $\boldsymbol{J}_{t,i}$, respectively. $\boldsymbol{J}_n$ is bounded and continuous by the properties of $\boldsymbol{\phi}$ and $\boldsymbol{\Gamma}$, while $\boldsymbol{J}_t$ has the same properties by assumption. These properties can be guaranteed, for instance, by the assumption that bodies' boundaries can be defined as piecewise-smooth with bounded curvature. A work-energy relationship dictates that the time evolution of the total kinetic energy in the system is governed by

$$\mathrm{d}K = \boldsymbol{v}^T \left(\boldsymbol{u} + \boldsymbol{J}_t^T \boldsymbol{\lambda}_t - \boldsymbol{G}\right) \mathrm{d}t\,, \tag{15}$$

because neither normal forces nor Coriolis forces do work on the system.

The contact forces $[\boldsymbol{\lambda}_n; \boldsymbol{\lambda}_t]$ must lie within the Coulomb friction cone; that is, for each contact $i \in \{1,\dots,m\}$,

$$\boldsymbol{\lambda}_{n,i}\boldsymbol{\phi}_i(\boldsymbol{q}) \leq 0\,, \tag{16}$$

$$\boldsymbol{\lambda}_{n,i}\boldsymbol{J}_{n,i}\boldsymbol{v} \leq 0\,, \tag{17}$$

$$\boldsymbol{\lambda}_{n,i} \geq 0\,, \tag{18}$$

$$\boldsymbol{\lambda}_{t,i} \in -\boldsymbol{\mu}_i\boldsymbol{\lambda}_{n,i}\mathrm{Unit}\left(\boldsymbol{J}_{t,i}\boldsymbol{v}\right)\,, \tag{19}$$

where $\boldsymbol{\mu}_i > 0$ is the friction coefficient for the ith contact. (16) and (17) restrict normal forces contacts which are active ($\boldsymbol{\phi}_i \leq 0$) and non-separating ($\boldsymbol{J}_{n,i}\boldsymbol{v} \leq 0$). (18) requires that normal forces push bodies apart. (19) is a *maximum dissipation* constraint, capturing the solution set of an optimization problem which maximizes the mechanical power lost due to friction:

$$\min_{\boldsymbol{\lambda}_{t,i}} \quad (\boldsymbol{\lambda}_{t,i}) \cdot (\boldsymbol{J}_{t,i}\boldsymbol{v})\,, \tag{20}$$

$$\text{s.t.} \quad \boldsymbol{\lambda}_{t,i} \in \mathrm{cl}(\mathrm{Ball}(\boldsymbol{\mu}_i\boldsymbol{\lambda}_{n,i}))\,. \tag{21}$$

We denote the set of Coulomb contact forces as

$$\mathrm{FC}\left(\boldsymbol{q},\boldsymbol{v}\right) = \left\{\boldsymbol{\lambda} : \forall i,\ (16)\text{–}(19)\text{ hold}\right\}\,. \tag{22}$$

We note in particular that, since $\mathrm{Unit}(\boldsymbol{v}) \subseteq \mathrm{Unit}(\boldsymbol{0})$,

$$\mathrm{FC}\left(\boldsymbol{q},\boldsymbol{v}\right) \subseteq \mathrm{FC}\left(\boldsymbol{q},\boldsymbol{0}\right)\,, \tag{23}$$

for any $\boldsymbol{q},\boldsymbol{v}$. Let $\mathcal{C} = \{1,\dots,m\}$ be understood as the collection of contacts. For an individual configuration $\boldsymbol{q}$, we denote the set of contacts that are active as

$$C_A(\boldsymbol{q}) = \left\{i \in 1,\dots,m : \boldsymbol{\phi}_i(\boldsymbol{q}) \leq 0\right\}\,, \tag{24}$$

and the set of interpenetrating contacts as

$$C_P(\boldsymbol{q}) = \left\{i \in 1,\dots,m : \boldsymbol{\phi}_i(\boldsymbol{q}) < 0\right\}\,. \tag{25}$$

We note that because $\boldsymbol{\phi}$ is continuous, $C_A(\boldsymbol{q})$ and $\mathcal{C} \setminus C_P(\boldsymbol{q})$ are u.s.c. in $\boldsymbol{q}$. From these functions we also define $\mathcal{Q}_A = \{\boldsymbol{q} : C_A(\boldsymbol{q}) \neq \emptyset\}$, the set of configurations with active contact, and $\mathcal{Q}_P = \{\boldsymbol{q} : C_P(\boldsymbol{q}) \neq \emptyset\}$, the set of interpenetrating configurations. Finally, we define the following for notational convenience:

$$\boldsymbol{J} = \begin{bmatrix}\boldsymbol{J}_n \\ \boldsymbol{J}_t\end{bmatrix}, \qquad \boldsymbol{J}_i = \begin{bmatrix}\boldsymbol{J}_{n,i} \\ \boldsymbol{J}_{t,i}\end{bmatrix}, \tag{26}$$

$$\boldsymbol{\lambda} = \begin{bmatrix}\boldsymbol{\lambda}_n \\ \boldsymbol{\lambda}_t\end{bmatrix}, \qquad \boldsymbol{\lambda}_i = \begin{bmatrix}\boldsymbol{\lambda}_{n,i} \\ \boldsymbol{\lambda}_{t,i}\end{bmatrix}, \tag{27}$$

$$\mathcal{I}(\boldsymbol{q}) = \left\{\boldsymbol{v} \in \mathbb{R}^{n_v} : \exists i \in C_A(\boldsymbol{q}),\ \boldsymbol{J}_{n,i}\boldsymbol{v} < 0\right\}, \tag{28}$$

$$\mathcal{S}(\boldsymbol{q}) = \left\{\boldsymbol{v} \in \mathbb{R}^{n_v} : \forall i \in C_A(\boldsymbol{q}),\ \boldsymbol{J}_{n,i}\boldsymbol{v} > 0\right\}. \tag{29}$$

For a given configuration, $\mathcal{I}(\boldsymbol{q})$ is the set of *impacting* velocities, for which an active contact is moving towards penetration and thus causes an impact. $\mathcal{S}(\boldsymbol{q})$ likewise is the set of *separating* velocities, where no impact can occur as all contacting surfaces are moving away from each other. While $\mathcal{I}(\boldsymbol{q})$ and $\mathcal{S}(\boldsymbol{q})$ are disjoint, there may be some velocities in *neither* set; these situations may require impacts, as in Painlevé's Paradox (Stewart 2000). By Assumption 12, when $\boldsymbol{q}$ is non-penetrating, $\mathcal{S}(\boldsymbol{q}) = \text{int}\left(\mathcal{I}(\boldsymbol{q})^c\right)$ and $\mathcal{I}(\boldsymbol{q}) = \text{int}\left(\mathcal{S}(\boldsymbol{q})^c\right)$.

2.6 Discrete-time Simulation

When generating solutions to the continuous dynamics (12), it is important to note the interplay between the dynamics, non-penetration constraints, and friction cone. Common ODE integration schemes are an incomplete approach to discrete time simulation, as arbitrarily selecting contact forces from the friction cone can cause penetration over a time-step. Many approaches (e.g. Halm and Posa (2018); Anitescu and Potra (1997)) resolve this issue with a constrained semi-implicit Euler scheme. Given a state $\boldsymbol{x} = [\boldsymbol{q}; \boldsymbol{v}]$, input $\boldsymbol{u}$, the state $[\boldsymbol{q}^+; \boldsymbol{v}^+] = [\boldsymbol{q} + \Delta\boldsymbol{q}; \boldsymbol{v} + \Delta\boldsymbol{v}]$ after a time-step of duration Δt is calculated as

$$\Delta\boldsymbol{q} = \Gamma(\boldsymbol{q})\boldsymbol{v}\Delta t\,, \tag{30}$$

$$\boldsymbol{M}(\boldsymbol{q}^+)\Delta\boldsymbol{v} = \left(\boldsymbol{J}(\boldsymbol{q}^+)^T\boldsymbol{\lambda} + \boldsymbol{u} - \boldsymbol{C}(\boldsymbol{x}) - \boldsymbol{G}(\boldsymbol{q})\right)\Delta t\,, \tag{31}$$

where $\boldsymbol{\lambda}\Delta t$ is the total contact impulse over the time step. What remains is to determine a value for $\boldsymbol{\lambda}$ that corresponds to physically reasonable motion.

2.6.1 Continuous Forces Anitescu and Potra (1997) select continuous forces for sustained contact via a natural first-order approximation to the friction cone constraint: only contacts that are already active (i.e. active at $\boldsymbol{q}$) are allowed to exert force; forces must prevent penetrating velocities at these contacts; and the forces must lie in the friction cone at $\boldsymbol{v}^+$:

$$\text{find} \quad \boldsymbol{\lambda}\,, \tag{32}$$

$$\forall i \in C_A(\boldsymbol{q}),\ \boldsymbol{J}_{n,i}(\boldsymbol{q}^+)\boldsymbol{v}^+ \geq \boldsymbol{0}\,, \tag{33}$$

$$\boldsymbol{\lambda} \in \text{FC}(\boldsymbol{q}^+, \boldsymbol{v}^+)\,. \tag{34}$$

Stewart and Trinkle (1996) and Anitescu and Potra (1997) both approximate the maximal dissipation constraint (19) embedded in this problem into an LCP. Given a set of unit vectors $\boldsymbol{d}_1, \ldots, \boldsymbol{d}_k$, the cone constraint in the maximum dissipation formulation (21) is approximated by the polygonal constraint

$$\boldsymbol{\lambda}_{t,i} \in \boldsymbol{\mu}_i\boldsymbol{\lambda}_{n,i}\text{co}\left(\{\boldsymbol{d}_1, \ldots \boldsymbol{d}_k\}\right)\,. \tag{35}$$

Via the definition of convex hull, by packing these vectors into the matrix $\boldsymbol{D} = [\boldsymbol{d}_1, \ldots, \boldsymbol{d}_k]$, we can equivalently search for a coefficient vector $\boldsymbol{\lambda}_{D,i}$, that solves

$$\begin{aligned} \min_{\boldsymbol{\lambda}_{D,i}} \quad & \boldsymbol{\lambda}_{D,i}^T\boldsymbol{D}^T\boldsymbol{J}_{t,i}(\boldsymbol{q}^+)\boldsymbol{v}^+\,, \\ \text{s.t.} \quad & \boldsymbol{\lambda}_{D,i} \geq \boldsymbol{0}\,, \\ & \|\boldsymbol{\lambda}_{D,i}\|_1 \leq \boldsymbol{\mu}_i\boldsymbol{\lambda}_{n,i}\,, \end{aligned} \tag{36}$$

and then reconstruct $\boldsymbol{\lambda}_{t,i} = \boldsymbol{D}\boldsymbol{\lambda}_{D,i}$. The solution set to this problem can be represented explicitly with a slack variable $\boldsymbol{\gamma}_i$ as the complementarity constraints

$$\boldsymbol{0} \leq \boldsymbol{\lambda}_{D,i} \quad \perp \quad \boldsymbol{J}_{D,i}(\boldsymbol{q}^+)\boldsymbol{v}^+ + \boldsymbol{1}\gamma_i \geq \boldsymbol{0}\,, \tag{37}$$

$$0 \leq \gamma_i \quad \perp \quad \boldsymbol{\mu}_i\boldsymbol{\lambda}_{n,i} - \boldsymbol{1}^T\boldsymbol{\lambda}_{D,i} \geq 0\,, \tag{38}$$

where $\boldsymbol{J}_{D,i} = \boldsymbol{D}^T\boldsymbol{J}_{t,i}$. For convenience, we define the lumped terms

$$\boldsymbol{\lambda}_D = \begin{bmatrix} \boldsymbol{\lambda}_{D,1} \\ \vdots \\ \boldsymbol{\lambda}_{D,m} \end{bmatrix}, \qquad \bar{\boldsymbol{\lambda}} = \begin{bmatrix} \boldsymbol{\lambda}_n \\ \boldsymbol{\lambda}_D \end{bmatrix}, \tag{39}$$

$$\boldsymbol{J}_D = \begin{bmatrix} \boldsymbol{J}_{D,1} \\ \vdots \\ \boldsymbol{J}_{D,m} \end{bmatrix}, \qquad \bar{\boldsymbol{J}} = \begin{bmatrix} \boldsymbol{J}_n \\ \boldsymbol{J}_D \end{bmatrix}. \tag{40}$$

Accordingly, we say that the contact forces $\bar{\boldsymbol{\lambda}}$ are contained in the *linear* friction cone if they comply with (16)–(18) and a $\boldsymbol{\gamma}$ exists such that (37)–(38) are satisfied:

$$\text{LFC}\left(\boldsymbol{q}, \boldsymbol{v}^+\right) = \left\{\bar{\boldsymbol{\lambda}} : \exists\gamma, \forall i,\ \text{(16)–(18), (37)–(38) hold}\right\}\,. \tag{41}$$

In particular, we note that when $\boldsymbol{v}^+ = \boldsymbol{0}$, any frictional force is maximally dissipating (as the objective of (36) is identically 0). Furthermore, we note that linearized cone is an inner approximation of the true Coulomb friction cone constraint $\|\boldsymbol{\lambda}_{t,i}\|_2 \leq \boldsymbol{\mu}_i\boldsymbol{\lambda}_{n,i}$, and therefore

$$\text{LFC}\left(\boldsymbol{q}, \boldsymbol{v}^+\right) \subseteq \text{LFC}\left(\boldsymbol{q}, \boldsymbol{0}\right)\,, \tag{42}$$

$$\bar{\boldsymbol{J}}^T\text{LFC}\left(\boldsymbol{q}, \boldsymbol{0}\right) \subseteq \boldsymbol{J}^T\text{FC}\left(\boldsymbol{q}, \boldsymbol{0}\right)\,. \tag{43}$$

More details on the linear friction cone and its embedding into LCP-based simulation can be found in Stewart and Trinkle (1996).

2.6.2 Event-based Simulation through Impact The above process is incomplete for simulating a system through time, as it assumes that no new contacts activate *within* a time-step. There are multiple resolutions to this issue, but we will focus on *event-based* formulations, which attempt to determine the sub-time-step instant t_{imp} at which a new contact is activated and resolve an instantaneous impact then via a subroutine $\text{ImpactLaw}(\boldsymbol{q}, \boldsymbol{v})$, if necessary. Anitescu and Potra (1997) present pseudocode for such an implementation, which is reproduced in our notation in Algorithm 1.

There are many choices for ImpactLaw (e.g. Anitescu and Potra (1997); Bhatt and Koechling (1995); Chatterjee and Ruina (1998); Seghete and Murphey (2014); Routh (1891); Drumwright and Shell (2010); Stronge (1990) and others), each with its own limitation. In this work, we will develop a tractable LCP-based simulation scheme that can be used to generate a suitable, individual output for ImpactLaw, as well to approximate the set of all such outputs for a given pre-impact state.

2.7 Resolving Inelastic Impacts

We focus on inelastic impulsive impacts, during which velocities change instantaneously and configurations remain

Algorithm 1: Event-Based Rigid Body Simulation

Input: Time-step h, initial state $\boldsymbol{x}_0$, input callback $\boldsymbol{u}(\boldsymbol{x}, t)$

Output: Final state $\boldsymbol{x}$

$t \leftarrow 0$;
$\boldsymbol{x} \leftarrow \boldsymbol{x}_0$;
$\boldsymbol{u} \leftarrow \boldsymbol{u}(\boldsymbol{x}, t)$;
while $t < T$ **do**
    $\Delta t \leftarrow \min(h, T - t)$;
    Calculate $\boldsymbol{\lambda}, \boldsymbol{q}^+, \boldsymbol{v}^+$ via (30)–(34);
    if a new contact is penetrating at $\boldsymbol{q}^+$ **then**
        Estimate t_{imp}, moment at which first new contact activates;
        $\Delta t \leftarrow t_{imp} - t$;
        Calculate $\boldsymbol{\lambda}, \boldsymbol{q}^+, \boldsymbol{v}^+$ via (30)–(34);
        $\boldsymbol{v}^+ \leftarrow \mathrm{ImpactLaw}(\boldsymbol{q}^+, \boldsymbol{v}^+)$;
    end
    $t \leftarrow t + \Delta t$;
    $\boldsymbol{x} \leftarrow [\boldsymbol{q}^+; \boldsymbol{v}^+]$;
    $\boldsymbol{u} \leftarrow \boldsymbol{u}(\boldsymbol{x}, t)$;
end

constant. Denoting $\boldsymbol{\Lambda} = \boldsymbol{\lambda}\Delta t$ and taking the limit of the discrete-time dynamics (31) as $\Delta t \to 0$ requires the pre- and post-impact velocities $\boldsymbol{v}$ and $\boldsymbol{v}^+$ to obey

$$\boldsymbol{v}^+(\boldsymbol{\Lambda}) = \boldsymbol{v} + \boldsymbol{M}(\boldsymbol{q})^{-1}\boldsymbol{J}(\boldsymbol{q})^T\boldsymbol{\Lambda}\,. \tag{44}$$

Models often select $\boldsymbol{\Lambda}$ via an impulsive analog to Coulomb's friction law (e.g. Routh (1891); Anitescu and Potra (1997)). We will later combine and generalize ideas from two categories of these laws: algebraic and differential (Chatterjee 1997).

2.7.1 Algebraic impact resolution Several methods (e.g. Anitescu and Potra (1997); Hurmuzlu and Marghitu (1994); Glocker and Pfeiffer (1995)) calculate $\boldsymbol{\Lambda}$ as the solution to a system of algebraic equations. In some of these models, all impacts are resolved simultaneously. For instance, Glocker and Pfeiffer (1995) and Anitescu and Potra (1997) solve for an impulse $\boldsymbol{\Lambda}$ which both prevents penetration and satisfies the (linear) Coulomb friction cone constraint only at the *end* of them impact; this is equivalent to the continuous time evolution (30)–(34) for $\Delta t = 0$. We particularly note that a velocity-based complementarity condition is enforced by this approach:

$$\boldsymbol{0} \leq \boldsymbol{\Lambda}_{n,i} \perp \boldsymbol{J}_{n,i}\boldsymbol{v}^+(\boldsymbol{\Lambda}) \geq \boldsymbol{0}, \forall i \in C_A(\boldsymbol{q})\,. \tag{45}$$

This behavior is often violated in real systems (Chatterjee 1999); for the system in Figure 1, this formulation can only generate the symmetric result. An alternative approach observed in several algebraic models (e.g. Ivanov (1995); Smith et al. (2012); Seghete and Murphey (2014)) is to consider multi-impact as a finite sequence of individual impacts; to summarize this technique,

1. Pick a single active contact $i \in C_A(\boldsymbol{q})$.
2. Generate an impulse $\boldsymbol{\Lambda}_i$, by resolving a single impact at contact i, ignoring all other contacts.
3. Increment $\boldsymbol{v} \leftarrow \boldsymbol{v} + \boldsymbol{M}^{-1}\boldsymbol{J}_i^T\boldsymbol{\Lambda}_i$.
4. Terminate and take $\boldsymbol{v}^+ = \boldsymbol{v}$ if it is non-impacting ($\boldsymbol{v} \notin \mathcal{I}(\boldsymbol{q})$); otherwise, return to 1.

Various methods differ in their choice of contact ordering as will as single-impact resolution methodology; furthermore, some methods are only able to guarantee that the process terminates under significant assumptions, e.g. two or less contacts (Seghete and Murphey 2014). We will compare our method to sequences of single impacts resolved using the method of Anitescu and Potra (1997).

2.7.2 Differential impact resolution As opposed to algebraic approaches, differential approaches consider continuous evolution of velocity from pre- to post-impact velocity, in which the total derivative satisfies a friction law in some form. We will now describe one of the oldest differential models for a single impact (Routh 1891), which we will later extend to the multi-contact case. For a single contact $C_A(\boldsymbol{q}) = \{i\}$, Routh (1891) proposed a method which satisfies Coulomb friction differentially. To summarize this technique,

1. Increase the normal impulse $\boldsymbol{\Lambda}_{n,i}$ with slope $\boldsymbol{\lambda}_i = 1$.
2. Increment the tangential impulse with slope $\boldsymbol{\lambda}_{t,i}$, satisfying to Coulomb friction, identical to (19) for the mid-impact velocity $\bar{\boldsymbol{v}} = \boldsymbol{v} + \boldsymbol{M}^{-1}\boldsymbol{J}_i^T\boldsymbol{\Lambda}_i$, the velocity after net impulse $\boldsymbol{\Lambda}_i$.
3. Terminate when the normal contact velocity vanishes* (i.e. $\boldsymbol{J}_{n,i}\bar{\boldsymbol{v}} = 0$) and take $\boldsymbol{v}^+ = \bar{\boldsymbol{v}}$.

As observed in Posa et al. (2016), this process is equivalent to a u.s.c. differential inclusion:

$$\dot{\boldsymbol{v}} \in F_{\boldsymbol{q},i}(\boldsymbol{v})\,, \tag{46}$$

where $F_{\boldsymbol{q},i}(\boldsymbol{v})$ is equal to the net increment in velocity due to the "force" applied in steps 1) and 2) of Routh's method:

$$F_{\boldsymbol{q},i}(\boldsymbol{v}) = \boldsymbol{M}^{-1}\left(\boldsymbol{J}_{n,i}^T - \boldsymbol{\mu}\boldsymbol{J}_{t,i}^T\mathrm{Unit}\left(\boldsymbol{J}_{t,i}\boldsymbol{v}\right)\right)\,. \tag{47}$$

For any $\dot{\boldsymbol{v}} \in F_{\boldsymbol{q},i}(\boldsymbol{v})$, we can associate a set of forces $\boldsymbol{\lambda}_i$ such that

$$\dot{\boldsymbol{v}} = \boldsymbol{M}^{-1}\boldsymbol{J}_i^T\boldsymbol{\lambda}_i\,, \tag{48}$$
$$\boldsymbol{\lambda}_{n,i} = 1\,, \tag{49}$$
$$\boldsymbol{\lambda}_i \in \mathrm{FC}(\boldsymbol{q}, \boldsymbol{v})\,. \tag{50}$$

Note that for a frictionless contact ($\boldsymbol{\mu} = 0$), this simplifies to

$$F_{\boldsymbol{q},i}(\boldsymbol{v}) = \left\{\boldsymbol{M}^{-1}\boldsymbol{J}_{n,i}^T\right\}\,. \tag{51}$$

A diagram depicting the resolution of a planar impact with this method is shown in Figure 3. Solutions may transition between sliding and sticking, and the direction of slip may even reverse as a result of each impact. While the path is piecewise linear in the planar case, this is not true in three dimensions. We additionally note that due to the definition of $F_{\boldsymbol{q},i}$, (46) would predict "forces" even when $\boldsymbol{v}$ is a separating velocity (i.e. $\boldsymbol{v} \in \mathcal{S}(\boldsymbol{q})$). However, Routh's method is intended to be used for velocity trajectories that

*To permit resolutions to Painlevé's Paradox, terminate only when consistency no longer requires an instantaneous change in velocity.

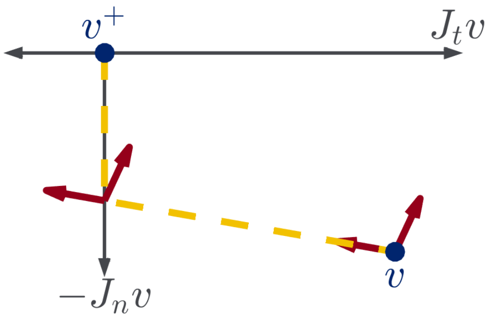

Figure 3. Velocity throughout an impact resolution by Routh's method (image adapted from Posa et al. (2016)). At the initial state, the velocity-projected extreme rays of the friction cone are shown as solid red arrows. The contact begins in a sliding regime. When $\boldsymbol{v}$, shown in the yellow dotted line, intersects $\boldsymbol{J}_t\boldsymbol{v} = \mathbf{0}$, the contact transitions to sticking and the impact terminates when $\boldsymbol{J}_n\boldsymbol{v} = \mathbf{0}$.

start in $\mathcal{I}(\boldsymbol{q})$ only until the first moment that a feasible post-impact velocity is achieved (i.e. $\boldsymbol{v} \notin \mathcal{I}(\boldsymbol{q})$), and therefore this non-physical behavior will never be encountered under the intended use of the system.

From this point forward, we will take s to be the variable of integration (i.e. "simulation time") during the resolution of an impact event; we note that evolution of s *does not correspond* to evolution of time, but rather measures the accumulation of impact impulse over an *instantaneous* collision. In a slight abuse of notation, we will consider total derivatives such as $\dot{\boldsymbol{v}}(s)$ to be taken with respect to s. We will also denote the impulse (i.e. the integrated force) on a contact i over a sub-interval $[s_1, s_2]$ of an impact resolution as $\boldsymbol{\Lambda}_i(s_1, s_2)$. Implicit in Routh's method is an assumption that the terminal condition in step 3) will eventually be reached by any valid choice of increment on $\boldsymbol{\Lambda}_i$; if it is possible to get "stuck" with $\boldsymbol{J}_{n,i}\boldsymbol{v} < 0$, then Routh's method would be ill-defined and not predict a post impact state. This does not happen in the frictionless case, as $\boldsymbol{J}_{n,i}\boldsymbol{v}$ has constant positive derivative $\boldsymbol{J}_{n,i}\dot{\boldsymbol{v}} = \|\boldsymbol{J}_{n,i}\|^2_{\boldsymbol{M}^{-1}}$. The frictional case requires more careful treatment. Intuitively, the added effect of the frictional impulse will be to dissipate kinetic energy quickly. One may conclude that termination happens eventually as zero velocity is a valid post-impact state:

Lemma 13. *Let $\boldsymbol{q} \notin \mathcal{Q}_P$ be a non-penetrating configuration, and $i \in C_A(\boldsymbol{q})$ be an active contact at $\boldsymbol{q}$. Then there exists $S(\boldsymbol{q}) > 0$ such that for any solution $\boldsymbol{v}(s) \in$ SOL $(F_{\boldsymbol{q},i}, [0, \|\boldsymbol{v}(0)\|_2 S(\boldsymbol{q})])$ of the single frictional contact system defined in (46) and (47), $\boldsymbol{v}(s)$ exits the impact at some $s^* \in [0, \|\boldsymbol{v}(0)\|_2 S(\boldsymbol{q})]$; i.e., $\boldsymbol{J}_{n,i}\boldsymbol{v}(s^*) \geq 0$.*

Proof. See Appendix C.2.

The implication of Lemma 13 is that *a priori*, one can determine an $S > 0$ proportional to the pre-impact speed $\|\boldsymbol{v}\|_2$ such that any solution to the DI (46) on $[0, S]$ can be used to construct the post-impact velocity $\boldsymbol{v}^+$. We will see, however, that the extension of this methodology to multiple concurrent impacts is non-trivial, and that physical systems associated with these models often exhibit a high degree of indeterminacy.

3 Simultaneous Impact Model

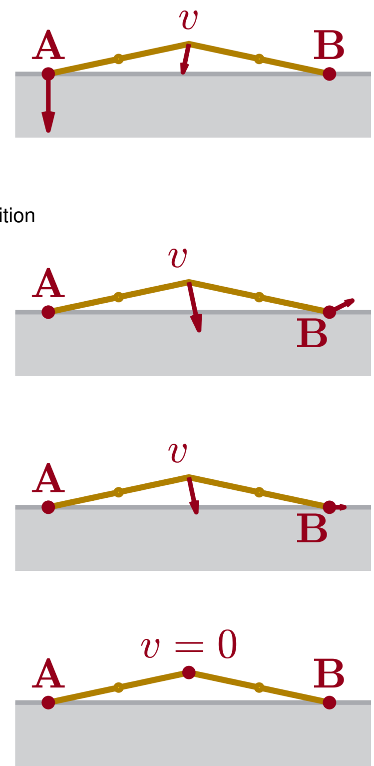

(a) Initial condition

(b) Simultaneous algebraic impacts

Figure 4. (a) A compass gait walker, consisting of two legs attached with a hinge joint at the hip, takes a step with hip velocity v and excites non-uniqueness in the model of Anitescu and Potra (1997). (b) A single impact at that the leading foot (point A) can cause the trailing foot (point B) to lift off the ground. Alternatively, impacts at both feet can cause the trailing foot to slide or come to rest.

We have seen in Figure 1 that two contacts impacting simultaneously can excite significant disagreement between models derived from seemingly similar principles. It is worth noting that making two points coming into contact at *exactly* the same is difficult in real life, and a measure-zero event in analytical models. However, when multiple bodies are in sustained contact, even a single impact is enough to generate non-uniqueness. In this section, we first offer two such common robotics examples—one related to legged locomotion and the other to manipulation—and show that simultaneous or sequenced impacts exhibit meaningful uncertainty; further details can be found in Appendix B. We then describe the principles, construction, and properties of our extension of Routh's method to arbitrarily-ordered multiple impacts.

3.1 Motivating Examples

One of the simplest models of bipedal walking is the compass gait walker, which consists of two rods (legs) connected with a revolute joint at the hip. A fundamental behavior of bipedal walking is to step with a leading foot while a trailing foot rests on the ground, as shown in Figure 4. As observed by Remy (2017), if a very wide step

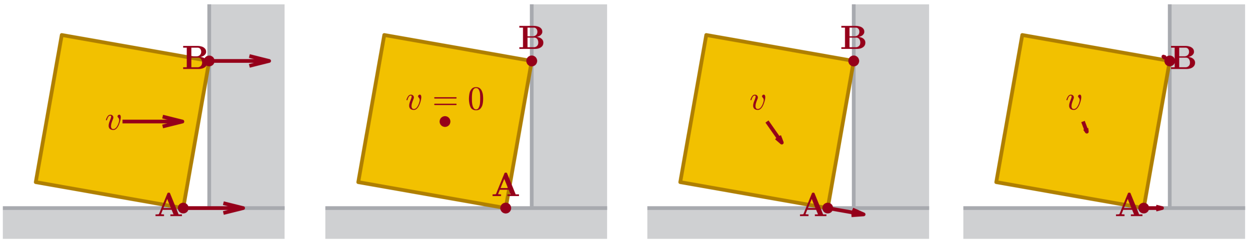

(a) Initial condition **(b)** Simultaneous algebraic impact **(c)** B-then-A sequential algebraic impact

Figure 5. Two subtly different solutions for a box sliding into a wall with velocity v (a) are shown. (b) When a simultaneous impact is generated via Anitescu and Potra (1997), the box comes to rest. (c) When point B has an individual impact before point A, a different outcome results; point A continues sliding, while point B lifts off the wall.

(156° between the legs) is taken by the model, then the simultaneous method of Anitescu and Potra (1997) results in three categorically different solutions. In one case, there is only an impact at the leading foot, and the trailing foot lifts of the ground. In two others, impacts at both feet can result in the trailing foot sliding or coming to rest.

In the second example, motivated by non-prehensile pushing of an object, we consider a box which slides on one corner on a floor before impacting a wall (Figure 5). If a single impact occurs between the box and the wall, it will trigger a second impact against the floor. Due to the position of the center of mass of the box, both impacts add counter-clockwise rotational momentum to the box, causing the contact with the wall to lift off. Alternatively, if both of these impacts are resolved simultaneously, the box will come to rest under sufficient friction.

3.2 Impact Model Construction

As post-impact velocity is sensitive to the ordering of individual impact resolutions, a model that captures all reasonable post-impact velocities is a useful tool for formal analysis of such behaviors. We will construct such a model by using as relaxed notion of impact resolutions as possible. A similar model, without theoretical results or a detailed understanding, was proposed by Posa et al. (2016) where it proved useful for stability analysis of robots undergoing simultaneous impact. We consider a formulation in which at any given instant during the resolution process, the impacts are allowed to concurrently resolve at *any* relative rate:

1. Monotonically increase the normal impulse on each non-separating contact i at rate $\boldsymbol{\lambda}_{n,i} \geq 0$ such that

$$\boldsymbol{\lambda}_{n,i} = 0, \forall i \notin C_A(\boldsymbol{q})\,, \tag{52}$$

$$\sum_i \boldsymbol{\lambda}_{n,i} = \|\boldsymbol{\lambda}_n\|_1 = 1\,. \tag{53}$$

2. Increment the tangential impulse for each contact at rate $\boldsymbol{\lambda}_{t,i}$ such that $\boldsymbol{\lambda} \in \mathrm{FC}(\boldsymbol{q}, \boldsymbol{v})$.
3. Terminate when $\boldsymbol{v} \notin \mathcal{I}(\boldsymbol{q})$.

We can understand the constraint (53) on $\boldsymbol{\lambda}$ as choosing a net force that comes from a convex combination of the forces that Routh's method might select for any of the individual contacts $i \in C_A(\boldsymbol{q})$. As in the single contact case, we might instead think of the selection of a $\boldsymbol{\lambda}$ as picking an element of a set of admissible values for $\dot{\boldsymbol{v}}$. As before, we construct a u.s.c. differential inclusion to capture this behavior:

$$\dot{\boldsymbol{v}} \in D_{\boldsymbol{q}}(\boldsymbol{v}) = \mathrm{co}\left(\bigcup_{i \in C_{\boldsymbol{q}}(\boldsymbol{v})} F_{\boldsymbol{q},i}(\boldsymbol{v})\right)\,, \tag{54}$$

$$C_{\boldsymbol{q}}(\boldsymbol{v}) = \begin{cases} \{i \in C_A(\boldsymbol{q}) : \boldsymbol{J}_{n,i}\boldsymbol{v} \leq 0\} & \boldsymbol{v} \in \mathrm{cl}\mathcal{I}(\boldsymbol{q})\,, \\ \arg\min_{i \in C_A(\boldsymbol{q})} \boldsymbol{J}_{n,i}\boldsymbol{v} & \text{otherwise}\,. \end{cases} \tag{55}$$

Similar to the single contact case, the behavior on $\mathrm{int}\left(\mathcal{I}(\boldsymbol{q})^c\right)$ (equivalently $\mathcal{S}(\boldsymbol{q})$ for $\boldsymbol{q} \notin \mathcal{Q}_P$) has been chosen to preserve upper semi-continuity, and is not encountered when resolving impacts. We denote total impulse over an interval $[s_1, s_2]$, $\boldsymbol{\Lambda}\,(s_1, s_2)$, as before. Similar to (50), one can extract $\boldsymbol{\lambda}(s)$ from a solution $\boldsymbol{v}(s)$ contained in $\mathrm{cl}\mathcal{I}(\boldsymbol{q})$ such that

$$\dot{\boldsymbol{v}} = \boldsymbol{M}^{-1}\boldsymbol{J}^T\boldsymbol{\lambda}\,, \tag{56}$$

$$\|\boldsymbol{\lambda}_n\|_1 = 1\,, \tag{57}$$

$$\boldsymbol{\lambda} \in \mathrm{FC}(\boldsymbol{q}, \boldsymbol{v})\,. \tag{58}$$

3.3 Properties

The construction of (54) is similar to that of the single contact system (46); it is furthermore equivalent when C_A is a singleton. We now detail properties of the multi-contact system that are useful for analyzing its solution set.

3.3.1 Existence and Closure For any configuration $\boldsymbol{q} \in \mathcal{Q}_A$, $D_{\boldsymbol{q}}(\boldsymbol{v})$ is non-empty, closed, uniformly bounded, and convex as it is constructed from the convex hull of a closed and non-empty set of bounded vectors. Therefore by Proposition 8, we obtain the following:

Lemma 14. *For all configurations $\boldsymbol{q} \in \mathcal{Q}_A$, velocities $\boldsymbol{v}_0$, and compact intervals $[a, b]$,* $\mathrm{SOL}\left(D_{\boldsymbol{q}}, [a, b]\right)$ *and* $\mathrm{IVP}\left(D_{\boldsymbol{q}}, \boldsymbol{v}_0, [a, b]\right)$ *are non-empty and closed under uniform convergence.*

Proof. See Appendix D.1.

3.3.2 Homogeneity As the set of allowable contact forces are only dependent on the direction of $\boldsymbol{v}$, $D_{\boldsymbol{q}}(\boldsymbol{v})$ is positively homogeneous in $\boldsymbol{v}$. That is to say, $\forall k > 0, \boldsymbol{v} \in \mathbb{R}^{n_v}$, $D_{\boldsymbol{q}}(\boldsymbol{v}) = D_{\boldsymbol{q}}(k\boldsymbol{v})$. Positive homogeneity induces a similar property on the solution set to the differential inclusion:

Lemma 15. Solution Homogeneity. *For all $\boldsymbol{q}$, $k > 0$, and compact intervals $[a, b]$, if $\boldsymbol{v}(s) \in \mathrm{SOL}\left(D_{\boldsymbol{q}}, [a, b]\right)$, $k\boldsymbol{v}(\frac{s}{k}) \in$* $\mathrm{SOL}\left(D_{\boldsymbol{q}}, [ka, kb]\right)$.

Proof. See Appendix D.2.

3.3.3 Energy Dissipation An essential behavior of inelastic impacts is that they dissipate kinetic energy. We now examine the dissipative properties of the model, which function both as a physical realism sanity check and as a device to prove critical theoretical properties. On inspection of (56)-(58), the kinetic energy $K(\boldsymbol{q}, \boldsymbol{v}(s))$ must be non-increasing during impact (i.e. when $\boldsymbol{v}(s) \in \mathrm{cl}\mathcal{I}(\boldsymbol{q})$) as the definition of the friction cone $\mathrm{FC}(\boldsymbol{q}, \boldsymbol{v})$ constraints both normal and frictional forces to be dissipative:

Lemma 16. Dissipation. *Let $\boldsymbol{q} \in \mathcal{Q}_A$, and let $[a, b]$ be a compact interval. If $\boldsymbol{v}(s) \in \mathrm{SOL}\,(D_{\boldsymbol{q}}, [a, b])$ and $\boldsymbol{v}([a, b]) \subseteq \mathrm{cl}\mathcal{I}(\boldsymbol{q})$, then $\|\boldsymbol{v}(s)\|_{\boldsymbol{M}}$ is non-increasing.*

Proof. See Appendix D.3.

K has total derivative

$$\dot{K} = \boldsymbol{v}^T \boldsymbol{J}^T \boldsymbol{\lambda}\,, \tag{59}$$

and furthermore it will strictly decrease unless the velocity is constant:

Theorem 17. *Let $\boldsymbol{q} \in \mathcal{Q}_A$, and let $[a, b]$ be a compact interval. If $\boldsymbol{v}(s) \in \mathrm{SOL}\,(D_{\boldsymbol{q}}, [a, b])$ and $\boldsymbol{v}\,([a, b]) \subseteq \mathrm{cl}\mathcal{I}(\boldsymbol{q})$, $\|\boldsymbol{v}(s)\|_{\boldsymbol{M}}$ constant implies $\boldsymbol{v}(s)$ constant.*

Proof. See Appendix D.4.

One might then wonder if K is strictly decreasing during impact; certainly, this would not be the case if $\boldsymbol{v}(s)$ could stay constant. Therefore, solutions to the differential inclusion must not be permitted to select $\dot{\boldsymbol{v}} = \boldsymbol{0}$, i.e., $\boldsymbol{0} \notin D_{\boldsymbol{q}}(\boldsymbol{v}^*)$ for every $\boldsymbol{v}^* \in \mathrm{cl}\mathcal{I}(\boldsymbol{q})$; we will therefore assume it to hold globally over valid (i.e. non-penetrating) configurations for the remainder of this work:

Assumption 18. $\forall \boldsymbol{q} \in \mathcal{Q}_A \setminus \mathcal{Q}_P$, $\boldsymbol{0} \notin D_{\boldsymbol{q}}(\mathrm{cl}\mathcal{I}(\boldsymbol{q}))$. *As $\boldsymbol{0} \in \mathrm{cl}\mathcal{I}(\boldsymbol{q})$, in particular,*

$$\boldsymbol{\lambda} \in \mathrm{FC}\,(\boldsymbol{q}, \boldsymbol{0}) \wedge \boldsymbol{\lambda}_n \neq \boldsymbol{0} \implies \boldsymbol{J}^T \boldsymbol{\lambda} \neq \boldsymbol{0}\,. \tag{60}$$

Critically, Assumption 18 covers most situations in robotics, including grasping and locomotion, with the notable exception being jamming between immovable surfaces. Furthermore, it guarantees strict dissipation during the impact process:

Theorem 19. Strict Dissipation. *Let $\boldsymbol{q} \in \mathcal{Q}_A \setminus \mathcal{Q}_P$ and $[a, b]$ be a compact interval. If $\boldsymbol{v}(s) \in \mathrm{SOL}\,(D_{\boldsymbol{q}}, [a, b])$ and $\boldsymbol{v}([a, b]) \subseteq \mathrm{cl}\mathcal{I}(\boldsymbol{q})$, $\|\boldsymbol{v}(s)\|_{\boldsymbol{M}}$ is strictly decreasing.*

Proof. Given that $\boldsymbol{v}$ is never constant on $\mathrm{cl}\mathcal{I}(\boldsymbol{q})$ via Assumption 18, $\|\boldsymbol{v}(s)\|_{\boldsymbol{M}}$ is non-constant by Theorem 17 and thus strictly decreasing by Lemma 16:

3.4 Linear Impact Termination

While solutions to the underlying differential inclusion are guaranteed to exist in the simultaneous impact model, we have yet to prove that they terminate the impact process, as in Routh's single-contact method. Termination proofs for other simultaneous impact models (e.g. Anitescu and Potra (1997); Drumwright and Shell (2010); Seghete and Murphey (2014) and others) exist, but these approaches rely on comparatively limited impulsive behaviors, and thus cannot generate the essential non-unique post-impact velocities highlighted in Section 3.1. We now show that our model exhibits what we understand to be the most permissive guaranteed termination behavior:

Proposition 20. Finite Termination. *For any configuration $\boldsymbol{q} \in \mathcal{Q}_A \setminus \mathcal{Q}_P$ and pre-impact velocity $\boldsymbol{v}(0)$, the differential inclusion (54) will resolve the impact by some $S(\boldsymbol{q})$ proportional to $\|\boldsymbol{v}(0)\|_{\boldsymbol{M}}$.*

We will prove this claim as a consequence of kinetic energy decreasing fast enough to force termination—a significant expansion of Theorem 19. Even though K must always decrease, Theorem 19 does not forbid $\frac{\mathrm{d}}{\mathrm{d}s}K \to 0$. In fact, it is not possible to create an instantaneous bound $\frac{\mathrm{d}}{\mathrm{d}s}K \leq -\epsilon < 0$. For example, consider a 2 DoF system with 2 frictionless, axis-aligned contacts such that $\boldsymbol{J}_n = \boldsymbol{I}_2$. For every $\epsilon > 0$, we can pick a velocity an corresponding impulse increment which satisfy $\dot{K} > -2\epsilon$:

$$\boldsymbol{v}_\epsilon = (1 + \epsilon) \begin{bmatrix} -1 \\ -\epsilon \end{bmatrix} \in \mathrm{cl}\mathcal{I}(\boldsymbol{q})\,, \tag{61}$$

$$\dot{\boldsymbol{v}}_\epsilon = \boldsymbol{J}_n^T \begin{bmatrix} \epsilon \\ 1 \end{bmatrix} \frac{1}{1+\epsilon} = \begin{bmatrix} \epsilon \\ 1 \end{bmatrix} \frac{1}{1+\epsilon} \in D_{\boldsymbol{q}}(\boldsymbol{v}_\epsilon)\,, \tag{62}$$

However as we take $\epsilon \to 0$, $\boldsymbol{v}_\epsilon$ converges to a non-impacting velcoity; therefore, $\dot{K}$ only remains small for a short duration before impact termination. It remains possible that the *aggregate energy dissipation* over an interval of fixed nonzero length can be bounded away from zero. We define this quality as $\alpha(s)$-dissipativity:

Definition 21. $\alpha(s)$-dissipativity. *For a positive definite function $\alpha(s) : \mathrm{cl}\mathbb{R}^+ \to [0, 1]$, the system $\dot{\boldsymbol{v}} \in D_{\boldsymbol{q}}(\boldsymbol{v})$ is said to be $\alpha(s)$-**dissipative** if for all $s > 0$, for all $\boldsymbol{v} \in \mathrm{SOL}\,(D_{\boldsymbol{q}}, [0, s])$ s.t. $\boldsymbol{v}\,([0, s]) \subseteq \mathrm{cl}\mathcal{I}(\boldsymbol{q})$, if $\|\boldsymbol{v}(0)\|_{\boldsymbol{M}} = 1$, $\|v(s)\|_{\boldsymbol{M}} \leq 1 - \alpha(s)$.*

Intuitively, if $K > 0$ on $\mathrm{cl}\mathcal{I}(\boldsymbol{q})$ and K decreases at a sufficient rate, any trajectory $\boldsymbol{v}(s)$ of the multi-contact system will exit $\mathrm{cl}\mathcal{I}(\boldsymbol{q})$ in finite time. The particular rate imposed by $\alpha(s)$-dissipativity implies that the exit time can be bounded linearly in $\|\boldsymbol{v}(0)\|_{\boldsymbol{M}}$:

Lemma 22. Aggregate Dissipation. *Let $\boldsymbol{q} \in \mathcal{Q}_A$ and let $\dot{\boldsymbol{v}} \in D_{\boldsymbol{q}}(\boldsymbol{v})$ be $\alpha_{\boldsymbol{q}}(s)$-dissipative. Then if $\boldsymbol{v}(s) \in \mathrm{SOL}\,(D_{\boldsymbol{q}}, [0, S])$ and $\boldsymbol{v}([0, S]) \subseteq \mathrm{cl}\mathcal{I}(\boldsymbol{q})$,*

$$S \leq \inf_{s>0} \frac{s\,\|\boldsymbol{v}(0)\|_{\boldsymbol{M}}}{\alpha_{\boldsymbol{q}}(s)}\,.$$

Proof. See Appendix D.5.

Proposition 20 arises from this behavior: *every $\boldsymbol{q} \in \mathcal{Q}_A \setminus \mathcal{Q}_P$* exhibits $\alpha(s)$-dissipativity. Without $\alpha(s)$-dissipativity, solutions that dissipate arbitrarily little would exist, and by closure of the solution set (Lemma 14), a non-dissipating solution $\boldsymbol{v}(s)$ would exist as well, violating Assumption 18:

Theorem 23. *For every configuration $\boldsymbol{q} \in \mathcal{Q}_A \setminus \mathcal{Q}_P$ there exists an $\alpha_{\boldsymbol{q}}(s)$ such that $\dot{\boldsymbol{v}} \in D_{\boldsymbol{q}}(\boldsymbol{v})$ is $\alpha_{\boldsymbol{q}}(s)$-dissipative.*

Proof. See Appendix D.6.

The u.s.c. structure of $D_{\boldsymbol{q}}$ has the additional useful implication that locally, there exists a *uniform* dissipation rate $\alpha(s)$ that holds regardless of the impact configuration:

Corollary 24. Uniform Dissipation. *For compact $\mathcal{Q} \subseteq \mathcal{Q}_A \setminus \mathcal{Q}_P$, there exists a single $\alpha_{\mathcal{Q}}(s)$ such that $\dot{\boldsymbol{v}} \in D_{\boldsymbol{q}}(\boldsymbol{v})$ is $\alpha_{\mathcal{Q}}(s)$-dissipative for all $\boldsymbol{q} \in \mathcal{Q}$.*

Proof. See Appendix D.7.

4 Continuous-Time Dynamics Model

We now describe how the simultaneous impact system can be embedded seamlessly into a full, continuous time dynamics model. As the impact model relies on integration over a variable other than time, rather than switching between integration spaces, we define time advancement t as a variable in an augmented state $\bar{\boldsymbol{x}}(s)$:

$$\bar{\boldsymbol{x}}(s) = \begin{bmatrix} \boldsymbol{x}(s) \\ t(s) \end{bmatrix} = \begin{bmatrix} \boldsymbol{q}(s) \\ \boldsymbol{v}(s) \\ t(s) \end{bmatrix} \in \mathbb{R}^{n_q+n_v+1} . \tag{63}$$

For any state $\bar{\boldsymbol{x}}(s)$ we can extract the relevant configuration, velocity, and time as by selecting the appropriate indices, e.g. as $\boldsymbol{q}(\bar{\boldsymbol{x}}(s))$. For notational compactness, whenever clear, we will write this construction in the shortened form $\boldsymbol{q}(s)$. We will also frequently make use of the sets

$$\bar{\mathcal{X}}_A = \{\bar{\boldsymbol{x}} : \boldsymbol{q}(\bar{\boldsymbol{x}}) \in \mathcal{Q}_A\} \ , \tag{64}$$
$$\bar{\mathcal{X}}_P = \{\bar{\boldsymbol{x}} : \boldsymbol{q}(\bar{\boldsymbol{x}}) \in \mathcal{Q}_P\} \ . \tag{65}$$

4.1 Model Construction

We now construct the dynamics model as a differential inclusion $\frac{\mathrm{d}}{\mathrm{d}s}\bar{\boldsymbol{x}}(s) \in D(\bar{\boldsymbol{x}}(s))$. Under this formulation, the velocity $\boldsymbol{v}(s)$ is continuous with respect to s, but can be *discontinuous* with respect to time $t(s)$ in the sense that $\boldsymbol{v}$ can evolve while t is held constant. To make the system autonomous, we represent the external forces $\boldsymbol{u}$ as set-valued, time-varying full-state feedback $\mathcal{U}(\bar{\boldsymbol{x}})$. In order for the system to be well-behaved, we assume that the convex-compact u.s.c. properties exploited in the impact dynamics carry over into the continuous time case, because $\mathcal{U}$ itself holds these properties:

Assumption 25. *$\mathcal{U}(\bar{\boldsymbol{x}})$ is convex-compact u.s.c. in $\bar{\boldsymbol{x}}$.*

We identify three distinct behaviors that $\frac{\mathrm{d}}{\mathrm{d}s}\bar{\boldsymbol{x}} \in D(\bar{\boldsymbol{x}})$ should comply with:

4.1.1 No Contact Forces Whenever all active contacts have separating velocities (including scenarios where no contacts are active), i.e.

$$\bar{\boldsymbol{x}}(s) \in \bar{\mathcal{X}}_{\mathcal{S}} = \{\bar{\boldsymbol{x}} : \boldsymbol{v}(\bar{\boldsymbol{x}}) \in \mathcal{S}(\boldsymbol{q}(\bar{\boldsymbol{x}}))\} \ , \tag{66}$$

$\bar{\boldsymbol{x}}(s)$ should evolve according to the manipulator equations (12) with no contact forces ($\boldsymbol{\lambda} = \boldsymbol{0}$), in the sense that

$$\boldsymbol{M}(\boldsymbol{q})\mathrm{d}\boldsymbol{v} \in (\mathcal{U}(\bar{\boldsymbol{x}}) - \boldsymbol{C}(\boldsymbol{x}) - \boldsymbol{G}(\boldsymbol{q}))\,\mathrm{d}s\,, \tag{67}$$
$$\mathrm{d}t = \mathrm{d}s\,. \tag{68}$$

these equations can be packaged into the differential inclusion form as

$$\dot{\bar{\boldsymbol{x}}} \in D_{\mathcal{S}}(\bar{\boldsymbol{x}}) = \begin{bmatrix} \boldsymbol{\Gamma}\boldsymbol{v} \\ \boldsymbol{M}^{-1}(\mathcal{U} - \boldsymbol{C} - \boldsymbol{G}) \\ 1 \end{bmatrix} . \tag{69}$$

4.1.2 Impact Whenever $\boldsymbol{v}(s)$ is a penetrating velocity over some interval $[a, b]$, i.e.

$$\bar{\boldsymbol{x}}([a,b]) \subseteq \bar{\mathcal{X}}_{\mathcal{I}} = \{\bar{\boldsymbol{x}} : \boldsymbol{v}(\bar{\boldsymbol{x}}) \in \mathcal{I}(\boldsymbol{q}(\bar{\boldsymbol{x}}))\} \ , \tag{70}$$

time and configuration should be frozen, and $\boldsymbol{v}$ should evolve according to our simultaneous impact model:

$$\dot{\bar{\boldsymbol{x}}} \in D_{\mathcal{I}}(\bar{\boldsymbol{x}}) = \begin{bmatrix} \boldsymbol{0} \\ D_{\boldsymbol{q}}(\boldsymbol{v}) \\ 0 \end{bmatrix} . \tag{71}$$

4.1.3 Sustained Contact In addition to impacts, the model must capture continuous state evolution with respect to time under finite contact forces, as in the manipulator equations (12). At the same time, proving that our differential inclusion model is well behaved via (8) will require that the right hand side $D(\bar{\boldsymbol{x}}(s))$ be convex-valued. A key concept in this model is that these sustained contact behaviors can be represented as an *convex combination* of contactless and impact dynamics:

$$\dot{\bar{\boldsymbol{x}}}(s) \in \mathrm{co}\left(D_{\mathcal{S}}(\bar{\boldsymbol{x}}) \cup D_{\mathcal{I}}(\bar{\boldsymbol{x}})\right) \ . \tag{72}$$

To demonstrate this property, we consider that the manipulator equations (12), the evolution of the state $\boldsymbol{q}$, $\boldsymbol{v}$ under sustained contact obeys

$$\mathrm{d}\boldsymbol{q} = \boldsymbol{\Gamma}\boldsymbol{v}\mathrm{d}t\,, \tag{73}$$
$$\boldsymbol{M}\mathrm{d}\boldsymbol{v} \in \left(\boldsymbol{J}^T\boldsymbol{\lambda} + \mathcal{U} - \boldsymbol{C} - \boldsymbol{G}\right)\mathrm{d}t\,, \tag{74}$$

for some finite, non-zero contact forces $\boldsymbol{\lambda} = [\boldsymbol{\lambda}_n;\ \boldsymbol{\lambda}_t] \in \mathrm{FC}(\boldsymbol{q}, \boldsymbol{v})$. One major difference between the contact force $\boldsymbol{\lambda}$ and those occuring within the impact inclusion is that $\|\boldsymbol{\lambda}_n\|_1 \neq 1$ in general. We therefore must restate the dynamics in terms of $\tilde{\boldsymbol{\lambda}} = \frac{\boldsymbol{\lambda}}{\|\boldsymbol{\lambda}_n\|_1} \in \mathrm{FC}(\boldsymbol{q}, \boldsymbol{v})$.

We free ourselves to do so by including t as a state in our formulation; it therefore has differential $\mathrm{d}t = \dot{t}\mathrm{d}s$. By selecting $\dot{t} = \frac{1}{1+\|\boldsymbol{\lambda}_n\|_1} \in (0, 1)$, we rewrite (73)–(74) as

$$\mathrm{d}\boldsymbol{q} = ((1-\dot{t})\boldsymbol{0} + \dot{t}\boldsymbol{\Gamma}\boldsymbol{v})\mathrm{d}s\,, \tag{75}$$
$$\boldsymbol{M}\mathrm{d}\boldsymbol{v} \in \Big((1-\dot{t})\boldsymbol{J}^T\tilde{\boldsymbol{\lambda}} + \dot{t}\,(\mathcal{U} - \boldsymbol{C} - \boldsymbol{G})\Big)\,\mathrm{d}s\,, \tag{76}$$
$$\mathrm{d}t = ((1-\dot{t})0 + \dot{t}1)\mathrm{d}s\,, \tag{77}$$

As $\tilde{\boldsymbol{\lambda}}$ is also in the friction cone, the convex combination differential inclusion (72) can generate sustained contact with this choice of $\dot{t}$. As a result, $t(s)$ neither evolves directly with s nor remains constant; effectively, simulation via (72) slows down time by a factor of $(1 + \|\boldsymbol{\lambda}_n\|_1)$. We will see in a later section that the averge slow-down factor does not grow arbitrarily large under mild assumptions.

We now combine these three modes of behavior into a single differential inclusion. While we might easily chose the contactless mode when $\bar{\boldsymbol{x}} \in \bar{\mathcal{X}}_{\mathcal{S}}$, arbitrating between impact and sustained contact when the velocity is non-seperating is less obvious. First, even if there exists an admissible, finite force $\boldsymbol{\lambda} \in \mathrm{FC}(\boldsymbol{q}, \boldsymbol{v})$ which would enforce $\dot{\boldsymbol{\phi}} \geq \boldsymbol{0}$ under sustained contact, (73)–(74), Painlevé's Paradox (see Stewart (2000) for details) might require impact dynamics to prevent penetration due to higher-order effects (e.g. $\ddot{\boldsymbol{\phi}} < \boldsymbol{0}$). Furthermore, almost all selections of $\dot{\bar{\boldsymbol{x}}}$

from $\mathrm{co}\,(D_{\mathcal{S}}(\bar{\boldsymbol{x}}) \cup D_{\mathcal{I}}(\bar{\boldsymbol{x}}))$ will correspond to non-physical behavior; a particular $\dot{\bar{\boldsymbol{x}}}$ must be chosen to *maintain* contact by exactly counteracting forces such that inter-body distance is *identically* zero during contact.

We resolve these issues in an implicit manner in the full differential inclusion

$$\dot{\bar{\boldsymbol{x}}} \in D(\bar{\boldsymbol{x}}) = \begin{cases} D_{\mathcal{S}}(\bar{\boldsymbol{x}}) & \bar{\boldsymbol{x}} \in \bar{\mathcal{X}}_{\mathcal{S}}\,, \\ D_{\mathcal{I}}(\bar{\boldsymbol{x}}) & \bar{\boldsymbol{x}} \in \mathrm{int}(\bar{\mathcal{X}}_{\mathcal{I}})\,, \\ \mathrm{co}\,(D_{\mathcal{S}}(\bar{\boldsymbol{x}}) \cup D_{\mathcal{I}}(\bar{\boldsymbol{x}})) & \text{otherwise}\,. \end{cases} \tag{78}$$

We will show that in this model, $\boldsymbol{\phi}(\boldsymbol{q}) = \boldsymbol{0}$ is effectively a *barrier*: solutions beginning at a non-penetrating configuration are forced to *never* penetrate.

4.2 Properties

4.2.1 Existence and Closure While proofs for existence of solutions for impact models and discrete-time simulation are commonplace (Stewart and Trinkle 1996; Anitescu and Potra 1997; Drumwright and Shell 2010), guarantees for continuous-time evolution through impact have thus far been limited. For example, Burden et al. (2016) studied discontinuous vector fields, with strong results and applications to robot impacts, but are restricted to frictionless contact; and Johnson et al. (2016) treated a limited form of friction, but assumed that contact occurs only at massless limbs. By contrast, our modeling philosophy of including a wide set of behaviors will allow us to guarantee existence of solutions via Proposition 8 only using bounded energy and input assumptions (Assumptions 26 and 27).

The continuous-time DI (78) already exhibits many of the properties required for application of Proposition 8. For any $\boldsymbol{q}$ and separating velocity $\boldsymbol{v} \in \mathcal{S}(\boldsymbol{q})$, we can pick an open neighborhood $\mathcal{Q} \times \mathcal{V}$ of $[\boldsymbol{q};\, \boldsymbol{v}]$ which also consists solely of separating velocities by continuity of $\boldsymbol{\phi}$ and $\boldsymbol{J}_n$. Therefore, the set of separating-velocity states $\bar{\mathcal{X}}_{\mathcal{S}}$ is open. $D(\bar{\boldsymbol{x}})$ must then be u.s.c., because it is constructed from two u.s.c. functions on disjoint open sets, and their convex hull on the remainder of the space. Furthermore, for any state $\bar{\boldsymbol{x}}$, $D(\bar{\boldsymbol{x}})$ is non-empty, compact, and convex. As $\boldsymbol{C}(\boldsymbol{x})$ can grow quadratically, D is not uniformly bounded; therefore Proposition 8 cannot be directly used to prove existence of solutions. However, nearly identical properties of the initial value problems can still be established in the following manner. Suppose first that terms that might contribute to growth of kinetic energy, $\mathcal{U}$ and $\boldsymbol{G}$, can only input power at a bounded rate:

Assumption 26. $\exists c > 0,\, \boldsymbol{v}^T(\mathcal{U} - \boldsymbol{G}) \leq c\,\|\boldsymbol{v}\|_{\boldsymbol{M}}$.

This condition is widely satisfied by many robotic systems, including those with globally bounded controllers and potential gradients (such as gravity). Assumption 26 implies that $\bar{\boldsymbol{x}}$ cannot diverge to infinity over a finite horizon. Furthermore, we will assume that if $\bar{\boldsymbol{x}}$ is bounded, $\dot{\bar{\boldsymbol{x}}}$ is bounded as well:

Assumption 27. *Over any compact set $\bar{\mathcal{X}}$, $\mathcal{U} - \boldsymbol{G}$ is bounded, and therefore $D(\bar{\mathcal{X}})$ is compact.*

In conjunction, Assumptions 26 and 27 imply that over a finite interval, the solutions $\bar{\boldsymbol{x}}(s)$ beginning from a compact set $\bar{\mathcal{X}}$ have bounded derivative and therefore inherit the key existence, closure, and u.s.c. structure for differential inclusions where the derivative is bounded everywhere:

Theorem 28. *Let $\bar{\mathcal{X}}$ be a compact set and $[a, b]$ be a compact interval. Then* $\mathrm{IVP}\left(D, \bar{\mathcal{X}}, [a, b]\right)$ *is compact and* $\mathrm{IVP}\left(D, \bar{\boldsymbol{x}}, [a, b]\right)$ *is non-empty, closed, convex, and u.s.c. in $\bar{\boldsymbol{x}}$ over $\bar{\mathcal{X}}$.*

Proof. See Appendix E.1.

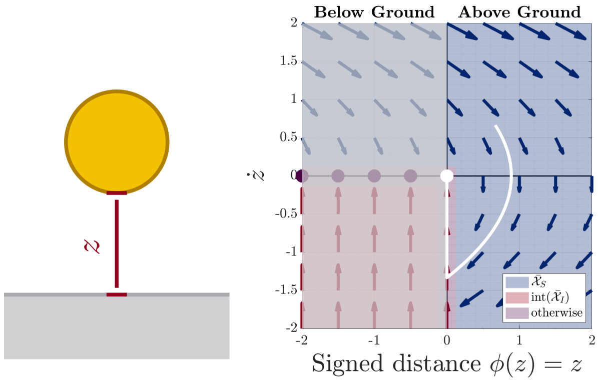

(a) 1D ball-ground system **(b)** 1D system phase portrait

Figure 6. A simple, 1D system of a non-rotating ball falling under gravity with configuration $\boldsymbol{q} = z = \phi(z)$ is shown (a). (b) A phase plot demonstrates why the structure of our differential inclusion prevents penetration; an example trajectory is shown in white. Penetration on this plot corresponds to crossing from the right-half- to the left-half-plane. This cross cannot happen on the top half of the vertical axis ($\phi = 0,\, \dot{z} >= 0$), as the flow of the system here by definition points rightward. The cross also cannot happen on the bottom half of the axis, as the third quadrant is constrained to purely-vertical flow ($\dot{\phi} = \dot{z}\mathrm{d}t = 0$).

4.2.2 Non-Penetration While there is no structure in $D(\bar{\boldsymbol{x}})$ that explicitly prevents penetration, $\boldsymbol{\phi}(\boldsymbol{q}) \geq \boldsymbol{0}$ is naturally, implicitly preserved; for each contact i, $\boldsymbol{\phi}_i(\boldsymbol{q}(s))$ crossing from positive to negative along a solution would require 2 contradicting conditions:

- $\dot{\boldsymbol{\phi}}_i < 0$ on $\mathrm{int}\left(\bar{\mathcal{X}}_{\mathcal{I}}\right)$ because the zero crossing forces $\bar{\boldsymbol{x}}$ to enter $\mathrm{int}\left(\bar{\mathcal{X}}_{\mathcal{I}}\right)$.
- $\dot{\boldsymbol{\phi}}_i = 0$ on $\mathrm{int}\left(\bar{\mathcal{X}}_{\mathcal{I}}\right)$ because $D(\bar{\boldsymbol{x}})$ requires $\dot{\boldsymbol{q}} = 0$ on $\mathrm{int}\left(\bar{\mathcal{X}}_{\mathcal{I}}\right)$.

An alternative, graphical argument is given for a 1D system in Figure 6.

Theorem 29. Non-Penetration. *Let $\bar{\boldsymbol{x}}_0 \notin \bar{\mathcal{X}}_P$ be a non-penetrating state, let $[a, b]$ be a compact interval, and let $\bar{\boldsymbol{x}}(s) \in \mathrm{IVP}\left(D, \bar{\boldsymbol{x}}_0, [a, b]\right)$. Then $\bar{\boldsymbol{x}}(s) \notin \bar{\mathcal{X}}_P$ for all $s \in [a, b]$.*

Proof. See Appendix E.2.

4.2.3 Correct Mode Selection Our requirements dictate that solutions $\bar{\boldsymbol{x}}(s)$ containing only separating velocities ($\bar{\boldsymbol{x}} \in \bar{\mathcal{X}}_{\mathcal{S}}$) should comply with contactless dynamics, and likewise with impact dynamics when $\bar{\boldsymbol{x}}(s)$ contains only impacting velocities and non-penetrating configurations ($\bar{\boldsymbol{x}} \in \bar{\mathcal{X}}_{\mathcal{I}} \setminus \bar{\mathcal{X}}_P$). The former is a trivial result of the construction of D, but the latter is only similarly trivial when $\bar{\boldsymbol{x}} \subseteq \mathrm{int}(\bar{\mathcal{X}}_{\mathcal{I}}) \setminus \bar{\mathcal{X}}_P$. However, all states $\bar{\boldsymbol{x}} \subseteq \bar{\mathcal{X}}_{\mathcal{I}}$ have penetrating velocity, and thus any contactless dynamics component in $\dot{\bar{\boldsymbol{x}}}$ would by definition cause $\bar{\boldsymbol{x}}$ to penetrate (i.e. enter $\bar{\mathcal{X}}_P$), allowing a proof by contradiction:

Theorem 30. Impact Dynamics. *Let $[a, b]$ be a compact interval and $\bar{\boldsymbol{x}}(s) \in \mathrm{SOL}\,(D, [a, b])$ with $\bar{\boldsymbol{x}}([a, b]) \subseteq \bar{\mathcal{X}}_{\mathcal{I}} \setminus \bar{\mathcal{X}}_P$. Then $\bar{\boldsymbol{x}}(s) \in \mathrm{SOL}\,(D_{\mathcal{I}}, [a, b])$.*

Proof. See Appendix E.3.

4.3 Linear Time Advancement

While Theorem 28 guarantees existence of solutions over any interval of s, practical application often requires reasoning about solution sets over intervals in time (over $t(s)$). To do so, solutions of the model must significantly advance time—i.e. for any T, all solutions of the model have $t(S) - t(0) > T$ for large enough S.

For small enough T, this property is only requires the solution to exit the impact dynamics regime, which by Theorem 23 cannot continue indefinitely:

Theorem 31. *Let $\bar{\mathcal{X}}$ be a compact set containing no configurations in $\mathcal{Q}_P$. Then there exists $S(\bar{\mathcal{X}}), T(\bar{\mathcal{X}}) > 0$, such that for all $S' > S(\bar{\mathcal{X}})$, if $\bar{\boldsymbol{x}}(s) \in \mathrm{IVP}\left(D, \bar{\mathcal{X}}, [0, S']\right)$, we must have $t(S') - t(0) > T(\bar{\mathcal{X}})$.*

Proof. See Appendix E.4.

If $t(S) - t(0) > T$ is guaranteed over a particular set $\bar{\mathcal{X}}$, then $t(s)$ must at least advance linearly at rate $\frac{T}{S}$ over arbitrarily long horizons:

Corollary 32. *Let $\bar{\mathcal{X}}$ be a compact set containing no configurations in $\mathcal{Q}_P$, such that*

$$\bar{\mathcal{X}}(S') = \left\{\bar{\boldsymbol{x}}(s) \in \mathrm{IVP}\left(D, \bar{\mathcal{X}}, [0, S]\right) : \bar{\boldsymbol{x}}([0, S]) \subseteq \bar{\mathcal{X}}\right\}, \tag{79}$$

is non-empty for all $S' > 0$. Define $S(\bar{\mathcal{X}}), T(\bar{\mathcal{X}}) > 0$ as in Theorem 31, and let

$$T'(S') = \min_{\bar{\boldsymbol{x}}(s) \in \bar{\mathcal{X}}(S')} t(\bar{\boldsymbol{x}}(S')) - t(\bar{\boldsymbol{x}}(0)). \tag{80}$$

Then $\liminf_{S' \to \infty} \frac{T'(S')}{S'} \geq \frac{T(\bar{\mathcal{X}})}{S(\bar{\mathcal{X}})}$.

Proof. See Appendix E.5.

5 Discrete Impact Integration

Sections 3 and 4 provide a rigorous theoretical framework yielding guaranteed existence of well-behaved solutions to our rigid body dynamics model; in this section, we develop a method to *compute* numerical approximations of these solutions. Given pre-impact condition $\boldsymbol{x}_0 = [\boldsymbol{q}_0;\ \boldsymbol{v}_0]$, we will show how one can develop an implicit, LCP-based integration scheme for our impact differential inclusion (54). We will bound the number of LCP solves required in two important scenarios: simulation and reachable-set approximation.

5.1 Model Construction

Just as forward Euler integration can cause penetration in continuous-time simulators (see Section 2.6), it can also cause impulses to act on separated contacts if applied to the impact differential inclusion (54). To rectify this issue, we develop an approximate, implicit, and discrete integration scheme. Our method seeks to find a contact impulse increment $\bar{\boldsymbol{\lambda}}$, such that

$$\boldsymbol{v}'(\bar{\boldsymbol{\lambda}}) = \boldsymbol{v} + \boldsymbol{M}^{-1}\bar{\boldsymbol{J}}^T\bar{\boldsymbol{\lambda}}\,, \tag{81}$$

$$\bar{\boldsymbol{\lambda}} \in \mathrm{LFC}(\boldsymbol{q}, \boldsymbol{v}'(\bar{\boldsymbol{\lambda}}))\,, \tag{82}$$

where $\bar{\boldsymbol{\lambda}}$ and $\bar{\boldsymbol{J}}$ are defined as in (39)–(40), and the dependence of $\boldsymbol{M}$ and $\bar{\boldsymbol{J}}$ on $\boldsymbol{q} = \boldsymbol{q}_0$ is supressed. Compared to the differential inclusion (54) which finds $\dot{\boldsymbol{v}} \in \boldsymbol{M}^{-1}\bar{\boldsymbol{J}}^T\mathrm{FC}(\boldsymbol{q}, \boldsymbol{v})$, this method approximates the derivative with a finite difference; enforces the friction cone constraint (82) at the incremented velocity $\boldsymbol{v}'$; and replaces the quadratic friction cone with the linear approximation. Our method may technically be described as algebraic, but it differs from most algebraic methods. While common methods do not attempt to capture any behavior between the beginning and end of the impact process (e.g. Glocker and Pfeiffer (1995); Anitescu and Potra (1997)), our method behaves differently because it is a direct numerical approximation of a differential process. For instance, these methods enforce complementarity between post-impact velocity and total impulse (45), a constraint which real systems do not satisfy (Chatterjee 1999). Our method circumvents this issue by instead enforcing complementarity between intermediate velocities and impulse increments. Despite these conceptual differences, the linear cone constraint in particular allows us to draw significant *computational* similarities to these methods by casting our method as a sequence of LCP's.

Algorithm 2: $\mathrm{Sim}(h, \boldsymbol{x}_0, N)$

Input: step size h, initial state $\boldsymbol{x}_0 = [\boldsymbol{q}_0; \boldsymbol{v}_0]$, max iteration count N
Output: final velocity $\boldsymbol{v}$

$\boldsymbol{v} \leftarrow \boldsymbol{v}_0$;
$i \leftarrow 0$;
while $\boldsymbol{v} \in \mathcal{I}(\boldsymbol{q}_0)$ *and* $i \leq N$ **do**
  $\boldsymbol{\lambda}_{n,max} \sim hp(\boldsymbol{\lambda}_n)$;
  Select $\boldsymbol{z} = [\boldsymbol{\beta}; \bar{\boldsymbol{\lambda}}; \boldsymbol{\gamma}]$ from $\mathrm{LCP}(\boldsymbol{W}_{\boldsymbol{q}_0}, \boldsymbol{w}_{\boldsymbol{q}_0}(\boldsymbol{v}, \boldsymbol{\lambda}_{n,max}))$;
  $\boldsymbol{v} \leftarrow \boldsymbol{v} + \boldsymbol{M}(\boldsymbol{q}_0)^{-1}\bar{\boldsymbol{J}}(\boldsymbol{q}_0)^T\bar{\boldsymbol{\lambda}}$;
  $i \leftarrow i + 1$;
end

As our model by construction can generate a set realistic outcomes, we frame resolving an impact as sampling from that set. We parameterize the sampling process with a normal impulse distribution $p(\boldsymbol{\lambda}_n)$ over the unit box; step size $h > 0$; and (possibly infinite) max iteration count N. While our theoretical results extend to any finite-density $p(\boldsymbol{\lambda}_n)$, we assume in this section that $p(\boldsymbol{\lambda}_n)$ is the uniform distribution for simplicity. We compute samples from our discrete approximation of Routh's method (Algorithm 2) as follows:

1. Generate a non-zero, maximum normal impulse increment $\boldsymbol{\lambda}_{n,max} \sim hp(\boldsymbol{\lambda}_n)$.
2. Find a set of forces $\bar{\boldsymbol{\lambda}}$ with normal component $\boldsymbol{\lambda}_n \leq \boldsymbol{\lambda}_{n,max}$ that solves (81)–(82).
3. Increment $\boldsymbol{v} \leftarrow \boldsymbol{v} + \boldsymbol{M}^{-1}\boldsymbol{J}^T\bar{\boldsymbol{\lambda}}$.
4. Terminate and take $\boldsymbol{v}^+ = \boldsymbol{v}$ if it is non-impacting ($\boldsymbol{v} \notin \mathcal{I}(\boldsymbol{q})$); otherwise, return to 1.

To satisfy the friction cone constraint (82), we recall that the linear friction cone is defined in (41) as linear complementarity constraints (16)–(18) and (37)–(38) with slack variables $\boldsymbol{\gamma}$. If some contacts are inactive, we may simply remove the associated elements from $\bar{\boldsymbol{\lambda}}$ and $\bar{\boldsymbol{J}}$; therefore, without loss of generality, $\boldsymbol{\phi}(\boldsymbol{q}) = \boldsymbol{0}$, and thus (16) is satisfied. To satisfy (17) and (18), we define slack variables $\boldsymbol{\beta} \in \mathbb{R}^m$ and enforce the following constraint:

$$\boldsymbol{0} \leq \boldsymbol{\beta} \perp \boldsymbol{\lambda}_{n,max} - \boldsymbol{\lambda}_n \geq \boldsymbol{0}\,, \tag{83}$$

$$\boldsymbol{0} \leq \boldsymbol{\lambda}_n \perp \boldsymbol{J}_n\boldsymbol{v}'(\bar{\boldsymbol{\lambda}}) + \boldsymbol{\beta} \geq \boldsymbol{0}\,. \tag{84}$$

Together, these constraints enforce $\boldsymbol{0} \leq \boldsymbol{\lambda}_n \leq \boldsymbol{\lambda}_{n,max}$; furthermore, for each contact, $\boldsymbol{\lambda}_{n,i} = \boldsymbol{\lambda}_{n,max_i}$ or the contact has terminated.

We can then find a impulse increment $\bar{\boldsymbol{\lambda}}$ which satisfies the constraints (83), (84), (37), and (38) by solving for $\boldsymbol{z} \in \mathrm{LCP}(\boldsymbol{W_q}, \boldsymbol{w_q}(\boldsymbol{v}, \boldsymbol{\lambda}_{n,max}))$:

$$\boldsymbol{z} = \begin{bmatrix} \boldsymbol{\beta} \\ \bar{\boldsymbol{\lambda}} \\ \boldsymbol{\gamma} \end{bmatrix}, \quad \boldsymbol{w_q}(\boldsymbol{v}, \boldsymbol{\lambda}_{n,max}) = \begin{bmatrix} \boldsymbol{\lambda}_{n,max} \\ \bar{\boldsymbol{J}}\boldsymbol{v} \\ \boldsymbol{0} \end{bmatrix}, \tag{85}$$

$$\boldsymbol{W_q} = \begin{bmatrix} \boldsymbol{0} & -\boldsymbol{I} & \boldsymbol{0} & \boldsymbol{0} \\ \boldsymbol{I} & \boldsymbol{J}_n\boldsymbol{M}^{-1}\boldsymbol{J}_n & \boldsymbol{J}_n\boldsymbol{M}^{-1}\boldsymbol{J}_D & \boldsymbol{0} \\ \boldsymbol{0} & \boldsymbol{J}_D\boldsymbol{M}^{-1}\boldsymbol{J}_n & \boldsymbol{J}_D\boldsymbol{M}^{-1}\boldsymbol{J}_D & \boldsymbol{E} \\ \boldsymbol{0} & \boldsymbol{\mu} & -\boldsymbol{E}^T & \boldsymbol{0} \end{bmatrix}, \tag{86}$$

where $\boldsymbol{q}$ is the configuration of the impacting state. We note in particular that by eliminating the columns and rows associated with $\boldsymbol{\beta}$ from this construction, we exactly recover the impact LCP from Anitescu and Potra (1997).

5.2 Properties

5.2.1 Existence The most essential property of our integration step is that, because $\boldsymbol{W_q}$ is copositive, we can leverage Proposition 10 to show that the constituent LCP has a solution:

Theorem 33. $\mathrm{LCP}(\boldsymbol{W_q}, \boldsymbol{w_q}(\boldsymbol{v}, \boldsymbol{\lambda}_{n,max}))$ *is non-empty for all states* $[\boldsymbol{q};\ \boldsymbol{v}]$*, and normal impulse* $\boldsymbol{\lambda}_{n,max} \geq \boldsymbol{0}$.

Proof. See Appendix E.6.

5.2.2 Dissipation As discussed in Section 3.3.3, an essential property of inelastic impacts is energy dissipation; because solutions to our model approximate the differential inclusion, the integration step (81)–(82) cannot increase kinetic energy:

Theorem 34. *Let* $[\boldsymbol{q};\ \boldsymbol{v}]$ *be any state with active contact, and let* $\boldsymbol{\lambda}_{n,max} \geq \boldsymbol{0}$ *be a normal impulse. Then all impulses* $\bar{\boldsymbol{\lambda}}$ *generated by the impact constraints (*$\mathrm{LCP}(\boldsymbol{W_q}, \boldsymbol{w_q}(\boldsymbol{v}, \boldsymbol{\lambda}_{n,max}))$*) dissipate kinetic energy:*

$$K(\boldsymbol{q}, \boldsymbol{v}'(\bar{\boldsymbol{\lambda}})) \leq K(\boldsymbol{q}, \boldsymbol{v})\,. \tag{87}$$

Proof. See Appendix E.7.

5.2.3 Impulse Advancement If $\boldsymbol{\lambda}_n = \boldsymbol{0}$ were allowed in the LCP solution at a penetrating velocity $\boldsymbol{v} \in \mathcal{I}(\boldsymbol{q})$, then $\boldsymbol{v} = \boldsymbol{v}'$ could be selected in an infinite loop, and Algorithm 2 might never terminate. The structure of the normal impulse constraints (83) and (84) prevents this behavior by design for $\boldsymbol{\lambda}_{n,max} > \boldsymbol{0}$:

Lemma 35. *Let* $[\boldsymbol{q};\ \boldsymbol{v}]$ *be an impacting state (*$\boldsymbol{v} \in \mathcal{I}(\boldsymbol{q})$*), and* $\boldsymbol{\lambda}_{n,max} > \boldsymbol{0}$*. Let* $\bar{\boldsymbol{\lambda}} = [\boldsymbol{\lambda}_n;\ \boldsymbol{\lambda}_D]$ *be an impulse generated by the impact constraints* $\mathrm{LCP}(\boldsymbol{W_q}, \boldsymbol{w_q}(\boldsymbol{v}, \boldsymbol{\lambda}_{n,max}))$*. Then either some contact i activates fully (*$\boldsymbol{\lambda}_{n,i} = \boldsymbol{\lambda}_{n,max_i}$*), or all contacts terminate (*$\boldsymbol{J}_n\boldsymbol{v}'(\bar{\boldsymbol{\lambda}}) \geq \boldsymbol{0}$*).*

Proof. See Appendix F.1 .

However, preventing the infinite loop also requires the stricter condition that the net impulse $\bar{\boldsymbol{J}}^T\bar{\boldsymbol{\lambda}}$ be non-zero. Assumption 18 in fact yields a stricter condition: the magnitude of the change in velocity $\boldsymbol{M}^{-1}\bar{\boldsymbol{J}}^T\bar{\boldsymbol{\lambda}}$ grows linearly in $\|\boldsymbol{\lambda}_n\|_1$.

Lemma 36. *Consider a configuration* $\boldsymbol{q} \in \mathcal{Q}_A \setminus \mathcal{Q}_P$*. There exists a nonzero vector* $\boldsymbol{r}(\boldsymbol{q}) \in \mathbb{R}^{n_v}$*, such that for each non-separating velocity* $\boldsymbol{v} \in \mathrm{cl}\mathcal{I}(\boldsymbol{q})$ *and contact force* $\bar{\boldsymbol{\lambda}} \in \mathrm{LFC}\,(\boldsymbol{q}, \boldsymbol{v})$*,*

$$\boldsymbol{r}(\boldsymbol{q}) \cdot \boldsymbol{M}^{-1}\bar{\boldsymbol{J}}(\boldsymbol{q})^T\bar{\boldsymbol{\lambda}} \geq \|\boldsymbol{\lambda}_n\|_1\,. \tag{88}$$

Proof. See Appendix F.2.

Furthermore, we now show that $\boldsymbol{r}(\boldsymbol{q})$ can be computed as a linear program (LP). We first observe that, for an individual contact i, the net impulse imparted is a convex combination of the extreme rays of the linear friction cone, i.e. the kth element of $\boldsymbol{\lambda}_{D,i}$ is equal to $\boldsymbol{\mu}_i\boldsymbol{\lambda}_{n,i}$ and all other elements of $\bar{\boldsymbol{\lambda}}$ are zero. The net impulse imparted in this case when $\boldsymbol{\lambda}_{n,i} = 1$ is

$$\boldsymbol{F}_{i,k} = \boldsymbol{J}_{n,i}^T + \boldsymbol{J}_{t,i}^T\,(\boldsymbol{\mu}_i\boldsymbol{d}_k)\,. \tag{89}$$

Any force in the linear friction cone with $\|\boldsymbol{\lambda}_n\|_1$ can therefore be expressed as a convex combination of these forces:

$$\bar{\boldsymbol{\lambda}} \in \mathrm{LFC}\,(\boldsymbol{q}, \boldsymbol{0}) \wedge \|\boldsymbol{\lambda}_n\|_1 = 1 \iff \bar{\boldsymbol{\lambda}} \in \mathrm{co}\left(\bigcup_{i,k}\{\boldsymbol{F}_{i,k}\}\right). \tag{90}$$

The condition (88) must then be satisfied by any solution to the following LP:

$$\min_{\boldsymbol{r}} \quad \|\boldsymbol{r}\|_1\,, \tag{91}$$

$$\text{s.t.} \quad \boldsymbol{M}^{-1}F_{i,k} \cdot \boldsymbol{r} \geq 1,\ \forall i, k\,. \tag{92}$$

5.3 Linear Impact Termination

In order to construct a continuous time simulation environment capable of generating non-unique impacts, we now show that Algorithm 2 can be used as an efficient implementation of the impact subroutine in Algorithm 1:

$$\mathrm{ImpactLaw}(\boldsymbol{q}, \boldsymbol{v}) \leftarrow \mathrm{Sim}(h, [\boldsymbol{q};\ \boldsymbol{v}], \infty)\,. \tag{93}$$

Let the random variable $Z(h, \boldsymbol{q}_0, \boldsymbol{v}_0)$ be the number of LCP solves required for $\mathrm{Sim}(h, [\boldsymbol{q}_0;\ \boldsymbol{v}_0], \infty)$ to terminate. Given that multiple impacts might occur in a single time-step, it is crucial that $Z(h, \boldsymbol{q}_0, \boldsymbol{v}_0)$ be as small as possible. Consider that Lemma 36 implies that the velocity takes large steps in the $\boldsymbol{r}$ direction with high probability, yet total movement in any direction is bounded by $2\|\boldsymbol{v}_0\|_{\boldsymbol{M}}$ as kinetic energy is non-increasing (Lemma 35). We can therefore show that with high probability, Z grows linearly with $\|\boldsymbol{v}_0\|_{\boldsymbol{M}}$:

Theorem 37. *Let $\boldsymbol{q}_0 \in \mathcal{Q}_A \setminus \mathcal{Q}_P$ be a pre-impact configuration, let σ be the minimum singular value of $\boldsymbol{M}(\boldsymbol{q}_0)$, let $h > 0$ be a step-size, and let*

$$c = 4\left\lceil \frac{(m+1)\|\boldsymbol{r}(\boldsymbol{q}_0)\|_2}{h\sqrt{\sigma}} \right\rceil, \tag{94}$$

where $\boldsymbol{r}(\boldsymbol{q}_0)$ is defined from Lemma 36 and m is the number of contacts. Then for all $k \in \mathbb{Z}^+$, and pre-impact velocities $\boldsymbol{v}_0 \in \mathcal{I}(\boldsymbol{q}_0)$,

$$P\left(Z(h, \boldsymbol{q}_0, \boldsymbol{v}_0) > c\left\lceil\|\boldsymbol{v}_0\|_{\boldsymbol{M}}\right\rceil + k\right) \leq \exp\left(-\frac{k}{(m+1)^2}\right). \tag{95}$$

Proof. See Appendix F.3.

As the probability density of Z exponentially decays, it has finite moments (including its mean and variance).

5.4 Post-Impact Set Approximation

In order to generate robust robot locomotion and manipulation, planning methods must be capable of reasoning about the uncertainty that contact introduces. We now describe a probabilistically complete method to approximate the uncertainty—that is, non-uniqueness—induced by the simultaneous impact behaviors modeled in our differential inclusion (54). First, we will examine a condition under which the full set of reachable post-impact velocities from Algorithm 2 is well-defined; then, we will reduce the problem of densely sampling this set to Proposition 4.

In order for computation of the set of possible outcomes of Algorithm 2 to be well-posed, we must consider a key practical ramification of the LCP solve on Line 5: numerical LCP solvers typically only find a *single* solution, and may be systematically biased in their selection among multiple solutions. For all claims in Section 5.4, we therefore make the additional assumption that this selection process does not affect the outcome of an individual integration step:

Assumption 38. *Consider a configuration with active contact $\boldsymbol{q} \in \mathcal{Q}_A \setminus \mathcal{Q}_P$. For each velocity $\boldsymbol{v} \in \mathbb{R}^{n_v}$ and normal impulse increment $\boldsymbol{\lambda}_{n,max} \geq \boldsymbol{0}$, every $\bar{\boldsymbol{\lambda}}$ generated from $\mathrm{LCP}(\boldsymbol{W}_{\boldsymbol{q}}, \boldsymbol{w}_{\boldsymbol{q}}(\boldsymbol{v}, \boldsymbol{\lambda}_{n,max}))$ results in the same incremented velocity $\boldsymbol{v}'$. Equivalently, there exists a function $\boldsymbol{f}_{\boldsymbol{q}} : \mathbb{R}^{n_v} \times \mathrm{cl}(\mathbb{R}^{m+}) \to \mathbb{R}^{n_v}$, such that*

$$\boldsymbol{v}' = \boldsymbol{v} + \boldsymbol{M}^{-1}\bar{\boldsymbol{J}}^T\bar{\boldsymbol{\lambda}} = \boldsymbol{f}_{\boldsymbol{q}}(\boldsymbol{v}, \boldsymbol{\lambda}_{n,max}). \tag{96}$$

Critically the time-step outcome $\boldsymbol{f}_{\boldsymbol{q}}(\boldsymbol{v}, \boldsymbol{\lambda}_{n,max})$ under Assumption 38 is only unique *given* $\boldsymbol{\lambda}_{n,max}$; different post-impact velocities can be generated by selecting different $\boldsymbol{\lambda}_{n,max}$. However, it is worth noting that Assumption 38 is violated in the rare cases when Anitescu and Potra (1997) produces multiple outcomes, including the compass gait and RAMone examples in Section 6. One can verify that the assumption holds for a particular scenario by solving a convex Semidefinite Program (Aydinoglu et al. 2020).

Under its limitations, Assumption 38 bestows several useful properties upon the impact simulation algorithm, including Lipschitz continuity of the single-step map:

Lemma 39. *For each non-penetrating configuration with active contact $\boldsymbol{q} \in \mathcal{Q}_A \setminus \mathcal{Q}_P$, $\boldsymbol{f}_{\boldsymbol{q}}(\boldsymbol{v}, \boldsymbol{\lambda}_{n,max})$ is Lipschitz continuous.*

Proof. We first note that because $\boldsymbol{v}'$ is unique, we must have that

$$\bar{\boldsymbol{J}}^T\bar{\boldsymbol{\lambda}} = \begin{bmatrix}\boldsymbol{0} & \bar{\boldsymbol{J}}^T & \boldsymbol{0}\end{bmatrix}\mathrm{LCP}(\boldsymbol{W}_{\boldsymbol{q}}, \boldsymbol{w}_{\boldsymbol{q}}(\boldsymbol{v}, \boldsymbol{\lambda}_{n,max})), \tag{97}$$

is a singleton over the convex domain $\boldsymbol{w}_{\boldsymbol{q}}(\mathbb{R}^{n_v}, \mathrm{cl}(\mathbb{R}^{m+}))$. Therefore by direct application of Proposition 11, $\boldsymbol{f}_{\boldsymbol{q}}$ is Lipschitz continuous.

Furthermore, the integration step LCP will select zero impulse in these scenarios:

Lemma 40. *Consider a configuration with active contact $\boldsymbol{q} \in \mathcal{Q}_A \setminus \mathcal{Q}_P$ and $\boldsymbol{\lambda}_{n,max} \geq \boldsymbol{0}$. Then if either $\boldsymbol{J}_n\boldsymbol{v} \geq \boldsymbol{0}$ or $\boldsymbol{\lambda}_{n,max} = \boldsymbol{0}$,*

$$\boldsymbol{v} = \boldsymbol{f}_{\boldsymbol{q}}(\boldsymbol{v}, \boldsymbol{\lambda}_{n,max}). \tag{98}$$

Proof. Observe that if either $\boldsymbol{\lambda}_{n,max} = \boldsymbol{0}$ or if $\boldsymbol{v}$ is not impacting ($\boldsymbol{J}_n\boldsymbol{v} \geq \boldsymbol{0}$), we can select zero normal impulse ($\boldsymbol{\lambda}_n = \boldsymbol{0}$ and thus $\boldsymbol{v}' = \boldsymbol{v}$) and satisfy the normal complementary equations (83) and (84). Setting the frictional impulses to zero and the slack variables $\boldsymbol{\beta}$ to the negative part of $\boldsymbol{J}_n\boldsymbol{v}$ constitutes a full solution to the LCP.

The continuity of $\boldsymbol{f}_{\boldsymbol{q}}$ allows for significant expansion of the $\boldsymbol{J}_n\boldsymbol{v} \geq \boldsymbol{0}$ case; if $\boldsymbol{v}$ is *almost* terminated, then only a single simulation step with a small $\boldsymbol{\lambda}_{n,max}$ is required to end the impact:

Lemma 41. *For all configurations $\boldsymbol{q} \in \mathcal{Q}_A \setminus \mathcal{Q}_P$, velocities $\boldsymbol{v} \in \mathbb{R}^{n_v}$, and $\varepsilon > 0$, there exists a $\delta(\varepsilon, \boldsymbol{v}_0)$, such that for any velocity $\bar{\boldsymbol{v}}$ which is almost non-impacting ($\boldsymbol{J}_n\bar{\boldsymbol{v}} \geq -\delta$) and sufficiently small ($\|\bar{\boldsymbol{v}}\|_{\boldsymbol{M}} \leq \|\boldsymbol{v}\|_{\boldsymbol{M}}$), we have that $\boldsymbol{f}_{\boldsymbol{q}}(\bar{\boldsymbol{v}}, \varepsilon\boldsymbol{1}) \notin \mathcal{I}(\boldsymbol{q})$.*

Proof. See Appendix F.4.

We now iteratively define the reachable set of Algorithm 2. Let $\mathcal{V}_N(\boldsymbol{x}_0, h)$ be the set of possible outputs of $\mathrm{Sim}(h, \boldsymbol{x}_0, N)$. Then we have that

$$\mathcal{V}_0(\boldsymbol{x}_0, h) = \{\boldsymbol{v}_0\}, \tag{99}$$

$$\mathcal{V}_N(\boldsymbol{x}_0, h) = \boldsymbol{f}_{\boldsymbol{q}}(\mathcal{V}_{N-1}(\boldsymbol{x}_0, h), [0, h]^m), \tag{100}$$

$$\mathcal{V}_N(\boldsymbol{x}_0, h) \supseteq \mathcal{V}_{N-1}(\boldsymbol{x}_0, h). \tag{101}$$

Here, we've used the $\boldsymbol{J}_n\boldsymbol{v} \geq \boldsymbol{0}$ condition in Lemma 40 to ignore early termination (i.e. $\boldsymbol{J}_n\boldsymbol{v} \geq \boldsymbol{0}$ before N loop

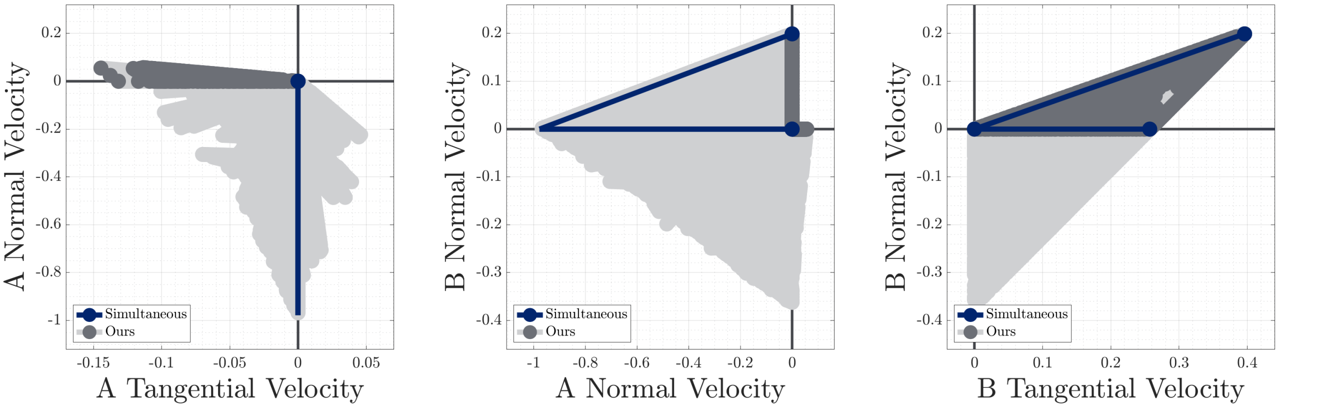

Figure 7. Evolution of the compass gait step. The center plot compares the normal velocities of the two contacts, while the left and right show velocities of points A and B, respectively. Our model produces the three outcomes in Figure 4b, as well as all reasonable intermediate velocities of point B. Furthermore, oscillation of impact between the feet allows point A to slide or lift off, while point B maintains contact.

iterations) in (100), and the $\boldsymbol{\lambda}_{n,max} = \mathbf{0}$ condition to establish the monotonic growth in (101). We can then construct the entire set of velocities reachable as

$$\mathcal{V}_\infty(\boldsymbol{x}_0, h) = \bigcup_{N \in \mathbb{N}} \mathcal{V}_N(\boldsymbol{x}_0, N)\,. \qquad (102)$$

$\mathcal{V}_N(\boldsymbol{x}_0, N)$ can approximate $\mathcal{V}_\infty(\boldsymbol{x}_0, h)$ with arbitrary precision:

Lemma 42. *Consider an initial configuration $\boldsymbol{q}_0 \in \mathcal{Q}_A \setminus \mathcal{Q}_P$, initial velocity $\boldsymbol{v}_0 \in \mathbb{R}^{n_v}$, and step-size $h \geq 0$. Then for each $\varepsilon > 0$, there exists an N, such that $\mathcal{V}_N([\boldsymbol{q}_0;\ \boldsymbol{v}_0], h)$ is an ε-net of $\mathcal{V}_\infty([\boldsymbol{q}_0;\ \boldsymbol{v}_0], h)$.*

Proof. $\mathcal{V}_N([\boldsymbol{q}_0;\ \boldsymbol{v}_0], h)$ is a monotonic (101) and uniformly bounded (via Theorem 34) sequence, and therefore it is convergent in the ε-net sense to some limiting set. $\mathcal{V}_\infty([\boldsymbol{q}_0;\ \boldsymbol{v}_0], h)$ is by definition the limit of this sequence.

Similarly, the post-impact reachable set is simply the reachable velocities which are non-penetrating:

$$\mathrm{Sim}(h, \boldsymbol{x}_0, \infty) \in \mathcal{V}_\infty(\boldsymbol{x}_0, h) \setminus \mathcal{I}(\boldsymbol{q}_0)\,. \qquad (103)$$

Algorithm 3: $\mathrm{Approximate}(h, \boldsymbol{x}_0, \varepsilon, N, M)$

Input: step size h, initial state $\boldsymbol{x}_0 = [\boldsymbol{q}_0;\ \boldsymbol{v}_0]$, approximation $0 < \varepsilon < h$, trajectory length N, trajectory count M
Output: post-impact set approximation $\tilde{\mathcal{V}}^+$

```
Ṽ⁺ ← {};
ψ ← σ_max (M⁻¹ J̄ᵀ) m(1 + max_i μ_i) + 1 ;
for i = 1 to M do
    v ← Sim(h, x₀, N);
    Ṽ⁺ ← Ṽ⁺ ∪ { f_{q₀}(v, ε/(3ψ) 1_m) };
end
Ṽ⁺ ← Ṽ⁺ \ I(q₀);
```

$\tilde{\mathcal{V}}^+ \leftarrow \{\}$;
$\psi \leftarrow \sigma_{max}\left(\boldsymbol{M}^{-1}\bar{\boldsymbol{J}}^T\right) m(1 + \max_i \boldsymbol{\mu}_i) + 1$;
for $i = 1$ **to** M **do**
  $\boldsymbol{v} \leftarrow \mathrm{Sim}(h, \boldsymbol{x}_0, N)$;
  $\tilde{\mathcal{V}}^+ \leftarrow \tilde{\mathcal{V}}^+ \cup \left\{\boldsymbol{f}_{\boldsymbol{q}_0}(\boldsymbol{v}, \frac{\varepsilon}{3\psi}\mathbf{1}_m)\right\}$;
end
$\tilde{\mathcal{V}}^+ \leftarrow \tilde{\mathcal{V}}^+ \setminus \mathcal{I}(\boldsymbol{q}_0)$;

We can finally use the above derived properties to construct a method, Algorithm 3, for approximating the post-impact set. Lemma 42 and Proposition 4 together show that M samples from $\mathrm{Sim}(h, \boldsymbol{x}_0, N)$ well-approximate $\mathcal{V}_\infty$, and can be forced to terminate with only a small additional step (Lemma 41). Therefore, Algorithm 3 is approximately complete:

Theorem 43. *Consider an initial configuration $\boldsymbol{q}_0 \in \mathcal{Q}_A \setminus \mathcal{Q}_P$, initial velocity $\boldsymbol{v}_0 \in \mathbb{R}^{n_v}$, and step-size $h > 0$. For all $\varepsilon, \delta > 0$, there exists $N, M > 0$, such that $\mathrm{Approximate}(h, \boldsymbol{x}_0, \varepsilon, N, M)$ returns an ε-net of $\mathcal{V}_\infty(\boldsymbol{x}_0, h) \setminus \mathcal{I}(\boldsymbol{q}_0)$ with probability at least $1 - \delta$.*

Proof. See Appendix F.5

6 Numerical Examples

We now show several examples of the post-impact velocity sets that can be generated by our model. The MATLAB code is available online[1], and LCP's were solved via the PATH solver (Dirkse and Ferris 1995). We begin by analyzing the three examples shown thus far: the phone drop (Fig. 1); compass gait step (Fig. 4); and box-wall impact (Fig. 5). We additionally discuss two further examples which highlight the applicability of our model to more complex systems. For each system, we provide plots of the evolution evolution of the velocity through the impact process with lines, projected onto the contact frames. Our method is shown in gray; simultaneous resolution via Anitescu and Potra (1997) is shown in blue; and sequential resolutions are shown in red and yellow. Samples of the post-impact velocity sets were generated using Algorithm 3, and are shown as circles; for visual clarity, the gray circles associated with are method are darkened. Sampling from the impulse distribution p is conducted with a Sobol quasi-random sequence, a method for reliably generating uniform-density ε-nets of unit hypercubes (Sobol 1967). For some examples, axes of symmetry were used to duplicate samples.

6.1 Phone Drop

We revisit the example of dropping a narrow, rectangular object onto the ground (Fig. 1), which may either result in the object coming to rest or pivoting on a corner. As shown in Figure 9, our method produces each of these symmetric

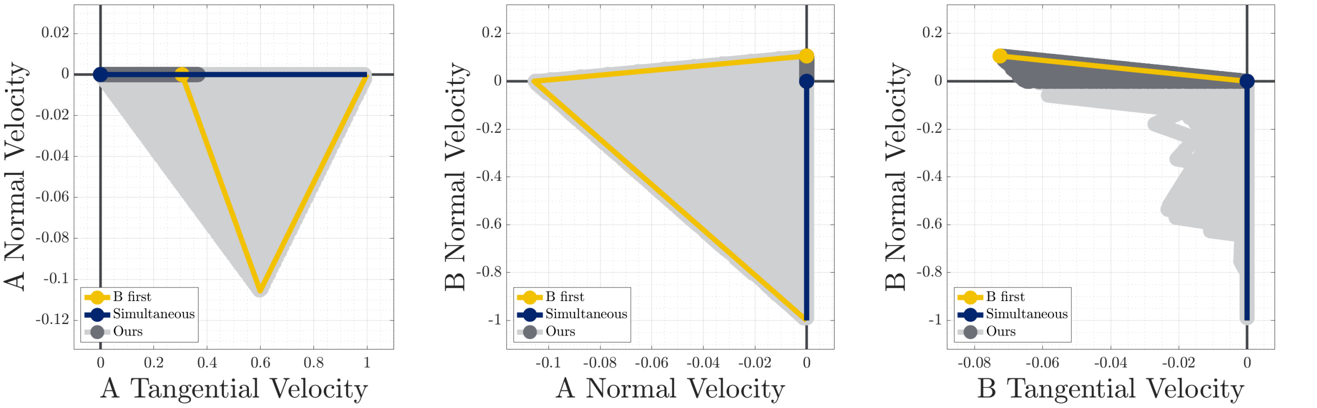

Figure 8. Evolution of the box-wall impact. The center plot compares the normal velocities of the two contacts, while the left and right show velocities of points A and B, respectively. Our model produces both the simultaneous and sequential outcome in Figure 5, as well as all reasonable intermediate velocities where A still slides and B lifts off. Furthermore, results are also generated where B slides instead of sticking or lifting off.

and sequential outcomes. During the entire impact process, our LCP always selects stiction at both contacts. Our model has the additional capability to temporarily reduce only the vertical component of $\boldsymbol{v}$ by evenly applying impulse at each contact. As a result, it can additionally generate scaled-down versions of the sequential outcomes (i.e., rolling on one foot with a smaller angular velocity).

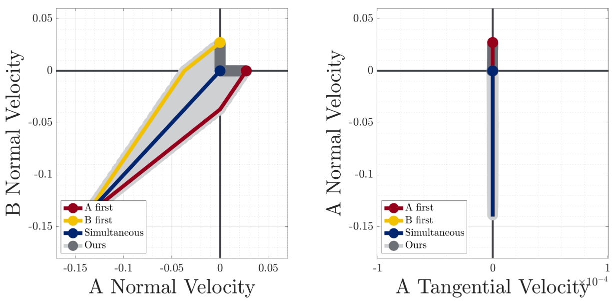

Figure 9. Evolution of the phone-drop impact. The left plot compares the normal velocities of the two contacts, while the right shows both normal and tangential velocity of point A. Point B's trajectory is omitted, as system symmetry makes it identical to that of point A. Our method generates the three outcomes depicted in Figure 1, as well as intermediate velocities between the symmetric and sequential impacts.

6.2 Compass Gait

We now analyze the outcomes of the compass gait walker model taking a wide step, as originally described in Figure 4. Previously, we shoed that the model of Anitescu and Potra (1997) always predicts that the leading foot sticks (point A), while the trailing foot (point B) could slide, stick, or lift off. As shown in Figure 7, for the compass gait step, our method generates each of these outcomes, as well as various convex combinations of these results. However, the model is also capable of generating oscillatory behavior where impulses at points A and B alternate during the impact process. This can potentially cause A to lift off, and B to remain on the ground instead.

6.3 Box and Wall

We examine our model's predictions on the scenario described in Figure 5, where a box impacts a wall (at point B) while sliding along flat ground (at point A). The model of Anitescu and Potra (1997) predicted an outcome where the box came to rest, and another where A continues sliding and B lifts off. As in the previous examples, our model reproduces both behaviors, as well as convex combinations of them (Figure 8). Additionally, some sequences allow A to slide even faster, while others allow B to slide instead of lifting or sticking.

6.4 RAMone

In this example, we examine a footfall event on a considerably more complex walking robot: a 5-link model of RAMone, the parameters of which are described in detail in Remy (2017). As shown in Figure 10, much like the compass gait example, Anitescu and Potra (1997) always predicts that the leading foot sticks, while the trailing foot can stick, slide, or lift. Our model reproduces the same results, as well as ones where the final contact velocities are scaled down.

6.5 Disk Stacking

In this example, we demonstrate our ability to generate non-unique results in a multi-object scenario motivated by manipulation: stacking disks. A tower of 3 discs (Figure 11) is created by dropping a disk on two others, which rest on the ground. The only prediction offered for this 5-contact collision offered by Anitescu and Potra (1997) is the entire tower coming to rest. While we cannot be sure that the numerical results cover all possible outputs of our model, we are able to generate various outcomes in which the tower falls apart. Figure 11b shows how the post-impact normal velocities compare in the left and right sides of the tower. The top ball always maintains contact with at least one of the left or right balls, and one of those balls always stays on the ground. The contacts that are maintained may slide, while the ball on the opposite side may even lift off the ground (Figure 11c).

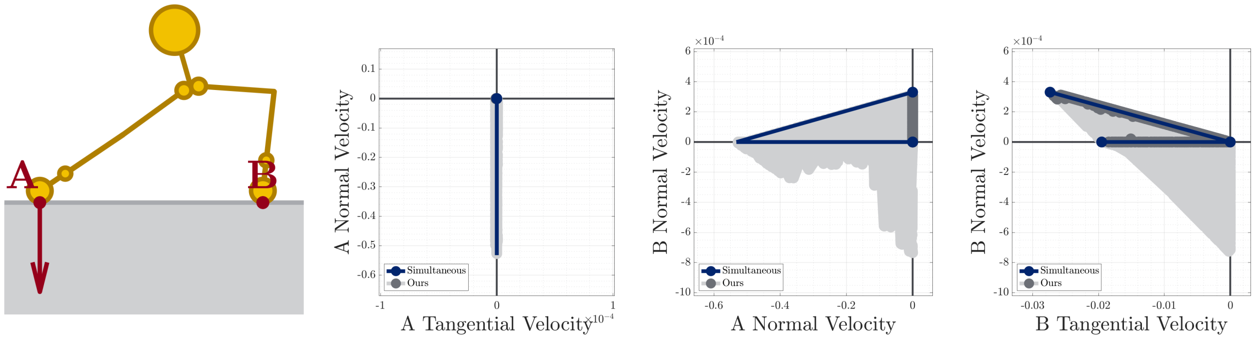

(a) RAMone initial condition **(b)** Footfall impact resolution process

Figure 10. Evolution of a footfall (a) of the RAMone robot. (b) Similar to the compass gait example, Anitescu and Potra (1997) predicts that the leading foot, point A, comes to rest, while point B may come to rest, slide, or lift off. All results from our model produce intermediate outcomes between these three results, and point A remains in stiction for the entire duration of the impact.

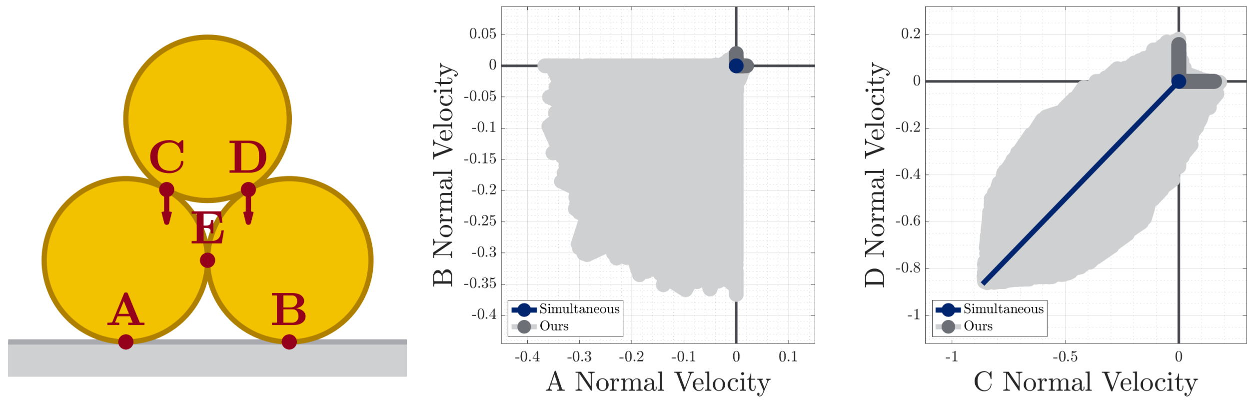

(a) Disk stack initial condition **(b)** Normal impact resolution process comparing left and right sides

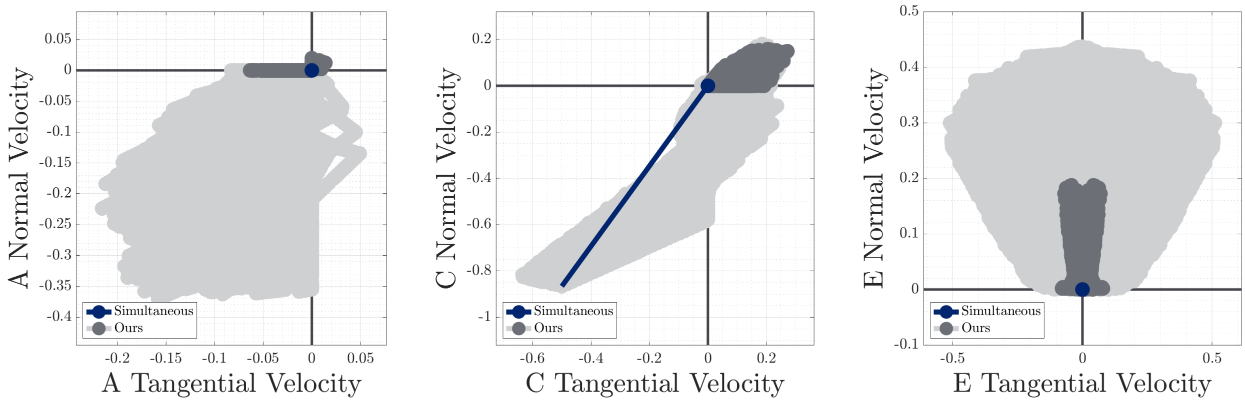

(c) Impact resolution process at individual contact points

Figure 11. Evolution of a stack of discs (a) as the top disk fall on the bottom two. Anitescu and Potra (1997) only predicts that the entire system comes to rest. (b) Our method additional predicts several scenarios where the top disk remains in contact with only one of the bottom two disks, while the other may roll away or even lift off the ground slightly. (c) various states of rolling, sliding, and lifting contact are shown for points A, C, and E; plots for B and D are omitted as they are symmetric with A and C, respectively.

7 Conclusion

Non-unique behavior is a pervasive complexity that is present in both real-world robotic systems and common models capturing frictional impacts between rigid bodies—and thus accurate incorporation of such phenomena is an essential component of robust planning, control, and estimation algorithms. Our model presents a state-of-the-art theoretical foundation for capturing these set-valued outcomes. Despite the high versatility of allowing impacts to resolve at arbitrary relative rates, both the continuous-time formulation and simulation method have termination guarantees.

Future development of our model will focus on capturing a wider array of contact-driven behaviors; improved theoretical guarantees; and more efficient computational approaches. For instance, while may models in robotics assume impacts are inelastic, capturing restitution would increase the accuracy of our model for some robotic systems. Additionally, while approximation of the post-impact set is probabilistically complete, there is currently no available method to compute the necessary bounds. Furthermore, in practice, the bounds were not tight enough to inform tractable computation in our examples. Future research could develop outer approximations of the post-impact set via Lyapunov-based reachability and sum-of-squares programming (Posa et al. 2016).

Funding

The authors disclosed receipt of the following financial support for the research, authorship, and/or publication of this article: This work was supported by the National Science Foundation under Grant No. CMMI-1830218, and an NSF Graduate Research Fellowship under Grant No. DGE-1845298.

Notes

1. `https://github.com/mshalm/routh-multi-impact`

References

M Anitescu and F A Potra. Formulating dynamic multi-rigid-body contact problems with friction as solvable linear complementarity problems. *Nonlinear Dynamics*, 14(3): 231–247, 1997.

Youcef Askoura. About extension of upper semicontinuous multi-valued maps and applications. *International Journal of Mathematical Analysis*, 3, 11 2008.

Jean-Pierre Aubin and Arrigo Cellina. *Differential Inclusions: Set-Valued Maps and Viability Theory (Grundlehren Der Mathematischen Wissenschaften)*. Springer Verlag, 1984. ISBN 0387131051.

Alp Aydinoglu, Victor M. Preciado, and Michael Posa. Stabilization of complementarity systems via contact-aware controllers, 2020.

V Bhatt and J Koechling. Three-dimensional frictional rigid-body impact. *Journal of Applied Mechanics*, 62:893, 1995.

B Brogliato. *Nonsmooth mechanics: models, dynamics, and control*. Springer Verlag, 1999.

Samuel A. Burden, S. Shankar Sastry, Daniel E. Koditschek, and Shai Revzen. Event–Selected Vector Field Discontinuities Yield Piecewise–Differentiable Flows. *SIAM Journal on Applied Dynamical Systems*, 15(2):1227–1267, jan 2016. ISSN 1536-0040. doi: 10.1137/15M1016588. URL `http://epubs.siam.org/doi/10.1137/15M1016588`.

A Chatterjee and A Ruina. A New Algebraic Rigid-Body Collision Law Based on Impulse Space Considerations. *Journal of Applied Mechanics*, 65(4):939–951, 1998.

Anindya Chatterjee. *Rigid Body Collisions: Some General Considerations, New Collision Laws, and Some Experimental Data*. PhD thesis, Cornell University, 7 1997.

Anindya Chatterjee. On the realism of complementarity conditions in rigid body collisions. *Nonlinear Dynamics*, 20(2):159–168, 1999. doi: 10.1023/a:1008397905242.

Nikhil Chavan-Dafle and Alberto Rodriguez. Stable Prehensile Pushing: In-Hand Manipulation with Alternating Sticking Contacts. oct 2017. URL `http://arxiv.org/abs/1710.11097`.

Richard W Cottle, Jong-Shi Pang, and Richard E Stone. *The linear complementarity problem*, volume 60. Siam, 2009.

Erwin Coumans and Erwin. Bullet physics simulation. In *ACM SIGGRAPH*, page 1, New York, New York, USA, 2015. ACM Press. ISBN 9781450336345. doi: 10.1145/2776880.2792704. URL `http://dl.acm.org/citation.cfm?doid=2776880.2792704`.

Steven P. Dirkse and Michael C. Ferris. The path solver: a nonmonotone stabilization scheme for mixed complementarity problems. *Optimization Methods and Software*, 5(2):123–156, 1995.

Evan Drumwright and Dylan A. Shell. Modeling Contact Friction and Joint Friction in Dynamic Robotic Simulation Using the Principle of Maximum Dissipation. pages 249–266. Springer, Berlin, Heidelberg, 2010. doi: 10.1007/978-3-642-17452-0_15. URL `http://link.springer.com/10.1007/978-3-642-17452-0{_}15`.

Francisco Facchinei and Jong-Shi Pang. *Finite-dimensional variational inequalities and complementarity problems*. Springer, New York, 2003. ISBN 978-0387955803.

Nima Fazeli, Samuel Zapolsky, Evan Drumwright, and Alberto Rodriguez. Fundamental Limitations in Performance and Interpretability of Common Planar Rigid-Body Contact Models. 2017. URL `https://arxiv.org/pdf/1710.04979.pdf`.

Ch. Glocker and F. Pfeiffer. Multiple impacts with friction in rigid multibody systems. *Nonlinear Dynamics*, 7(4):471–497, jun 1995. ISSN 0924-090X. doi: 10.1007/BF00121109. URL `http://link.springer.com/10.1007/BF00121109`.

Mathew Halm and Michael Posa. A Quasi-static Model and Simulation Approach for Pushing, Grasping, and Jamming. In *To appear in the Workshop on the Algorithmic Foundations of Robotics (WAFR)*, 2018.

Mathew Halm and Michael Posa. Modeling and Analysis of Non-unique Behaviors in Multiple Frictional Impacts. In *Robotics: Science and Systems*, 2019. URL `http://arxiv.org/abs/1902.01462`.

Francois Robert Hogan and Alberto Rodriguez. Feedback Control of the Pusher-Slider System: A Story of Hybrid and Underactuated Contact Dynamics. nov 2016. URL `http://arxiv.org/abs/1611.08268`.

Peter C. Horak and Jeff C. Trinkle. On the Similarities and Differences Among Contact Models in Robot Simulation. *IEEE Robotics and Automation Letters*, 4(2):493–499, apr 2019. ISSN 2377-3766. doi: 10.1109/LRA.2019.2891085. URL `https://ieeexplore.ieee.org/document/8603801/`.

Yildirim Hurmuzlu and Dan B. Marghitu. Rigid Body Collisions of Planar Kinematic Chains With Multiple Contact Points. *The International Journal of Robotics Research*, 13(1):82–92, feb 1994. ISSN 0278-3649. doi: 10.1177/027836499401300106. URL `http://journals.sagepub.com/doi/10.1177/027836499401300106`.

A.P Ivanov. On multiple impact. *Journal of Applied Mathematics and Mechanics*, 59(6):887–902, jan 1995. ISSN 0021-8928. doi: 10.1016/0021-8928(95)00122-0. URL https://www.sciencedirect.com/science/article/pii/0021892895001220.

Aaron M Johnson, Jennifer E King, and Siddhartha Srinivasa. Convergent planning. *IEEE Robotics and Automation Letters*, 1(2):1044–1051, 2016.

Sertac Karaman and Emilio Frazzoli. Sampling-based algorithms for optimal motion planning. *The International Journal of Robotics Research*, 30(7):846–894, 2011. doi: 10.1177/0278364911406761. URL https://doi.org/10.1177/0278364911406761.

Danny M Kaufman, Shinjiro Sueda, Doug L James, and Dinesh K Pai. Staggered projections for frictional contact in multibody systems. In *ACM Transactions on Graphics (TOG)*, volume 27, page 164. ACM, 2008.

Charles Kemp, Aaron Edsinger, and Eduardo Torres-Jara. Challenges for robot manipulation in human environments [Grand Challenges of Robotics]. *IEEE Robotics & Automation Magazine*, 14(1):20–29, mar 2007. ISSN 1070-9932. doi: 10.1109/MRA.2007.339604. URL http://ieeexplore.ieee.org/document/4141029/.

Igor Mordatch, Kendall Lowrey, and Emanuel Todorov. Ensemble-CIO: Full-body dynamic motion planning that transfers to physical humanoids. In *Intelligent Robots and Systems (IROS), 2015 IEEE/RSJ International Conference on*, pages 5307–5314. IEEE, 2015.

Michael Posa, Cecilia Cantu, and Russ Tedrake. A direct method for trajectory optimization of rigid bodies through contact. *The International Journal of Robotics Research (IJRR)*, 33(1): 69–81, 2014. URL https://posa.seas.upenn.edu/wp-content/uploads/Posa14.pdfhttp://ijr.sagepub.com/content/33/1/69.shorthttps://www.dropbox.com/s/a26rzvil81am4l8/ijrr_compressed.avi?dl=0.

Michael Posa, Mark Tobenkin, and Russ Tedrake. Stability analysis and control of rigid-body systems with impacts and friction. *IEEE Transactions on Automatic Control (TAC)*, 61 (6):1423–1437, 2016.

C David Remy. Ambiguous collision outcomes and sliding with infinite friction in models of legged systems. *The International Journal of Robotics Research*, 36(12): 1252–1267, oct 2017. ISSN 0278-3649. doi: 10.1177/0278364917731820. URL http://journals.sagepub.com/doi/10.1177/0278364917731820.

R. Tyrrell Rockafellar. *Convex Analysis*. Princeton University Press, 1970. ISBN 9780691015866. URL http://www.jstor.org/stable/j.ctt14bs1ff.

E J Routh. *Dynamics of a system of rigid bodies*. MacMillan and co. London, 1891.

Walter Rudin. *Real and Complex Analysis*. McGraw-Hill Education, 1986. ISBN 0070542341.

Walter Rudin. *Functional Analysis*. McGraw-Hill Science/Engineering/Math, 1991. ISBN 0070542368.

Seyed Sina Mirrazavi Salehian and Aude Billard. A Dynamical-System-Based Approach for Controlling Robotic Manipulators During Noncontact/Contact Transitions. *IEEE Robotics and Automation Letters*, 3(4):2738–2745, oct 2018. ISSN 2377-3766. doi: 10.1109/LRA.2018.2833142. URL https://ieeexplore.ieee.org/document/8354896/.

Vlad Seghete and Todd D. Murphey. A Propagative Model of Simultaneous Impact: Existence, Uniqueness, and Design Consequences. *IEEE Transactions on Automation Science and Engineering*, 11(1):154–168, jan 2014. ISSN 1545-5955. doi: 10.1109/TASE.2013.2267731. URL http://ieeexplore.ieee.org/document/6572900/.

Breannan Smith, Danny M. Kaufman, Etienne Vouga, Rasmus Tamstorf, and Eitan Grinspun. Reflections on simultaneous impact. *ACM Transactions on Graphics*, 31(4):1–12, jul 2012. ISSN 07300301. doi: 10.1145/2185520.2185602. URL http://dl.acm.org/citation.cfm?doid=2185520.2185602.

Ilya M. Sobol. On the distribution of points in a cube and the approximate evaluation of integrals. *USSR Computational Mathematics and Mathematical Physics*, 7(4):86 – 112, 1967. ISSN 0041-5553. doi: https://doi.org/10.1016/0041-5553(67)90144-9. URL http://www.sciencedirect.com/science/article/pii/0041555367901449.

David Stewart and J. C. Trinkle. An Implicit Time-Stepping Scheme for Rigid Body Dynamics with Coulomb Friction. *International Journal for Numerical Methods in Engineering*, 39(15):2673—-2691, 1996. URL http://citeseerx.ist.psu.edu/viewdoc/summary?doi=10.1.1.61.1260.

David E. Stewart. *Rigid-Body Dynamics with Friction and Impact*, volume 42. jan 2000. ISBN 0036144599360. doi: 10.1137/S0036144599360110. URL http://epubs.siam.org/doi/abs/10.1137/S0036144599360110.

D. Stoianovici and Y. Hurmuzlu. A critical study of the applicability of rigid-body collision theory. *Journal of Applied Mechanics*, 63(2):307–316, June 1996. doi: 10.1115/1.2788865. URL https://doi.org/10.1115/1.2788865.

W J Stronge. Rigid body collisions with friction. *Proceedings of the Royal Society of London. Series A: Mathematical and Physical Sciences*, 431(1881):169–181, 1990.

Thomas K Uchida, Michael A Sherman, and Scott L Delp. Making a meaningful impact: modelling simultaneous frictional collisions in spatial multibody systems. *Proceedings of the Royal Society of London A: Mathematical, Physical and Engineering Sciences*, 471(2177):20140859–20140859, 2015. ISSN 1364-5021. doi: 10.1098/rspa.2014.0859. URL http://rspa.royalsocietypublishing.org/content/471/2177/20140859.abstract.

Y.-T. Wang, V. Kumar, and J. Abel. Dynamics of rigid bodies undergoing multiple frictional contacts. In *Proceedings 1992 IEEE International Conference on Robotics and Automation*, pages 2764–2769. IEEE Comput. Soc. Press, 1992. ISBN 0-8186-2720-4. doi: 10.1109/ROBOT.1992.220016. URL http://ieeexplore.ieee.org/document/220016/.

Pierre-Brice Wieber, Russ Tedrake, and Scott Kuindersma. Modeling and Control of Legged Robots. In *Springer Handbook of Robotics*, pages 1203–1234. Springer International Publishing, Cham, 2016. doi: 10.1007/978-3-319-32552-1_48. URL http://link.springer.com/10.1007/978-3-319-32552-1{_}48.

A Notation

Here, we include a summary of the notation used in this paper in Table 2.

Table 2. Frequently-used constants and operations on sets A, A_i, A', B, scalars c, vectors $\boldsymbol{v}, \boldsymbol{w}$, matrices $\boldsymbol{M}, \boldsymbol{N}$, and functions $f : A \to B$, $\boldsymbol{g}(t) : \mathbb{R} \to \mathbb{R}^n$, $D : A \to \mathbb{P}(B)$. For notational brevity, we frequently write a singleton set $\{a\}$ without braces.

Expression	Meaning
A^c	complement of A
$\mathrm{int}(A)$	interior of A
$\mathrm{cl}(A)$	closure of A
$\mathrm{co}(A)$	convex hull of A
$\mathbb{P}(A)$	power set of A
$\boldsymbol{M}A$	scaled set, $\{\boldsymbol{M}a : a \in A\}$
$-A$	$(-1)A$
$A + B$	Minkowski sum of A and B
$A - B$	Minkowski sum of A and $-B$
$[A_1; \ldots A_k]$	Cartesian product $A_1 \times \cdots \times A_k$
$f(A')$	image of $A' \subseteq A$, $\cup_{a' \in A'} \{f(a')\} \subseteq B$
$D(A')$	image of $A' \subseteq A$, $\cup_{a' \in A'} D(a') \subseteq B$
$\dot{\boldsymbol{g}}(t)$	total (Lebesgue) derivative of $\boldsymbol{g}$
$\boldsymbol{M}_i$	ith row of $\boldsymbol{M}$
$\boldsymbol{v}_i$	ith element of $\boldsymbol{v}$
$\sigma_{max}(\boldsymbol{M})$	maximum singular value of $\boldsymbol{M}$
$\sigma_{min}(\boldsymbol{M})$	minimum singular value of $\boldsymbol{M}$
$\boldsymbol{M} \succ \boldsymbol{N}$	$\boldsymbol{M} - \boldsymbol{N}$ is positive definite
$\boldsymbol{M} \succeq \boldsymbol{N}$	$\boldsymbol{M} - \boldsymbol{N}$ is positive semi-definite
$\boldsymbol{v} > \boldsymbol{w}$	$\boldsymbol{v}_i > \boldsymbol{w}_i$ for each i
$\boldsymbol{v} \geq \boldsymbol{w}$	$\boldsymbol{v}_i \geq \boldsymbol{w}_i$ for each i
$A > 0$	each element of A is positive
$A \geq 0$	each element of A is non-negative
$\|\boldsymbol{A}\|_F$	Frobenius norm of A
$\|\boldsymbol{v}\|_p$	l_p norm of $\boldsymbol{v}$ for $p > 0$
$\|\boldsymbol{v}\|_{\boldsymbol{M}}$	norm, $\sqrt{\boldsymbol{v}^T\boldsymbol{M}\boldsymbol{v}}$, induced by $\boldsymbol{M} \succ \boldsymbol{0}$
$\widehat{\boldsymbol{v}}$	unit direction, $\frac{\boldsymbol{v}}{\|\boldsymbol{v}\|_2}$, of $\boldsymbol{v} \neq \boldsymbol{0}$
$\mathrm{Ball}(c)$	c-radius open ball, $\left\{\boldsymbol{v} : \|\boldsymbol{v}\|_2 < c\right\}$
$\boldsymbol{1}$	matrix/vector kl; m,of all 1's
$\boldsymbol{0}$	matrix/vector of all 0's
$\mathbb{R}^{n+}$	n-dimensional positive vectors

B Example Details

Here, we list relevant details on the examples in Section 6. The code may be run by downloading the MATLAB codebase[†] and running `Results()`. To run the results, the PATH LCP solver (Dirkse and Ferris 1995) must be installed, and `pathlcp.m` must be available from the MATLAB path. All geometric, inertial, and simulation quantities necessary for construction of the examples are listed in Tables 3–7, and the listed symbols match the variable names used int he codebase. For the RAMone example, we refer the reader to Remy (2017) for a full description of the system's inertial and geometric properties. Unless otherwise stated, all objects have uniform density and zero mass.

C Background Proofs

C.1 Proof of Proposition 4

Let $g(x) : \mathbb{R}^n \to \mathbb{R}^m$ be Lipschitz continuous with constant L and let $h > 0$. Let $\mathcal{X} = \{x_1, \ldots, x_N\}$ be a set of N uniform i.i.d. samples from $[0, h]^n$. We first note that that

Table 3. Geometric, inertial, and simulation parameters for the phone drop example

Parameter	Symbol	Value
Phone width	a	$7.444\,\mathrm{cm}$
Phone height	b	$16.094\,\mathrm{cm}$
Phone mass	m	$190\,\mathrm{g}$
Init. downward velocity	v_0	$14.01\,\mathrm{cm\,s^{-1}}$
Friction coefficient	μ	1
Step size	h	$0.3\,\mathrm{N\,s}$
Trajectory length	N	10
Number of trajectories	M	2^{14}

Table 4. Geometric, inertial, and simulation parameters for the compass gait example

Parameter	Symbol	Value
Leg length	l	$1\,\mathrm{m}$
Mass-to-foot length	$s_{\|}$	$0.5\,\mathrm{m}$
Leg mass	m	$1\,\mathrm{kg}$
Trailing leg pitch	φ_{tr}	78°
Leading leg pitch	φ_{le}	-78°
Trailing leg init. angular velocity	$\dot{\varphi}_{tr,0}$	$0.5\,\mathrm{rad\,s^{-1}}$
Leading leg init. angular velocity	$\dot{\varphi}_{le,0}$	$0.5\,\mathrm{rad\,s^{-1}}$
Friction coefficient	μ	5
Step size	h	$1\,\mathrm{N\,s}$
Trajectory Length	N	5
Number of Trajectories	M	2^{20}

Table 5. Geometric, inertial, and simulation parameters for the box and wall example

Parameter	Symbol	Value
Box side length	w	$1\,\mathrm{m}$
Box mass	m	$1\,\mathrm{kg}$
Angle box and ground	θ	10°
Init. horizontal velocity	v_0	$1\,\mathrm{m\,s^{-1}}$
Friction coefficient	μ	1
Step size	h	$2\,\mathrm{N\,s}$
Trajectory Length	N	5
Number of Trajectories	M	2^{18}

Table 6. Geometric, inertial, and simulation parameters for the RAMone example

Parameter	Symbol	Value
Trunk pitch	Φ	16°
Leading hip angle	α_{le}	-70°
Trailing hip angle	α_{tr}	70°
Leading knee angle	β_{le}	-2°
Trailing knee angle	β_{tr}	-92.48°
Trunk init. horizontal velocity	$\dot{x}_0$	$-0.4114\,\mathrm{m\,s^{-1}}$
Trunk init. vertical velocity	$\dot{y}_0$	$-0.2105\,\mathrm{m\,s^{-1}}$
Trunk init. angular velocity	$\dot{\Phi}_0$	$1\,\mathrm{rad\,s^{-1}}$
Leading hip init. velocity	$\dot{\alpha}_{le,0}$	0°
Trailing hip init. velocity	$\dot{\alpha}_{tr,0}$	0°
Leading knee init. velocity	$\dot{\beta}_{le,0}$	0°
Trailing knee init. velocity	$\dot{\beta}_{tr,0}$	0°
Friction coefficient	μ	10^5
Step size	h	$1\,\mathrm{N\,s}$
Trajectory Length	N	10
Number of Trajectories	M	2^{20}

[†] `https://github.com/mshalm/routh-multi-impact`

Table 7. Geometric, inertial, and simulation parameters for the disk stacking example

Parameter	Symbol	Value
Disk radius	R	$1\,\mathrm{m}$
Disk mass	m	$1\,\mathrm{kg}$
Initial vertical velocity	v_0	$-1\,\mathrm{m\,s^{-1}}$
Friction coefficient	μ	$\sqrt{3}$
Step size	h	$1\,\mathrm{N\,s}$
Trajectory Length	N	10
Number of Trajectories	M	2^{20}

$\|g(x)-g(x')\|_2 \leq L\|x-x'\|_2$. Therefore, $g(\mathcal{X})$ is a ε-net of $g([0,h]^n)$ if $\mathcal{X}$ is an $\frac{\varepsilon}{L}$-net of $[0,h]^n$; we will bound probability on the latter.

Consider the following set, a regularly-spaced grid of cardinality M^n:

$$\mathcal{X}' = \left\{\frac{h}{2M}, \frac{3h}{2M}, \dots, \frac{(2M-1)h}{2M}\right\}^n . \tag{104}$$

$\mathcal{X}'$ is by construction a $\frac{h\sqrt{n}}{2M}$-net of $[0,h]^n$d. Thus, setting $M = \left\lceil \frac{hL\sqrt{n}}{\varepsilon}\right\rceil$, $\mathcal{X}'$ is an $\frac{\varepsilon}{2L}$-net of $[0,h]^n$. Consider the case where $\mathcal{X}$ contained a close approximation of the entire grid; that is, for each $x \in \mathcal{X}'$, $\mathcal{X}$ contains an x_i with

$$x_i \in x + \left[-\frac{h}{2M}, \frac{h}{2M}\right]^n \subseteq [0,h]^n , \tag{105}$$

and thus $\|x_i - x\|_2 \leq \frac{\varepsilon}{2L}$. Then by triangle inequality, $\mathcal{X}$ is an $\frac{\varepsilon}{L}$-net of $[0,h]^n$ when (105) holds for each x_i. For a single $x \in \mathcal{X}'$, as the elements of $\mathcal{X}$ are chosen uniform i.i.d, the probability of (105) *not* holding is

$$(1 - M^{-n})^N . \tag{106}$$

Then by union bound, the probability of (105) holding for every x is at least

$$1 - M^n(1-M^{-n})^N . \tag{107}$$

The proof holds as $M^{-n} = \Omega$.

C.2 Proof of Lemma 13

We may assume WLOG that $\boldsymbol{M} = \boldsymbol{I}$ by applying a coordinate transformation of $\boldsymbol{M}^{\frac{1}{2}}$ to $\boldsymbol{v}$. Let $\boldsymbol{R}$ be a matrix with columns that constitute an orthogonal basis of $\mathrm{Range}\left(\boldsymbol{J}_i^T\right)$. By equivalence of norms there exists $\varepsilon > 0$ such that

$$\|\boldsymbol{J}_{n,i}\boldsymbol{v}\| + \|\boldsymbol{J}_{t,i}\boldsymbol{v}\|_2 \geq \varepsilon \left\|\boldsymbol{R}^T\boldsymbol{v}\right\|_2 . \tag{108}$$

We will show that $S = (\varepsilon \min(\boldsymbol{\mu}_i, 1))^{-1}$ satisfies the claim. Let $V(s) = \left\|\boldsymbol{R}^T\boldsymbol{v}(s)\right\|_2^2$. Assume WLOG that $\boldsymbol{v}(s)$ is an impacting velocity (i.e. $\boldsymbol{v}(s) \in \mathcal{I}(\boldsymbol{q})$) at least until $s^* = \left\|\boldsymbol{R}^T\boldsymbol{v}(0)\right\|_2 S \leq \|\boldsymbol{v}(0)\|_2 S$. Then, on the interval $[0, s^*)$,

$$\begin{aligned}
\dot{V} &= 2\dot{\boldsymbol{v}}^T\boldsymbol{R}\boldsymbol{R}^T\boldsymbol{v} , & (109)\\
&\in 2\left(\boldsymbol{J}_{n,i} - \boldsymbol{\mu}_i \mathrm{Unit}\left(\boldsymbol{J}_{t,i}\boldsymbol{v}\right)^T \boldsymbol{J}_{t,i}\right)\boldsymbol{R}\boldsymbol{R}^T\boldsymbol{v} , & (110)\\
&= -2\|\boldsymbol{J}_{n,i}\boldsymbol{v}\| - 2\boldsymbol{\mu}_i\|\boldsymbol{J}_{t,i}\boldsymbol{v}\|_2 , & (111)\\
&\leq -2\varepsilon\min(\boldsymbol{\mu}_i, 1)\sqrt{V} , & (112)\\
&\leq -\frac{2}{S}\sqrt{V} . & (113)
\end{aligned}$$

The unique solution to the IVP $\dot{x} = -\frac{2}{S}\sqrt{x}$,

$$x(s) = \left(\sqrt{x(0)} - \frac{s}{S}\right)^2 , \tag{114}$$

therefore bounds V from above on $[0, s^*)$. Thus,

$$\begin{aligned}
V(s^*) &\leq \left(\sqrt{V(0)} - \frac{s^*}{S}\right)^2 , & (115)\\
&= \left(\left\|\boldsymbol{R}^T\boldsymbol{v}(s^*)\right\|_2 - \frac{S\left\|\boldsymbol{R}^T\boldsymbol{v}(s^*)\right\|_2}{S}\right)^2 , & (116)\\
&= 0 . & (117)
\end{aligned}$$

Therefore $\boldsymbol{R}^T\boldsymbol{v}(s^*) = \boldsymbol{0}$, $\boldsymbol{J}_{n,i}\boldsymbol{v}(s^*) = 0$, and $\boldsymbol{v}(s^*) \notin \mathcal{I}(\boldsymbol{q})$.

D Impact Model Proofs

D.1 Proof of Lemma 14

The final claim may be reached via direct application of Theorem 1, as long as $D_{\boldsymbol{q}}(\boldsymbol{v})$ is non-empty, uniformly bounded, closed-valued, convex-valued, and u.s.c. We will demonstrate that each of these properties hold.

We first observe that the set of contacts $C_{\boldsymbol{q}}(\boldsymbol{v})$, used in the construction of $D_{\boldsymbol{q}}(\boldsymbol{v})$ in (54), is non-empty by construction. Furthermore, $C_{\boldsymbol{q}}(\boldsymbol{v})$ is u.s.c. in $\boldsymbol{v}$, because it is constructed from non-strict inequalities of linear functions of $\boldsymbol{v}$. Next, we note that for each i, $F_{\boldsymbol{q},i}(\boldsymbol{v})$ is non-empty, uniformly bounded, closed-valued, and u.s.c. as it is an affine transformation of $\mathrm{Unit}(\cdot)$. Finally, we characterize $D_{\boldsymbol{q}}(\boldsymbol{v})$. $D_{\boldsymbol{q}}(\boldsymbol{v})$ is non-empty, uniformly bounded, and close-convex valued, because it is constructed from the convex hull of a non-zero number of the sets $F_{\boldsymbol{q},i}(\boldsymbol{v})$. Now, consider an arbitrary velocity $\boldsymbol{v}_0$ and neighborhood $\dot{\mathcal{V}}_0 \supset D_{\boldsymbol{q}}(\boldsymbol{v}_0)$. As $C_{\boldsymbol{q}}(\boldsymbol{v})$ is u.s.c., we can select a neighborhood $\mathcal{V}$ with $C_{\boldsymbol{q}}(\mathcal{V}) \subseteq C_{\boldsymbol{q}}(\boldsymbol{v}_0)$. Therefore on $\mathcal{V}$,

$$D_{\boldsymbol{q}}(\boldsymbol{v}) \subseteq D_0(\boldsymbol{v}) = \mathrm{co}\left(\cup_{i\in C_{\boldsymbol{q}}(\boldsymbol{v}_0)} F_{\boldsymbol{q},i}(\boldsymbol{v})\right) . \tag{118}$$

$D_0(\boldsymbol{v})$ is u.s.c. by its construction from a convex hull of u.s.c. functions, and furthermore $D_{\boldsymbol{q}}(\boldsymbol{v}_0) = D_0(\boldsymbol{v}_0)$. Therefore by definition of u.s.c. there exists a neighborhood $\mathcal{V}_0$ of $\boldsymbol{v}_0$ such that

$$D_{\boldsymbol{q}}(\mathcal{V}_0) \subseteq D_0(\mathcal{V}_0) \subseteq \dot{\mathcal{V}}_0 . \tag{119}$$

$D_{\boldsymbol{q}}(\mathcal{V})$ is therefore by definition u.s.c. and the claim is satified.

D.2 Proof of Lemma 15

Consider a configuration $\boldsymbol{q} \in \mathbb{R}^{n_q}$ and compact interval $[a,b]$.

We first demonstrate that the impact differential inclusion mapping $D_{\boldsymbol{q}}(\boldsymbol{v})$ is positively homogeneous in $\boldsymbol{v}$. Consider a velocity $\boldsymbol{v}$ and $k > 0$. As the function $\mathrm{Unit}(\cdot)$ is positively homogeneous, by its definition (47), $F_{\boldsymbol{q},i}(\boldsymbol{v})$ is positively homogeneous:

$$\begin{aligned}
F_{\boldsymbol{q},i}(\boldsymbol{v}) &= \boldsymbol{M}^{-1}\left(\boldsymbol{J}_{n,i}^T - \boldsymbol{\mu}\boldsymbol{J}_{t,i}^T\mathrm{Unit}\left(\boldsymbol{J}_{t,i}\boldsymbol{v}\right)\right) & (120)\\
&= \boldsymbol{M}^{-1}\left(\boldsymbol{J}_{n,i}^T - \boldsymbol{\mu}\boldsymbol{J}_{t,i}^T\mathrm{Unit}\left(\boldsymbol{J}_{t,i}k\boldsymbol{v}\right)\right) & (121)\\
&= F_{\boldsymbol{q},i}(k\boldsymbol{v}) . & (122)
\end{aligned}$$

Furthermore, we observe that the set of contacts $C_{\boldsymbol{q}}(\boldsymbol{v})$, used in the construction of $D_{\boldsymbol{q}}(\boldsymbol{v})$ in (54), is also positively homogeneous in $\boldsymbol{v}$. Therefore, $D_{\boldsymbol{q}}(\boldsymbol{v})$ is positively homogeneous.

We now prove the final claim. Consider a solution $\boldsymbol{v}(s)$ to the impact DI $\dot{\boldsymbol{v}} \in D_{\boldsymbol{q}}(\boldsymbol{v})$ over $[a, b]$, and $k > 0$. The function $k\boldsymbol{v}(\frac{s}{k})$ is well-defined and absolutely continuous over the interval $[ka, kb]$, and has derivative equal to $\dot{\boldsymbol{v}}(\frac{s}{k})$ a.e. on $[ka, kb]$. Then $\dot{\boldsymbol{v}}(\frac{s}{k}) \in D_{\boldsymbol{q}}(\boldsymbol{v}(\frac{s}{k})) = D_{\boldsymbol{q}}(k\boldsymbol{v}(\frac{s}{k}))$ a.e., and $k\boldsymbol{v}(\frac{s}{k}) \in \mathrm{SOL}\,(D_{\boldsymbol{q}}, [ka, kb])$.

D.3 Proof of Lemma 16

Let $\boldsymbol{q} \in \mathcal{Q}_A$, and let $[a, b]$ be a compact interval. Consider a solution of the impact DI $\boldsymbol{v}(s) \in \mathrm{SOL}\,(D_{\boldsymbol{q}}, [a, b])$ with impact velocity ($\boldsymbol{v}([a, b]) \subseteq \mathrm{cl}\mathcal{I}(\boldsymbol{q})$). We will show that $\|\boldsymbol{v}(s)\|_{\boldsymbol{M}}$ is non-increasing by proving that $\dot{K}(\boldsymbol{q}, \boldsymbol{v}(s))$ is non-positive almost everywhere. Pick any $s \in [a, b]$ where $\dot{\boldsymbol{v}}(s) \in D_{\boldsymbol{q}}(\boldsymbol{v}(s))$. By construction of $D_{\boldsymbol{q}}(\boldsymbol{v})$ (54) and the definition of the convex hull, there exists coefficients $c_i \in [0, 1]$ for each impacting contact such that

$$\dot{\boldsymbol{v}}(s) \in \sum_{i:\boldsymbol{J}_{n,i}\boldsymbol{v}(s)\leq 0} c_i F_{\boldsymbol{q},i}(\boldsymbol{v}(s))\,. \tag{123}$$

We observe that

$$\dot{K}(\boldsymbol{q}, \boldsymbol{v}(s)) \in \sum_{i:\boldsymbol{J}_{n,i}\boldsymbol{v}(s)\leq 0} c_i \boldsymbol{v}(s)^T \boldsymbol{M}(\boldsymbol{q}) F_{\boldsymbol{q},i}(\boldsymbol{v}(s))\,, \tag{124}$$

$\dot{K}$ is then non-positive as each term in this sum is non-positive by construction of $F_{\boldsymbol{q},i}(\boldsymbol{v})$:

$$\boldsymbol{v}(s)^T \boldsymbol{M}(\boldsymbol{q}) F_{\boldsymbol{q},i}(\boldsymbol{v}(s)) = \boldsymbol{v}(s)^T \boldsymbol{J}_{n,i}^T - \boldsymbol{\mu}_i \left\|\boldsymbol{J}_{t,i}\boldsymbol{v}(s)\right\|_2\,. \tag{125}$$

D.4 Proof of Theorem 17

Let $\boldsymbol{q} \in \mathcal{Q}_A$ be a configuration with active contact, and $\boldsymbol{v}(s) \in \mathrm{SOL}\,(D_{\boldsymbol{q}}, [a, b])$ a solution to the associated impact differential inclusion. We additionally assume that $\boldsymbol{v}(s)$ is non-constant, and that it remains in $\mathrm{cl}\mathcal{I}(\boldsymbol{q})$, the closure of the impacting velocities over the entire interval $[a, b]$. Let $\boldsymbol{\lambda}(s)$ be the associated vector of force variables.

We now prove the claim by showing that $\|\boldsymbol{v}(b)\|_{\boldsymbol{M}} < \|\boldsymbol{v}(a)\|_{\boldsymbol{M}}$; such behavior occurs because any change in $\boldsymbol{v}(s)$ must result from a strictly dissipative contact. As $\boldsymbol{v}(s)$ is continuous, we may select $a < s^* < b$ such that $\forall \delta > 0$, $\boldsymbol{v}(s)$ is non-constant on $[s^*, s^* + \delta]$. Let $A = \{i \in C_A(\boldsymbol{q}) : \boldsymbol{J}_{n,i}\boldsymbol{v}(s^*) \leq 0\}$ be the set of non-separating contacts at $s = s^*$. Let B be the set of contacts $b \in A$ with zero contact velocity ($\boldsymbol{J}_b\boldsymbol{v}(s^*) = \boldsymbol{0}$). As $\boldsymbol{v}(s)$ is continuous, $\exists\delta_\varepsilon > 0$ and $\varepsilon > 0$ such that $\forall s \in [s^*, s^* + \delta_\varepsilon] \subseteq [a, b]$,

- All contacts not in A are separating ($\boldsymbol{J}_{n,i}\boldsymbol{v}(s) > \varepsilon\,, \forall i \in C_A \setminus A$)
- All contacts $i \in A \setminus B$ are moving, with $\boldsymbol{J}_{n,i}\boldsymbol{v}(s) < -\varepsilon$ or $\|\boldsymbol{J}_{t,i}\boldsymbol{v}(s)\|_2 > \frac{1}{\boldsymbol{\mu}_i}\varepsilon$.

Select an s from $[s^*, s^* + \delta_\varepsilon]$ with $\boldsymbol{v}(s) \neq \boldsymbol{v}(s^*)$. By Lemma 16,

$$0 \geq \frac{1}{2}\|\boldsymbol{v}(s)\|_{\boldsymbol{M}}^2 - \frac{1}{2}\|\boldsymbol{v}(s^*)\|_{\boldsymbol{M}}^2\,, \tag{126}$$

$$= \boldsymbol{v}(s^*)^T \boldsymbol{M}\left(\boldsymbol{v}(s) - \boldsymbol{v}(s^*)\right) + \frac{1}{2}\|\boldsymbol{v}(s) - \boldsymbol{v}(s^*)\|_{\boldsymbol{M}}^2\,, \tag{127}$$

$$= \left(\boldsymbol{J}\boldsymbol{v}(s^*)\right)^T \boldsymbol{\Lambda}(s^*, s) + \frac{1}{2}\|\boldsymbol{v}(s) - \boldsymbol{v}(s^*)\|_{\boldsymbol{M}}^2\,. \tag{128}$$

Therefore, there must exist a contact $a \in A \setminus B$ that generates nonzero impulse $\|\boldsymbol{\Lambda}_a(s^*, s)\|_1 > 0$ as (128) is non-positive. Finally,

$$K(\boldsymbol{v}(s)) = K(\boldsymbol{v}(s^*)) + \int_{s^*}^{s} (\boldsymbol{J}\boldsymbol{v}(\tau))^T \boldsymbol{\lambda}_c(\tau)\mathrm{d}\tau\,, \tag{129}$$

$$\leq K(\boldsymbol{v}(s^*)) - \varepsilon||\boldsymbol{\Lambda}_a(s^*, s)||_1\,, \tag{130}$$

$$< K(\boldsymbol{v}(s^*))\,. \tag{131}$$

Therefore $\|\boldsymbol{v}\|_{\boldsymbol{M}}$ is non-constant.

D.5 Proof of Lemma 22

Suppose not, so there exists a configuration $\boldsymbol{q} \in \mathcal{Q}_A$, dissipation rate $\alpha_{\boldsymbol{q}}(s)$ such that $\dot{\boldsymbol{v}} \in D_{\boldsymbol{q}}(\boldsymbol{v})$ is $\alpha_{\boldsymbol{q}}(s)$-dissipative, $s > 0$ and $S > \|\boldsymbol{v}(0)\|_{\boldsymbol{M}} \frac{s}{\alpha_{\boldsymbol{q}}(s)}$, and $\boldsymbol{v}(s) \in \mathrm{SOL}\,(D_{\boldsymbol{q}}, [0, S])$ with $\boldsymbol{v}([0, S]) \subseteq \mathrm{cl}\mathcal{I}(\boldsymbol{q})$. Assume WLOG by Lemma 15 that $\|\boldsymbol{v}(0)\|_{\boldsymbol{M}} = 1$. As $\dot{\boldsymbol{v}} \in D_{\boldsymbol{q}}(\boldsymbol{v})$ is $\alpha_{\boldsymbol{q}}(s)$-dissipative, $\exists s_1 \in [0, s]$ such that $\|\boldsymbol{v}(s_1)\|_{\boldsymbol{M}} \leq 1 - \alpha_{\boldsymbol{q}}(s)$. A sequence $(s_k)_{k\in\mathbb{N}}$ can be iteratively constructed by Lemma 15 such that

$$s_k \in s_{k-1} + \left[0, s\left(1 - \alpha_{\boldsymbol{q}}(s)\right)^{k-1}\right] \subseteq \left[0, \frac{s}{\alpha_{\boldsymbol{q}}(s)}\right]\,, \tag{132}$$

$$\frac{\|\boldsymbol{v}(s_k)\|_{\boldsymbol{M}}}{\|\boldsymbol{v}(s_{k-1})\|_{\boldsymbol{M}}} \leq \left(1 - \alpha_{\boldsymbol{q}}(s)\right)\,. \tag{133}$$

Therefore $\exists s_\infty \in \left[0, \frac{s}{\alpha_C(s)}\right]$ with $s_n \to s_\infty < S$ and by continuity of $\boldsymbol{v}$, $\boldsymbol{v}(s_\infty) = \boldsymbol{0} \in \mathrm{cl}\mathcal{I}(\boldsymbol{q})$. But then by Theorem 19 $\|\boldsymbol{v}(s)\|_{\boldsymbol{M}}$ must decrease below 0 on $[s_\infty, S]$, a contradiction.

D.6 Proof of Theorem 23

Suppose not. Then there exists a $\boldsymbol{q} \in \mathcal{Q}_A \setminus \mathcal{Q}_P$, an $S > 0$ and a corresponding sequence of solutions $\left(\boldsymbol{v}^j(s)\right)_{j\in\mathbb{N}}$, $\boldsymbol{v}^j(s) \in \mathrm{SOL}\,(D_{\boldsymbol{q}}, [0, S])$, all starting with kinetic energy $\frac{1}{2}$ (i.e. $\left\|\boldsymbol{v}^j(0)\right\|_{\boldsymbol{M}} = 1$) and never exiting $\mathrm{cl}\mathcal{I}(\boldsymbol{q})$, which dissipate less and less energy:

$$\lim_{j\to\infty} \left\|\boldsymbol{v}^j(S)\right\|_{\boldsymbol{M}} = 1\,. \tag{134}$$

As $D_{\boldsymbol{q}}$ is bounded and each solution $\boldsymbol{v}^j(s)$ never exceeds kinetic energy $\frac{1}{2}$ (by Lemma 16), the sequence is equicontinuous and bounded. By Theorem 1, a subsequence of $\boldsymbol{v}^j(s)$ converges uniformly to a function $\boldsymbol{v}_\infty(s)$, and because kinetic energy is non-increasing, Lemma 16 implies $\|\boldsymbol{v}_\infty(s)\|_{\boldsymbol{M}} = 1$ for all $s \in [0, S]$. By Lemma 14 $\boldsymbol{v}_\infty(s)$ is a solution to the differential inclusion $\dot{\boldsymbol{v}} \in D_{\boldsymbol{q}}(\boldsymbol{v})$. Therefore as $\boldsymbol{v}_\infty(s)$ does not dissipate kinetic energy, it is constant by Theorem 17, and thus $\boldsymbol{0} \in D_{\boldsymbol{q}}(\boldsymbol{v}_\infty(s))$. But as each $\boldsymbol{v}^j(s) \in \mathrm{cl}\mathcal{I}(\boldsymbol{q})$, we must also have $\boldsymbol{v}_\infty(s) \in \mathrm{cl}\mathcal{I}(\boldsymbol{q})$, which contradicts Assumption 18.

D.7 Proof of Corollary 24

Let $\mathcal{Q} \subseteq \mathcal{Q}_A \setminus \mathcal{Q}_P$ be compact set of non-penetrating configurations with active contact. Let $S > 0$. Define the differential inclusion

$$\begin{bmatrix} \dot{\boldsymbol{q}} \\ \dot{\boldsymbol{v}} \end{bmatrix} = \dot{\boldsymbol{x}} \in D'(\boldsymbol{x}) = \begin{bmatrix} \mathbf{0} \\ D_{\boldsymbol{q}}(\boldsymbol{v}) \end{bmatrix} . \tag{135}$$

As C_A is u.s.c. and $\boldsymbol{M}, \boldsymbol{\phi}, \boldsymbol{J}$ are continuous, D' is compact-convex, uniformly bounded, and u.s.c.. Now consider the sets

$$\mathcal{X}_0 = \left\{ \begin{bmatrix} \boldsymbol{q}_0 \\ \boldsymbol{v}_0 \end{bmatrix} : \boldsymbol{q}_0 \in \mathcal{Q} \wedge \|\boldsymbol{v}_0\|_{\boldsymbol{M}(\boldsymbol{q}_0)} = 1 \right\} , \tag{136}$$

$$\mathcal{X}_S = \{\boldsymbol{x}(S) : \boldsymbol{x}(s) \in \mathrm{IVP}\,(D', \mathcal{X}_0, [0, S])\} . \tag{137}$$

$\mathcal{X}_0$ represents all initial conditions with configurations in $\mathcal{Q}$ and initial kinetic energy $\frac{1}{2}$, and $\mathcal{X}_S$ is set of states reachable from $\mathcal{X}_0$ via solutions to the dynamics (135) for a duration S. As $\mathcal{X}_0$ is compact, $\mathrm{IVP}\,(D', \mathcal{X}_0, [0, S])$ and therefore $\mathcal{X}_S$ is closed and non-empty by Proposition 8. Any solution $[\boldsymbol{q}(s);\ \boldsymbol{v}(s)] \in \mathrm{IVP}\,(D', \mathcal{X}_0, [0, S])$ must have constant $\boldsymbol{q}(s) = \boldsymbol{q}(0) \in \mathcal{Q}$, because the inclusion (135) prescribes $\dot{\boldsymbol{q}} = \mathbf{0}$. Therefore, $\boldsymbol{v}(s)$ must be a solution to the associated impact differential inclusion $\dot{\boldsymbol{v}} \in D_{\boldsymbol{q}(0)}(\boldsymbol{v})$. Therefore, by Theorem 23,

$$\alpha_{\mathcal{Q}}(S) = 1 - \max_{[\boldsymbol{q}_S;\ \boldsymbol{v}_S] \in \mathcal{X}_S} \|\boldsymbol{v}_S\|_{\boldsymbol{M}(\boldsymbol{q}_S)} \in (0, 1] . \tag{138}$$

Setting $\alpha_{\mathcal{Q}}(0) = 0$ and selecting an arbitrary configuration $\boldsymbol{q} \in \mathcal{Q}$, we now show that $\dot{\boldsymbol{v}} \in D_{\boldsymbol{q}}(\boldsymbol{v})$ is $\alpha_{\mathcal{Q}}(s)$-dissipative. Let $S > 0$, $\|\boldsymbol{v}_0\|_{\boldsymbol{M}(\boldsymbol{q})} = 1$, and $\boldsymbol{v}(s) \in \mathrm{IVP}\,(D_{\boldsymbol{q}}, \boldsymbol{v}_0, [0, S])$. By Definition 5, $\boldsymbol{x}(s) = [\boldsymbol{q};\ \boldsymbol{v}(s)] \in \mathrm{IVP}\,(D', \mathcal{X}_0, [0, S])$ and thus $\|\boldsymbol{v}(s)\|_{\boldsymbol{M}(\boldsymbol{q})} \leq 1 - \alpha_{\mathcal{Q}}(s) < 1$ for all $s \in [0, S]$.

E Continuous-time Model Proofs

E.1 Proof of Theorem 28

Let $[a, b]$ and $\bar{\mathcal{X}}$ be compact. As $D(\bar{\boldsymbol{x}})$ neither depends on $t(\bar{\boldsymbol{x}})$ nor s, WLOG $[a, b] = [0, S]$ and $t(\bar{\boldsymbol{x}}) = 0$ for each $\bar{\boldsymbol{x}} \in \bar{\mathcal{X}}$. We will prove that $\mathrm{IVP}\,(D, \bar{\boldsymbol{x}}, [0, S])$ has the claimed properties in the following manner:

1. We will bound kinetic energy growth (via Assumption 26), which will guarantee that solutions starting in $\bar{\mathcal{X}}$ remain in a larger compact set, $\bar{\mathcal{X}}'$.
2. We will show that, restricted to $\bar{\mathcal{X}}'$, $\dot{\bar{\boldsymbol{x}}} \in D(\bar{\boldsymbol{x}})$ is equivalent to another differential inclusion, $\dot{\bar{\boldsymbol{x}}} \in \tilde{D}(\bar{\boldsymbol{x}})$, which complies with the requirements of Theorem 1.

First, we construct a suitable $\bar{\mathcal{X}}'$. As $\bar{\mathcal{X}}$ is compact, we may pick $c > 0$ such that $\bar{\mathcal{X}} \subseteq \mathrm{Ball}_c$. Let $\bar{\boldsymbol{x}}(s) \in \mathrm{IVP}\left(D, \bar{\mathcal{X}}, [0, S]\right)$. We begin by establishing a bound on $\boldsymbol{v}(\bar{\boldsymbol{x}}(s))$ over $[0, S]$. Let $K(\bar{\boldsymbol{x}}) = K(\boldsymbol{q}(\bar{\boldsymbol{x}}), \boldsymbol{v}(\bar{\boldsymbol{x}}))$. By Assumption 26 and (15), $\exists c_K > 0$ such that for all $\bar{\boldsymbol{x}}$,

$$\frac{\partial K}{\partial \bar{\boldsymbol{x}}} D_C(\bar{\boldsymbol{x}}) = \boldsymbol{v}^T\left(\mathcal{U} - \boldsymbol{G}\right) \leq \sqrt{2} c_K \|\boldsymbol{v}\|_{\boldsymbol{M}} . \tag{139}$$

As the impact dynamics dissipate energy (Lemma 16), $\frac{\partial K}{\partial \bar{\boldsymbol{x}}} D_I(\bar{\boldsymbol{x}}) \leq 0$ and thus

$$\dot{K}(\bar{\boldsymbol{x}}(s)) \in \frac{\partial K}{\partial \bar{\boldsymbol{x}}} D(\bar{\boldsymbol{x}}) \leq 2 c_K \sqrt{K(\bar{\boldsymbol{x}})} . \tag{140}$$

Similar to the argument in Appendix C.2, we can compare (140) to the differential equation $\dot{x} = 2 c_K \sqrt{x}$, and upper bound K as

$$K(\boldsymbol{q}(s), \boldsymbol{v}(s)) \leq \left(\sqrt{K(\boldsymbol{q}(0), \boldsymbol{v}(0))} + c_K s\right)^2 . \tag{141}$$

The growth of $\|\boldsymbol{v}(s)\|_2$ can be similarly bounded; picking $c_{\boldsymbol{M}}$ such that $c_{\boldsymbol{M}}^{-1} \|\boldsymbol{v}\|_{\boldsymbol{M}} \leq \sqrt{2}\|\boldsymbol{v}\|_2 \leq c_{\boldsymbol{M}} \|\boldsymbol{v}\|_{\boldsymbol{M}}$,

$$\|\boldsymbol{v}(s)\|_2 \leq c_{\boldsymbol{M}} \sqrt{K(\boldsymbol{q}(s), \boldsymbol{v}(s))} , \tag{142}$$

$$\leq c_{\boldsymbol{M}} \left(\sqrt{K(\boldsymbol{q}(0), \boldsymbol{v}(0))} + c_K s\right) , \tag{143}$$

$$\leq c_{\boldsymbol{M}}^2 \|\boldsymbol{v}(0)\|_2 + c_{\boldsymbol{M}} c_K s . \tag{144}$$

Now, we bound $\boldsymbol{q}(\bar{\boldsymbol{x}}(s))$. Given that $\|\dot{\boldsymbol{q}}\|_2 \leq \|\boldsymbol{\Gamma}\|_F \|\boldsymbol{v}\|_2$, $\|\boldsymbol{q}(s)\|_2$ can be bounded by selecting $c_{\boldsymbol{\Gamma}} = \sup_{\boldsymbol{q}} \|\boldsymbol{\Gamma}\|_F$, and applying the triangle inequality:

$$\|\boldsymbol{q}(s)\|_2 \leq \|\boldsymbol{q}(0)\|_2 + c_{\boldsymbol{\Gamma}} s \max_{s' \in [0, s]} \|\boldsymbol{v}(s')\|_2 . \tag{145}$$

Finally, we bound $\|t(s)\| \leq s$ from $\dot{t} \leq 1$. As $\|\bar{\boldsymbol{x}}(0)\|_2 < c$,

$$\|\bar{\boldsymbol{x}}(s)\|_2 \leq \|\boldsymbol{q}(s)\|_2 + \|\boldsymbol{v}(s)\|_2 + \|t(s)\| , \tag{146}$$

$$\leq c + (c_{\boldsymbol{\Gamma}} s + 1)\left(c_{\boldsymbol{M}}^2 c + c_{\boldsymbol{M}} c_K s\right) + s . \tag{147}$$

Therefore, $\bar{\boldsymbol{x}}(s)$ does not exit $\bar{\mathcal{X}}' = \mathrm{clBall}_{c'}$, where

$$c' = c + (c_{\boldsymbol{\Gamma}} S + 1)\left(c_{\boldsymbol{M}}^2 c + c_{\boldsymbol{M}} c_K S\right) + S . \tag{148}$$

By Assumption 27 and element-wise application of Theorem 1 of Askoura (2008), there exists a bounded, non-empty, compact-convex valued u.s.c. function $\tilde{D}(\bar{\boldsymbol{x}})$ defined over $\mathbb{R}^n$ such that $\tilde{D}|_{\bar{\mathcal{X}}'} = D|_{\bar{\mathcal{X}}'}$. Therefore, by Theorem 1, $\mathrm{IVP}\left(\tilde{D}, \bar{\boldsymbol{x}}, [0, S]\right)$ is non-empty, closed under uniform convergence, and u.s.c. on $\bar{\mathcal{X}}$. As D and $\tilde{D}$ are locally equivalent, any solution $\bar{\boldsymbol{x}}(s)$ to $\dot{\bar{\boldsymbol{x}}} \in \tilde{D}(\bar{\boldsymbol{x}})$ that is fully contained in $\bar{\mathcal{X}}'$ is also a solution to $\dot{\bar{\boldsymbol{x}}} \in D(\bar{\boldsymbol{x}})$, and vice versa. As all solutions beginning on $\bar{\mathcal{X}}$ remain in $\bar{\mathcal{X}}'$ over $[0, S]$, $\mathrm{IVP}\left(\tilde{D}, \bar{\boldsymbol{x}}, [0, S]\right) = \mathrm{IVP}\,(D, \bar{\boldsymbol{x}}, [0, S])$ on $\bar{\mathcal{X}}$ and the claim is proven.

E.2 Proof of Theorem 29

Suppose not. Then there exists a non-penetrating initial state $\bar{\boldsymbol{x}}_0 = [\boldsymbol{q}_0;\ \boldsymbol{v}_0;\ t_0] \notin \bar{\mathcal{X}}_P$, compact interval $[0, S]$, and corresponding solution $\bar{\boldsymbol{x}}(s) = [\boldsymbol{q}(s); \boldsymbol{v}(s); t(s)] \in \mathrm{IVP}\,(D, \bar{\boldsymbol{x}}_0, [0, S])$ that penetrates at some $s_P \in [0, S]$ ($\bar{\boldsymbol{x}}(s_P) \in \bar{\mathcal{X}}_P$). Thus some contact $i \in \mathcal{C}$ penetrates at s_P ($\boldsymbol{\phi}_i(\boldsymbol{q}(s_P)) < 0$). Let $k(s) = \dot{t}(s) \in [0, 1]$; a.e. on $[0, S]$,

$$\dot{\bar{\boldsymbol{x}}} \in (1 - k(s)) D_{\mathcal{I}}(\bar{\boldsymbol{x}}(s)) + k(s) D_{\mathcal{S}}(\bar{\boldsymbol{x}}(s)) . \tag{149}$$

By the intermediate value theorem, we may select $s_A \in [0, s_P]$ such that $\boldsymbol{\phi}_i(\boldsymbol{q}(s_P)) < \boldsymbol{\phi}_i(\boldsymbol{q}(s_A)) < 0$ and contact i penetrates on the entire interval $[s_A, s_P]$. In order for $\boldsymbol{\phi}_i$ to decrease, there must exist a non-zero mesure set $\mathcal{S} \subseteq [s_A, s_P]$ with

$$\dot{\boldsymbol{\phi}}_i = \frac{\partial \boldsymbol{\phi}_i}{\partial \boldsymbol{q}} \dot{\boldsymbol{q}} = \boldsymbol{J}_{n,i} \boldsymbol{v}(s) k(s) < 0 , \tag{150}$$

on $\mathcal{S}$. But then both $\boldsymbol{\phi}_i$ and $\dot{\boldsymbol{\phi}}_i$ are strictly negative on $\mathcal{S}$, and thus $\bar{\boldsymbol{x}}(\mathcal{S}) \subseteq \mathrm{int}\left(\bar{\mathcal{X}}_{\mathcal{I}}\right)$. Therefore only impact dynamics are active on $\mathcal{S}$, i.e. $k(s) = 0$ a.e. on $\mathcal{S}$. But then $\dot{\boldsymbol{\phi}}_i = 0$ a.e. on $\mathcal{S}$, a contradiction.

E.3 Proof of Theorem 30

Suppose not. Then there exists a compact interval $[a, b]$; solution $\bar{\boldsymbol{x}}(s) \in \mathrm{SOL}\,(D, [a, b])$ with $\bar{\boldsymbol{x}}(s)$ impacting but not penetrating, $\bar{\boldsymbol{x}}([a, b]) \subseteq \bar{\mathcal{X}}_{\mathcal{I}} \setminus \bar{\mathcal{X}}_P$; and set $\mathcal{S} = \left\{s : \dot{\bar{\boldsymbol{x}}}(s) \in D(\bar{\boldsymbol{x}}(s)) \setminus D_{\mathcal{I}}(\bar{\boldsymbol{x}}(s))\right\}$ with positive measure. Furthermore, $\dot{t}(s)|_{\mathcal{S}} > 0$ and $\dot{\boldsymbol{q}}(s) = \boldsymbol{\Gamma}(\boldsymbol{q}(s))\boldsymbol{v}(s)\dot{t}(s)$.

We will now show that allowing $\dot{t}(s)|_{\mathcal{S}} > 0$ must lead to penetration and therefore a contradiction. By Lebesgue's density theorem, we may select a point of density $a < s_1 < b$, i.e., for all $\delta > 0$, $[s_1, s_1 + \delta] \cap \mathcal{S}$ has non-zero measure. As $\bar{\boldsymbol{x}}(s)$ remains in $\bar{\mathcal{X}}_{\mathcal{I}}$, by continuity of $\boldsymbol{J}(\boldsymbol{q})$ and $\bar{\boldsymbol{x}}(s)$ we may select $\delta > 0$ and a contact i that is active $\boldsymbol{\phi}_i(\boldsymbol{q}(s)) = 0$ with negative time derivative $\boldsymbol{J}_{n,i}\boldsymbol{v}(s) < 0$ on $[s_1, s_1 + \delta] \subseteq [a, b]$. Let $\dot{\boldsymbol{\phi}}_{\max} = \max_{s\in[s_1,s_1+\delta]} \boldsymbol{J}_{n,i}\boldsymbol{v}(s) < 0$. Then

$$\boldsymbol{\phi}_i(s_1 + \delta) = \int_{[s_1,s_1+\delta]} \boldsymbol{J}_{n,i}\boldsymbol{v}(s)\dot{t}(s)\mathrm{d}s\,, \tag{151}$$

$$\leq \dot{\boldsymbol{\phi}}_{\max} \int_{[s_1,s_1+\delta]\cap\mathcal{S}} \dot{t}(s)\mathrm{d}s\,, \tag{152}$$

$$< 0\,, \tag{153}$$

and thus $\bar{\boldsymbol{x}}(s_1 + \delta) \in \bar{\mathcal{X}}_P$, a contradiction.

E.4 Proof of Theorem 31

Let $\bar{\mathcal{X}}$ be compact containing no penetrating states ($\bar{\mathcal{X}} \cap \bar{\mathcal{X}}_P = \emptyset$). By Corollary 24 there exists a dissipation rate $\alpha_{\bar{\mathcal{X}}}(s)$ such that the impact differential inclusion $\dot{\boldsymbol{v}} \in D_{\boldsymbol{q}}(\boldsymbol{v})$ for each configuration $\boldsymbol{q} \in \boldsymbol{q}(\bar{\mathcal{X}})$ is $\alpha_{\bar{\mathcal{X}}}(s)$-dissipative. Let $\bar{K} = \max_{\bar{\mathcal{X}}} \|\boldsymbol{v}\|_{\boldsymbol{M}(\boldsymbol{q})}$.

Suppose the claim is not true. Then, for some $S' > S(\bar{\mathcal{X}}) = \frac{\bar{K}}{\alpha_{\bar{\mathcal{X}}}(1)}$, there must exist a sequence of solutions $(\bar{\boldsymbol{x}}_j(s))_{j\in\mathbb{N}}$, $\bar{\boldsymbol{x}}_j(s) \in \mathrm{IVP}\left(D, \bar{\mathcal{X}}, [0, S']\right)$, for which the elaped times grows arbitrarily small: $t_j(S') - t_j(0) \to 0$. By Theorem 28, $\mathrm{IVP}\left(D, \bar{\mathcal{X}}, [0, S']\right)$ is compact, and therefore by Assumption 27, the derivatives $\dot{\bar{\boldsymbol{x}}}_j(s)$ are uniformly bounded. Therefore $(\bar{\boldsymbol{x}}_j(s))_{j\in\mathbb{N}}$ is equicontinuous. Thus by Theorem 1, a subsequence of $\bar{\boldsymbol{x}}_j(s)$ converges uniformly to some $\bar{\boldsymbol{x}}_\infty(s)$ with $t_\infty([0, S']) = t_\infty(0)$. As $\mathrm{IVP}\left(D, \bar{\mathcal{X}}, [0, S']\right)$ is closed (Theorem 28), $\bar{\boldsymbol{x}}_\infty(s)$ must also be a solution to the initial value problem.

We now show that a contradiction arises because $\bar{\boldsymbol{x}}_\infty(s)$ follows impact dynamics longer than $\frac{\bar{K}}{\alpha_{\bar{\mathcal{X}}}(1)}$. Furthermore, as $t_\infty(s)$ is constant, $\dot{t}_\infty(s) = 0$, and thus $\bar{\boldsymbol{x}}_\infty(s)$ must follow only impact dynamics, $\bar{\boldsymbol{x}}_\infty(s) \in \mathrm{IVP}\left(D_{\mathcal{I}}, \bar{\mathcal{X}}, [0, S']\right)$. In order for $\dot{\bar{\boldsymbol{x}}}_\infty(s)$ to be selected from $D_{\mathcal{I}}$, we must have $\bar{\boldsymbol{x}}_\infty(s) \notin \bar{\mathcal{X}}_{\mathcal{S}}$ a.e., and thus $\boldsymbol{v}_\infty(s) \notin \mathcal{S}(\boldsymbol{q}_\infty(s))$ a.e. Additionally, as $\bar{\boldsymbol{x}}_\infty(s)$ only follows impact dynamics, the configuration is constant, i.e. $\boldsymbol{q}_\infty([0, S']) = \boldsymbol{q}_\infty(0) = \boldsymbol{q}_\infty$. Therefore $\boldsymbol{v}_\infty(s)$ is a solution of $\dot{\boldsymbol{v}} \in D_{\boldsymbol{q}_\infty}(\boldsymbol{v})$, and $\boldsymbol{v}_\infty(s) \in \mathrm{cl}\mathcal{I}(\boldsymbol{q}_\infty)$. Therefore $\mathcal{I}(\boldsymbol{q}_\infty)$ is non-empty and therefore has active contact ($\boldsymbol{q}_\infty \in \mathcal{Q}_A$). Furthermore, as $\bar{\mathcal{X}}$ contains no penetrating states, $\boldsymbol{q}_\infty \notin \mathcal{Q}_P$ (via Theorem 29), and thus $\dot{\boldsymbol{v}} \in D_{\boldsymbol{q}_\infty}(\boldsymbol{v})$ is $\alpha_{\bar{\mathcal{X}}}(s)$-dissipative. Finally, by Lemma 22, $S' < \frac{\|\boldsymbol{v}_\infty(0)\|_{\boldsymbol{M}}}{\alpha_{\bar{\mathcal{X}}}(1)} \leq S(\bar{\mathcal{X}})$, a contradiction.

E.5 Proof of Corollary 32

As $\bar{\mathcal{X}}(S')$ is non-empty and compact for all $S' > 0$, $T'(S')$ is well-defined. Then, $\liminf_{S'\to\infty} \frac{T'(S')}{S'} \in [0, 1]$ as the impact DI (78) enforces $\dot{t}(s) \in [0, 1]$. Consider a particular $S' > 0$, and let $\bar{\boldsymbol{x}}(s) \in \mathrm{IVP}\left(D, \bar{\mathcal{X}}, [0, S']\right)$. By Theorem 31, $t(s)$ increases by $T(\bar{\mathcal{X}})$ over each interval of length $S(\bar{\mathcal{X}})$, bounding

$$t(S') \geq T(\bar{\mathcal{X}}) \left\lfloor \frac{S'}{S(\bar{\mathcal{X}})} \right\rfloor \geq S' \frac{T(\bar{\mathcal{X}})}{S(\bar{\mathcal{X}})} - T(\bar{\mathcal{X}})\,. \tag{154}$$

Therefore, $\liminf_{S'\to\infty} \frac{T'(S')}{S'} \geq \frac{T(\bar{\mathcal{X}})}{S(\bar{\mathcal{X}})}$.

E.6 Proof of Theorem 33

Consider some state $[\boldsymbol{q};\ \boldsymbol{v}]$ and normal impulse $\boldsymbol{\lambda}_{n,max} \geq \boldsymbol{0}$. Let

$$\boldsymbol{z} = \begin{bmatrix} \boldsymbol{\beta} \\ \bar{\boldsymbol{\lambda}} \\ \boldsymbol{\gamma} \end{bmatrix} \geq \boldsymbol{0}\,. \tag{155}$$

Then we have

$$\boldsymbol{z}^T\boldsymbol{W}_{\boldsymbol{q}}\boldsymbol{z} = \frac{1}{2}\boldsymbol{z}^T\left(\boldsymbol{W}_{\boldsymbol{q}} + \boldsymbol{W}_{\boldsymbol{q}}^T\right)\boldsymbol{z}\,, \tag{156}$$

$$= \left\|\bar{\boldsymbol{J}}^T\bar{\boldsymbol{\lambda}}\right\|^2_{\boldsymbol{M}^{-1}} + \boldsymbol{\lambda}_n^T\boldsymbol{\mu}\boldsymbol{\gamma}\,, \tag{157}$$

$$\geq 0\,, \tag{158}$$

where the final inequality holds because $\boldsymbol{\mu}$ has positive entries and $\boldsymbol{M} \succ 0$. Therefore, $\boldsymbol{M}_{\boldsymbol{q}}$ is copositive.

Suppose further that$\boldsymbol{z} \in \mathrm{LCP}(\boldsymbol{W}_{\boldsymbol{q}}, \boldsymbol{0})$, thus $\boldsymbol{W}_{\boldsymbol{q}}\boldsymbol{z} \geq \boldsymbol{0}$ and $\boldsymbol{z}^T\boldsymbol{W}_{\boldsymbol{q}}\boldsymbol{z} = 0$. $\boldsymbol{W}_{\boldsymbol{q}}\boldsymbol{z} \geq \boldsymbol{0}$ implies by construction that

$$\boldsymbol{\lambda}_n \leq \boldsymbol{0}\,, \tag{159}$$

$$\boldsymbol{E}^T\boldsymbol{\lambda}_D \leq \boldsymbol{\mu}\boldsymbol{\lambda}_n \leq \boldsymbol{0}\,. \tag{160}$$

Therefore as $\boldsymbol{\lambda}_n, \boldsymbol{\lambda}_D \geq \boldsymbol{0}$, $\boldsymbol{\lambda}_n = \boldsymbol{0}$ and $\boldsymbol{\lambda}_D = \boldsymbol{0}$. Finally, as $\boldsymbol{\lambda}_{n,max}$ and $\boldsymbol{\beta}$ are non-negative,

$$\boldsymbol{z}^T\boldsymbol{w}_{\boldsymbol{q}}(\boldsymbol{v}, \boldsymbol{\lambda}_{n,max}) = \boldsymbol{\beta}^T\boldsymbol{\lambda}_{n,max} \geq \boldsymbol{0}\,. \tag{161}$$

Therefore by Proposition 10, $\mathrm{LCP}(\boldsymbol{W}_{\boldsymbol{q}}, \boldsymbol{w}_{\boldsymbol{q}}(\boldsymbol{v}, \boldsymbol{\lambda}_{n,max}))$ is non-empty.

E.7 Proof of Theorem 34

Consider a state $[\boldsymbol{q};\ \boldsymbol{v}]$, normal impulse increment $\boldsymbol{\lambda}_{n,max} \geq \boldsymbol{0}$, and solution to the impact LCP $\boldsymbol{z} = [\boldsymbol{\beta};\ \bar{\boldsymbol{\lambda}};\ \boldsymbol{\gamma}] \in \mathrm{LCP}(\boldsymbol{W}_{\boldsymbol{q}}, \boldsymbol{w}_{\boldsymbol{q}}(\boldsymbol{v}, \boldsymbol{\lambda}_{n,max}))$. Let $\boldsymbol{v}' = \boldsymbol{v} + \boldsymbol{M}^{-1}\bar{\boldsymbol{J}}^T\bar{\boldsymbol{\lambda}}$. Then from the complementarity condition we have

$$0 = \boldsymbol{z}^T\left(\boldsymbol{W}_{\boldsymbol{q}}\boldsymbol{z} + \boldsymbol{w}_{\boldsymbol{q}}(\boldsymbol{v}, \boldsymbol{\lambda}_{n,max})\right)\,, \tag{162}$$

$$= \left(\bar{\boldsymbol{\lambda}}^T\bar{\boldsymbol{J}}\right)\boldsymbol{v}' + \boldsymbol{\lambda}_n^T\boldsymbol{\mu}\boldsymbol{\gamma} + \boldsymbol{\beta}^T\boldsymbol{\lambda}_{n,max}\,, \tag{163}$$

$$= (\boldsymbol{v}' - \boldsymbol{v})^T\boldsymbol{M}\boldsymbol{v}' + \boldsymbol{\lambda}_n^T\boldsymbol{\mu}\boldsymbol{\gamma} + \boldsymbol{\beta}^T\boldsymbol{\lambda}_{n,max}\,. \tag{164}$$

As $\boldsymbol{\lambda}_n^T\boldsymbol{\mu}\boldsymbol{\gamma} + \boldsymbol{\beta}^T\boldsymbol{\lambda}_{n,max} \geq 0$,

$$(\boldsymbol{v}' - \boldsymbol{v})^T\boldsymbol{M}\boldsymbol{v}' \leq 0\,. \tag{165}$$

(165) is equivalent to $\|\boldsymbol{v}'\|^2_{\boldsymbol{M}} \leq \boldsymbol{v}^T\boldsymbol{M}\boldsymbol{v}'$. The Cauchy-Schwartz inequality then gives $\|\boldsymbol{v}'\|^2_{\boldsymbol{M}} \leq \|\boldsymbol{v}\|_{\boldsymbol{M}}\|\boldsymbol{v}'\|_{\boldsymbol{M}}$, and therefore $K(\boldsymbol{q}, \boldsymbol{v}') - K(\boldsymbol{q}, \boldsymbol{v}) \leq 0$.

F Simulation Proofs

F.1 Proof of Lemma 35

Let $[\boldsymbol{q};\ \boldsymbol{v}]$ be an impacting state ($\boldsymbol{v} \in \mathcal{I}(\boldsymbol{q})$), and let $\boldsymbol{\lambda}_{n,max} > \boldsymbol{0}$ be a normal impulse. Consider an impact LCP solution

$$[\boldsymbol{\beta};\ \boldsymbol{\lambda}_n;\ \boldsymbol{\lambda}_D;\ \gamma] \in \mathrm{LCP}(\boldsymbol{W}_{\boldsymbol{q}}, \boldsymbol{w}_{\boldsymbol{q}}(\boldsymbol{v}, \boldsymbol{\lambda}_{n,max}))\,.$$

such that

$$\boldsymbol{\lambda}_n < \boldsymbol{\lambda}_{n,max}\,. \tag{166}$$

Therefore for each contact i, the complementary equation (83) yields $\boldsymbol{\beta}_i = 0$ as $\boldsymbol{\lambda}_{n,max_i} - \boldsymbol{\lambda}_{n,i} > 0$. Then from complementarity equation (84), $\boldsymbol{J}_{n,i}\boldsymbol{v}' \geq 0$.

F.2 Proof of Lemma 36

Consider a configuration $\boldsymbol{q} \in \mathcal{Q}_A \setminus \mathcal{Q}_P$. It is sufficient to prove the claim for $\boldsymbol{v} = \boldsymbol{0}$ as $\mathrm{LFC}\,(\boldsymbol{q}, \bar{\boldsymbol{v}}) \subseteq \mathrm{LFC}\,(\boldsymbol{q}, \boldsymbol{0})$ for any velocity $\bar{\boldsymbol{v}}$ (see (42)). Furthermore, as $\boldsymbol{M}$ is full rank, we may assume WLOG that $\boldsymbol{M} = \boldsymbol{I}$. Consider the set of forces in the linear friction cone with total normal force 1:

$$\Lambda = \mathrm{LFC}\,(\boldsymbol{q}, \boldsymbol{0}) \cap \left\{\bar{\boldsymbol{\lambda}} : \|\boldsymbol{\lambda}_n\|_1 = 1\right\}\,. \tag{167}$$

As $\mathrm{LFC}\,(\boldsymbol{q}, \boldsymbol{0})$ is a convex cone, any vector $\boldsymbol{r}$ satisfies the claim if $\boldsymbol{r} \cdot \bar{\boldsymbol{J}}^T \Lambda > 1$.

As the linear friction cone is a subset of the Coulomb friction cone (see (43)), by Assumption 18, $\boldsymbol{0} \notin \bar{\boldsymbol{J}}^T \Lambda$. Furthermore, $\bar{\boldsymbol{J}}^T \Lambda$ is compact, non-empty, and convex. Therefore, $\boldsymbol{0} \notin \bar{\boldsymbol{J}}^T \Lambda - (-\bar{\boldsymbol{J}}^T \Lambda) = 2\bar{\boldsymbol{J}}^T \Lambda$, and by Theorem 11.4 of Rockafellar (1970) $\bar{\boldsymbol{J}}^T \Lambda$ and $-\bar{\boldsymbol{J}}^T \Lambda$ are strongly separated by some hyperplane. Then by definition there exists some vector $\tilde{\boldsymbol{r}}$ such that

$$\min_{\boldsymbol{F} \in \bar{\boldsymbol{J}}^T \Lambda} \boldsymbol{F} \cdot \tilde{\boldsymbol{r}} > \max_{\boldsymbol{F} \in -\bar{\boldsymbol{J}}^T \Lambda} \boldsymbol{F} \cdot \tilde{\boldsymbol{r}} = -\min_{\boldsymbol{F} \in \bar{\boldsymbol{J}}^T \Lambda} \boldsymbol{F} \cdot \tilde{\boldsymbol{r}}\,. \tag{168}$$

Setting $\varepsilon = \min_{\boldsymbol{F} \in \bar{\boldsymbol{J}}^T \Lambda} \boldsymbol{F} \cdot \tilde{\boldsymbol{r}} > 0$, $\boldsymbol{r} = \frac{\tilde{\boldsymbol{r}}}{\varepsilon}$ satisfies the claim.

F.3 Proof of Theorem 37

Let $\boldsymbol{q}_0 \in \mathcal{Q}_A \setminus \mathcal{Q}_P$ be a pre-impact configuration and let $\boldsymbol{v}_0 \in \mathcal{I}(\boldsymbol{q}_0)$ be a pre-impact velocity. As each $\boldsymbol{\lambda}_{n,max}$ is selected from the uniform distribution over the unit box, we have that

$$c_p = \mathbb{E}_{\boldsymbol{\lambda}_{n,max} \sim p}\left[\min_i \boldsymbol{\lambda}_{n,max_i}\right] = \frac{1}{m+1}\,. \tag{169}$$

We assume WLOG that p is supported on the interior of the unit box $(0,1)^m$, as the probability of being on the boundary is 0. Let $\sigma > 0$ be the minimum singular value of $\boldsymbol{M} = \boldsymbol{M}(\boldsymbol{q}_0)$. We can bound the norm of the initial velocity from below by

$$\sqrt{\sigma}\,\|\boldsymbol{v}\|_2 \leq \|\boldsymbol{v}\|_{\boldsymbol{M}}\,. \tag{170}$$

Now, select $\boldsymbol{r}$ for $\boldsymbol{q}_0$ as defined in Lemma 36. We will now show that the existence of $\boldsymbol{r}$ in conjunction with dissipation (Theorem 34), allows us to create a useful sufficient condition for impact termination.

Consider any execution of Algorithm 2 with initial state $[\boldsymbol{q}_0;\ \boldsymbol{v}_0]$, and let $\boldsymbol{\lambda}^k_{n,max}$, $\bar{\boldsymbol{\lambda}}^k = [\boldsymbol{\lambda}^k_n;\ \boldsymbol{\lambda}^k_D]$ and $\boldsymbol{v}_k$ be the maximum normal impulse; selected impulse; and velocity computed on lines 4–6 on the kth iteration of the loop. If the loop has not terminated after K steps, then for all loop iterations $k \in \{1, \ldots, K\}$, $\boldsymbol{v}_k \in \mathcal{I}(\boldsymbol{q}_0)$. By Theorem 34 and Lemmas 35–36, we have that

$$\begin{aligned}
\|\boldsymbol{v}_0\|_{\boldsymbol{M}} &\geq \|\boldsymbol{v}_K\|_{\boldsymbol{M}}\,, && (171)\\
&\geq \sqrt{\sigma}\,\|\boldsymbol{v}_K\|_2\,, && (172)\\
&\geq \sqrt{\sigma}\frac{\boldsymbol{r}}{\|\boldsymbol{r}\|_2} \cdot \boldsymbol{v}_K && (173)\\
&\geq \frac{\sqrt{\sigma}}{\|\boldsymbol{r}\|_2}\left(\boldsymbol{r} \cdot \boldsymbol{v}_0 + \sum_{k=1}^{K}\left\|\boldsymbol{\lambda}^k_{n,max}\right\|_1\right)\,, && (174)\\
&\geq -\sqrt{\sigma}\,\|\boldsymbol{v}_0\|_2 + \frac{\sqrt{\sigma}}{\|\boldsymbol{r}\|_2}\sum_{k=1}^{K}\left\|\boldsymbol{\lambda}^k_{n,max}\right\|_1\,, && (175)\\
&\geq -\|\boldsymbol{v}_0\|_{\boldsymbol{M}} + \sum_{k=1}^{K}\frac{\sqrt{\sigma}}{\|\boldsymbol{r}\|_2}\min_i \boldsymbol{\lambda}^k_{n,max_i}\,. && (176)
\end{aligned}$$

For this inequality to hold, and thus for $\boldsymbol{v}_K$ to remain in $\mathcal{I}(\boldsymbol{q}_0)$, it must be true that the summation in (176) is no greater than $2\,\|\boldsymbol{v}_0\|_{\boldsymbol{M}}$. Therefore, termination of the impact within K steps (i.e. $Z(h, \boldsymbol{q}_0, \boldsymbol{v}_0) \leq K$) is implied by $Z_K > c_Z\,\|\boldsymbol{v}_0\|_{\boldsymbol{M}}$, where

$$c_Z = \frac{2\,\|\boldsymbol{r}\|_2}{h\sqrt{\sigma}}\,, \tag{177}$$

$$Z_K = \sum_{k=1}^{K}\frac{1}{h}\min_i \boldsymbol{\lambda}^k_{n,max_i}\,. \tag{178}$$

Given that the $\boldsymbol{\lambda}_{n,max} \sim hp$ are selected i.i.d. we have that $\mathbb{E}\left[Z_K\right] = Kc_p$. Thus we would expect an impact to terminate proportional to

$$K^* = \left\lceil\frac{c_Z}{c_p}\right\rceil\left\lceil\|\boldsymbol{v}_0\|_{\boldsymbol{M}}\right\rceil\,. \tag{179}$$

We now explicitly bound the termination time Z using Hoeffding's inequality, applied below in (183); for $k \in \mathbb{Z}^+$ and $K = 2K^* + k$,

$$\begin{aligned}
P\left(Z \geq K\right) &\leq P\left(Z_K \leq c_Z\,\|\boldsymbol{v}_0\|_{\boldsymbol{M}}\right)\,, && (180)\\
&\leq P\left(Z_K \leq K^* c_p\right)\,, && (181)\\
&= P\left(Z_K - Kc_p \leq -\left(K^* + k\right)c_p\right)\,, && (182)\\
&\leq \exp\left(-\frac{2}{K}\left(K^* + k\right)^2 c_p^2\right)\,, && (183)\\
&\leq \exp\left(-\left(K^* + k\right)c_p^2\right)\,, && (184)\\
&\leq \exp\left(-kc_p^2\right)\,. && (185)
\end{aligned}$$

Thus the claim is satisfied.

F.4 Proof of Lemma 41

Suppose not. Then there exists a configuration $\boldsymbol{q} \in \mathcal{Q}_A \setminus \mathcal{Q}_P$, velocity $\boldsymbol{v}$, and $\varepsilon > 0$, such that for all $N \in \mathbb{N}$, there exists a $\boldsymbol{v}_N$, $\boldsymbol{J}_n\boldsymbol{v}_N \geq -\frac{1}{N}$, $\|\boldsymbol{v}_N\|_{\boldsymbol{M}} \leq \|\boldsymbol{v}\|_{\boldsymbol{M}}$, and yet $\boldsymbol{v}_N = \boldsymbol{f}_{\boldsymbol{q}}(\boldsymbol{v}'_N, \varepsilon\boldsymbol{1}) \in \mathcal{I}(\boldsymbol{q})$.

Due to energy dissipation (Theorem 34) and the boundedness of $\boldsymbol{v}_N$, the sequence $\boldsymbol{v}'_N$ is bounded as well. Without loss of generality we can therefore assume that $\boldsymbol{v}_N \to \boldsymbol{v}_\infty$ and $\boldsymbol{v}'_N \to \boldsymbol{v}'_\infty$. As $\boldsymbol{J}_n\boldsymbol{v}_N \geq -\frac{1}{N}$, it must be that $\boldsymbol{J}_n \boldsymbol{v}_\infty \geq 0$. Therefore, $\boldsymbol{v}'_\infty = \boldsymbol{f}_{\boldsymbol{q}}(\boldsymbol{v}_\infty, \varepsilon \mathbf{1}_m) = \boldsymbol{v}_\infty$ via Lemma 40. As $\boldsymbol{v}_N$ and $\boldsymbol{v}'_N$ converge to each other, there exists an N^*, with LCP-selected force $\bar{\boldsymbol{\lambda}}_{N^*} = [\boldsymbol{\lambda}_n;\ \boldsymbol{\lambda}_D]$ such that

$$\|(\boldsymbol{v}'_{N^*} - \boldsymbol{v}_{N^*})\|_2 = \left\|\boldsymbol{M}^{-1}\bar{\boldsymbol{J}}^T\bar{\boldsymbol{\lambda}}_{N^*}\right\|_2 < \frac{\varepsilon}{\|\boldsymbol{r}(\boldsymbol{q})\|_2}\,, \tag{186}$$

where $\boldsymbol{r}(\boldsymbol{q})$ comes from Lemma 36. However, by Lemma 35, as $\boldsymbol{v}'_{N^*} \in \mathcal{I}(\boldsymbol{q})$, at least one contact must fully activate, and thus $\|\boldsymbol{\lambda}_n\|_1 \geq \varepsilon$. But then again by Lemma 36, $\left\|\boldsymbol{M}^{-1}\bar{\boldsymbol{J}}^T\bar{\boldsymbol{\lambda}}_{N^*}\right\|_2 \geq \frac{\varepsilon}{\|\boldsymbol{r}(\boldsymbol{q})\|_2}$, a contradiction.

F.5 Proof of Theorem 43

First we will show that generating an ε-net of $\mathcal{V}_\infty(\boldsymbol{x}_0, h) \setminus \mathcal{I}(\boldsymbol{q}_0)$ can be reduced to generating an ε'-net of $\mathcal{V}_N(\boldsymbol{x}_0, h)$ for a suitable (ε', N). We will then show that $\mathcal{V}_N(\boldsymbol{x}_0, h)$ is the image of a box under a Lipschitz continuous function, reducing the claim to Proposition 4.

Select an initial condition $\boldsymbol{x}_0 = [\boldsymbol{q}_0;\ \boldsymbol{v}_0] \in (\mathcal{Q}_A \setminus \mathcal{Q}_P) \times \mathbb{R}^{n_v}$; step size $h > 0$; and approximation constants $\varepsilon, \delta > 0$. By Lemma 42, we can select N such that $\mathcal{V}_N(\boldsymbol{x}_0, h)$ is an $\frac{\varepsilon}{3}$-net of $\mathcal{V}_\infty(\boldsymbol{x}_0, h)$. Consider a run of $\mathrm{Approximate}(h, \boldsymbol{x}_0, \epsilon, N, M)$ for some $M > 0$. Define ψ as it is constructed on line 2 of Algorithm 3. Furthermore, suppose that the M samples from $\mathcal{V}_N(\boldsymbol{x}_0, h)$ generated on line 4 of Algorithm 3 constitute a ε' net of $\mathcal{V}_N(\boldsymbol{x}_0, h)$, where

$$\varepsilon' = \min\left(\frac{\varepsilon}{3}, \frac{\delta\left(\frac{\varepsilon}{3\psi}, \boldsymbol{v}_0\right)}{\sigma_{max}(\boldsymbol{J}_n)}\right)\,, \tag{187}$$

and $\delta\left(\frac{\varepsilon}{3\psi}, \boldsymbol{v}_0\right)$ comes from Lemma 41.

Consider any possible post-impact velocity $\boldsymbol{v}_1 \in \mathcal{V}_\infty(\boldsymbol{x}_0, h) \setminus \mathcal{I}(\boldsymbol{q}_0)$. Then there exists a $\boldsymbol{v}_2 \in \mathcal{V}_N(\boldsymbol{x}_0, h)$ with $\|\boldsymbol{v}_1 - \boldsymbol{v}_2\|_2 < \frac{\varepsilon}{3}$. Select the closest velocity $\boldsymbol{v}_3 \in \mathcal{V}_N(\boldsymbol{x}_0, h) \subseteq \mathcal{V}_\infty(\boldsymbol{x}_0, h)$ to $\boldsymbol{v}_2$ selected on line 4 during a run of $\mathrm{Approximate}(h, \boldsymbol{x}_0, \epsilon, N, M)$. From (187), we can determine two key facts: $\|\boldsymbol{v}_3 - \boldsymbol{v}_2\|_2 \leq \frac{\varepsilon}{3}$, and $\boldsymbol{J}_n \boldsymbol{v}_3 \geq -\delta\left(\frac{\varepsilon}{3\psi}, \boldsymbol{v}_0\right)$. This same $\boldsymbol{v}_3$ is used to generate $\boldsymbol{v}_4 = \boldsymbol{f}_{\boldsymbol{q}_0}(\boldsymbol{v}_3, \frac{\varepsilon}{3\psi}\mathbf{1}_m)$ on line 5, and $\boldsymbol{J}_n \boldsymbol{v}_4 \geq \mathbf{0}$ via Lemma 41.

$\boldsymbol{v}_4$ is in the post-impact set $\mathcal{V}_\infty(\boldsymbol{x}_0, h) \setminus \mathcal{I}(\boldsymbol{q}_0)$ by Lemma 41, and it will be output by $\mathrm{Approximate}(h, \boldsymbol{x}_0, \epsilon, N, M)$. Furthermore suppose that $\bar{\boldsymbol{\lambda}} = [\boldsymbol{\lambda}_n;\ \boldsymbol{\lambda}_D]$ was the LCP-selected force in the calculation of $\boldsymbol{v}_4$; we then have that

$$\|\boldsymbol{v}_4 - \boldsymbol{v}_3\|_2 \leq \left\|\boldsymbol{M}^{-1}\bar{\boldsymbol{J}}^T\bar{\boldsymbol{\lambda}}\right\|_2\,, \tag{188}$$

$$\leq \sigma \left\|\bar{\boldsymbol{\lambda}}\right\|_1\,, \tag{189}$$

$$\leq \sigma \|\boldsymbol{\lambda}_n\|_1 (1 + \max_i \boldsymbol{\mu}_i)\,, \tag{190}$$

$$\leq \frac{\varepsilon}{3}\,, \tag{191}$$

where $\sigma = \sigma_{max}\left(\boldsymbol{M}^{-1}\bar{\boldsymbol{J}}^T\right)$ and the final inequality comes from the construction of ψ on line 2 of Algorithm 3. Thus, by triangle inequality, $\|\boldsymbol{v}_4 - \boldsymbol{v}_1\|_2$ is bounded above by

$$\|\boldsymbol{v}_2 - \boldsymbol{v}_1\|_2 + \|\boldsymbol{v}_3 - \boldsymbol{v}_2\|_2 + \|\boldsymbol{v}_4 - \boldsymbol{v}_3\|_2 \leq \varepsilon\,. \tag{192}$$

Therefore, the claim is true if the samples from $\mathcal{V}_N(\boldsymbol{x}_0, h)$ generated on line 4 of Algorithm 3 are a ε' net of $\mathcal{V}_N(\boldsymbol{x}_0, h)$ with probability $1 - \delta$; we conclude by calculating an M that guarantees this property.

Consider the sequence of functions

$$\boldsymbol{f}^1(\boldsymbol{\lambda}_n^1) = \boldsymbol{f}_{\boldsymbol{q}_0}(\boldsymbol{v}_0, \boldsymbol{\lambda}_n^1)\,, \tag{193}$$

$$\boldsymbol{f}^k(\boldsymbol{\lambda}_n^1, \ldots, \boldsymbol{\lambda}_n^k) = \boldsymbol{f}_{\boldsymbol{q}_0}(\boldsymbol{f}^{k-1}(\boldsymbol{\lambda}_n^1, \ldots, \boldsymbol{\lambda}_n^{k-1}), \boldsymbol{\lambda}_n)\,. \tag{194}$$

Examining (100), we see that the sequence $\boldsymbol{f}^N$ can be used to construct the N-step reachable velocities:

$$\mathcal{V}_N(\boldsymbol{x}_0, h) = \boldsymbol{f}^N([0, h]^{Nm})\,. \tag{195}$$

Furthermore, if $f_{\boldsymbol{q}_0}$ has Lipschitz constant L, then $\boldsymbol{f}^N$ is Lipschitz continuous on $[0, h]^{Nm}$ with constant L^N by Proposition 2. Under Assumption 38, $\mathrm{Sim}(h, \boldsymbol{x}_0, N)$ yields a uniform sample of $[0, h]^{Nm}$ mapped under $\boldsymbol{f}^N$. Therefore, the claim holds, with M given by Proposition 4:

$$M \geq \frac{\ln(\delta\Omega)}{\ln(1 - \Omega)}\,, \tag{196}$$

$$\Omega = \left\lceil \frac{hL^N\sqrt{Nm}}{\varepsilon} \right\rceil^{-Nm}\,. \tag{197}$$